

THE HARD START PHENOMENA IN HYPERGOLIC ENGINES

VOLUME V. RCS ENGINE DEFORMATION AND DESTRUCT TESTS

by

Yael Miron and H. E. Perlee

Prepared for
Manned Spacecraft Center
National Aeronautics and Space Administration
Houston, Texas
Order No. T-39882 (G)

UNITED STATES DEPARTMENT OF THE INTERIOR
Rogers C. B. Morton, Secretary

BUREAU OF MINES
Thomas V. Falkie, Director

PITTSBURGH MINING AND SAFETY RESEARCH CENTER

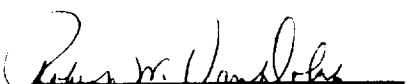
INTERIM REPORT NO. 1646

THE HARD START PHENOMENA IN HYPERGOLIC ENGINES
VOLUME V. RCS ENGINE DEFORMATION AND DESTRUCT TESTS

By

Yael Miron and H. E. Perlee

APPROVED:



Robert W. Van Dolah
Research Director
Pittsburgh Mining and
Safety Research Center

U.S. Department of the Interior
Bureau of Mines
Pittsburgh, Pennsylvania 15213
March 22, 1974

CONTENTS

	<u>Page</u>
Introduction.....	6
Experimental background.....	7
Procedures and results.....	9
Set I. Deformation experiments.....	9
Engine deformation experiments.....	9
Impulse measurements.....	20
Explosion pressure.....	25
Set II. Destruct experiments.....	29
SS engine fragmentation experiments.....	29
Panel-engine destruct experiments.....	31
Set III. Fragmentation studies.....	39
Fragment kinematics.....	39
Penetration of Vycor window and mylar H-film blanket by steel projectiles.....	74
Impulse due to an explosion in the engine.....	79
Rise in temperature of engine wall due to an internal explosion....	79
Summary.....	81
References.....	83
Appendix I. Theoretical background.....	84

ILLUSTRATIONS

Fig.

1. RCS molybdenum engine.....	10
2. Stainless steel prototype Apollo attitude control engine used by the MSC in their qualifying tests.....	11
3. Drawing of simulated rocket engine combustion chamber.....	12
4. Scaled drawing of the assembled components used in the destruct experiments with the simulated combustion chambers.....	13
5. Drawing showing the three charge locations used in the destruct experiments.....	14
6. Engine destruct test assembly.....	15
7. Percent increase in engine diameter as a function of tetryl charge (exclusive of detonator) and TNT equivalence (inclusive of detonator).....	17
8. Simulated engine deformation resulting from the explosion of 3.0, 6.0, and 7.5 g of tetryl located at the center of the engine.....	18
9. Cross section of the deformed combustion chamber resulting from the explosion of 7.5 g of tetryl located at the center of the combustion chamber.....	19
10. Deformed simulated engines resulting from the explosion of 6 g of tetryl fired in an air environment with the charge located (a) on the engine's axis near the injector; (b) at the engine's center, and (c) at mid-height near the engine wall.....	21
11. Scaled drawing of the simulated mortar engine.....	22

ILLUSTRATIONS

<u>Fig.</u>	<u>Page</u>
12. Impulse resulting from the explosion of various amounts of tetryl fired in the simulated mortar engine.....	24
13. Electronic circuitry used in conjunction with the resistor pressure transducer for recording explosion pressures.....	26
14. Resistor pressure transducer used for recording peak explosion pressures at the chamber wall.....	27
15. Resistor pressure transducer record obtained at the wall opposite a 9-g tetryl charge located at the chamber's mid-center position.....	28
16. Resistor pressure transducer record obtained with 10.5 g tetryl at the center of the engine.....	32
17. Panel-engine destruct test assembly.....	33
18. Resultant damage to the outer surface of the RCS panel by the explosively destroyed molybdenum combustion chamber.....	35
19. Resultant damage to inner RCS panel.....	36
20. Recovered molybdenum combustion chamber.....	38
21. Stainless steel engine halves containing 1.3- and 0.6-cm diam blowout plugs.....	41
22. Quartered stainless steel engines containing 0.6-, 1.3-, 1.9-, and 2.5-cm diam blowout plugs.....	42
23. Assembled stainless steel engine including explosive train containing NG-EGDN-cellulose wick.....	44
24. Front half of the destructed MSC engine.....	46
25. Rear half of the destructed MSC engine.....	47
26. Front half of the destructed TMC engine (042).....	48
27. Rear half of the destructed TMC engine (042).....	49
28. Front half of the destructed TMC engine (379).....	50
29. Rear half of the destructed TMC engine (379).....	51
30. Front half of the destructed TMC engine (542).....	52
31. Rear half of the destructed TMC engine (542).....	53
32. Stainless steel engine section loaded with a single layer of the NG-EGDN-cellulose explosive film.....	54
33. Stainless steel engine section showing Primacord loaded on the engine wall.....	55
34. Molybdenum engine fragments resulting from the explosion of 0.75 g of explosive film (NG-EGDN-cellulose) covering half the engine internal surface.....	56
35. Molybdenum engine fragments resulting from the explosion of 0.5 g of PETN (Primacord) covering half the engine internal surface.....	57
36. Ratio of fragment translational velocities as a function of the ratio of their area-to-mass ratios common to an explosion.....	59
37. High speed frame sequence of exploding engine halves.....	62
38. Pressure transducer traces for detonating stoichiometric C_2H_4/O_2 mixtures in the stainless steel engines for two heights of the ignition source above the transducer (a) 4.0 cm and (b) 1.4 cm.....	64
39. Pressure distribution behind an C_2H_4/O_2 detonation front.....	65

ILLUSTRATIONS

<u>Fig.</u>		<u>Page</u>
40.	Angular velocity of stainless steel fragments as a function of their translational (radial) velocity.....	66
41.	Fragment velocities from the explosion of the stainless steel engines with the NG-EGDN-cellulose layers, the PETN cord, and the C_2H_4/O_2 gas detonations.....	67
42.	Side and top views of the experimental arrangement of components in the engine explosion experiments.....	70
43.	Molybdenum engine fragments resulting from the explosion of 0.50 g of PETN (Primacord) completely covering the interior of the engine.....	71
44.	Molybdenum engine fragments resulting from the explosion of 0.75 g of PETN (Primacord) completely covering the interior of the engine.....	72
45.	Molybdenum engine fragments resulting from the explosion of 0.75 g of PETN (Primacord) completely covering the interior of the engine.....	73
46.	Velocity of 1.61 g blunt and 1.44 g pointed steel projectile required to crack or puncture a 30-cm square, 0.32-cm thick Vycor plate.....	76
47.	Typical maximum damage to Vycor plate by the blunt nose 1.61 g projectile (also shown).....	77
48.	Depth of penetration of a 12-layer H-film blanket by a blunt 1.61 g projectile as a function of projectile velocity.....	78
49.	Ballistic pendulum apparatus.....	80
A-1.	Wave pattern and pressure distribution associated with thin film detonation.....	85
A-2.	Illustration of (a) the high pressure zone behind the detonation front and (b) the quasi-steady chamber pressure (P_V) in producing rotation of a fragment.....	90

TABLES

1.	Results of simulated engine experiments.....	16
2.	Peak shock pressures resulting from the explosion of various weights of tetryl located at the center of the combustion chamber and striking the wall adjacent to the charge center.	29
3.	Fragment weight distribution.....	30
4.	Fragment penetration distribution in the wax blocks.....	30
5.	Fragment weight distribution, panel shot No. 1.....	34
6.	Fragment penetration in the wax blocks, panel shot No. 1.....	34
7.	Distribution of total fragment weight and number as a function of engine component.....	37
8.	Recovered fragments from the destructed molybdenum engines and their average weight and velocity range.....	58
9.	Fragment velocities (m/sec) obtained in the C_2H_4/O_2 detonation studies in sectioned SS engines.....	60
10.	Mass and area-to-mass ratio for the SS, aluminum, and molybdenum fragments.....	61
11.	Number of fragments recovered, average weight, and velocity range obtained in the molybdenum engine explosions.....	69
12.	Temperature rise of SS engines following detonation of various weights of Primacord.....	81

THE HARD START PHENOMENA IN HYPERGOLIC ENGINES
VOLUME V. RCS ENGINE DEFORMATION AND DESTRUCT TESTS

by

Yael Miron¹ and H. E. Perlee²

INTRODUCTION

Apollo Reaction Control (RCS) engines experienced high pressure peaks at ignition in a space simulated environment that destroyed the engine. More than two engines have failed during testing at the Marquardt Corporation (TMC) test facility and another seven at the Manned Space Center (MSC) in Houston, Tex. Furthermore, the possibility existed that under flight conditions the fragments of the damaged engine contain sufficient momentum to damage the surrounding Apollo spacecraft as well as vulnerable areas (windows, and so forth) of the adjacent Lunar Module (LM). Thus, there existed a need for simulating similar engine destructions and assessing the degree of damage imparted to the surrounding vehicles by the resulting fragments.

The RCS engines are expensive and only seven were available for these studies. Therefore, for exploratory study purposes, less-expensive engines were machined from No. 347 stainless steel (SS) having internal dimensions identical to the RCS engines. These SS engines were used in almost all the experiments described in this volume.

The Bureau program was subdivided into three sets, with each set interrelated to the previous one. In the first set of experiments, the extent of deformation of the engine was measured as a function of the size and position of an explosive charge in the engine. The total impulse imparted (in the direction of thrust) by an explosion of a condensed-phase charge in the engine combustion chamber also was measured. Finally, the internal pressure exerted on the walls of the engine during the explosion also was measured.

In the second set of experiments, explosive charges large enough to fragment SS engines were used and the fragment size distribution and the fragment velocity or energy (the combined phenomena is termed

¹Chemical research engineer.

²Chief, Theoretical Support.

Both authors are with the Pittsburgh Mining and Safety Research Center, Bureau of Mines, U. S. Department of the Interior, Pittsburgh, Pa.

"fragment-kinematics") resulting from the exploded engines were analyzed. Partly on the basis of these results, charge sizes were calculated for subsequent use in exploding two molybdenum engines, mounted on Apollo AFRM Service Module Reaction Control System panels; one engine to a panel. These tests afforded a survey of the damage to the panels by the flying fragments. The explosive used in these two sets was tetryl (2, 4, 6-Trinitrophenyl methyl nitramine), initiated by a No. 8 Du Pont³ electric detonator.

In the third set of experiments, a more detailed study was made of the fragment-kinematics of the SS engines. In this study, the engines were quartered or halved and some of these sections contained cylindrical blowout plugs of various sizes. Besides the advantage of having fragments of known size, weight, and shape, this arrangement also decreased the total number of engines required for the tests. Two types of explosive systems were used in this phase of the program. One was a gas-phase detonation of a stoichiometric mixture of ethylene and oxygen. The second, intended to simulate a thin layer detonation, consisted of either lens paper saturated with an explosive solution of NG-EGDN (a 50:50 mixture of nitroglycerin and ethylene glycol dinitrate) covering the internal engine surfaces or thin Primacord⁴ wound around the internal surface in such a manner as to simulate a thin layer of explosive on the surface of the engine. For this phase, two molybdenum engines were available for the final experiments. The impulse given to the engines by the gas-phase detonation and by the thin layer detonation was measured in a ballistic mortar type equipment. The temperature rise in the wall of the engine due to the detonation also was measured.

In the last group of experiments, the energy required by various projectiles to penetrate or otherwise damage a Vycor window and a Mylar H-film blanket was measured. Both materials are used in the LM vehicle. The Vycor window is located about 2 meters away from an attitude control engine and protects another, more fragile, window from meteorites. The Mylar blanket covers the LM outer surface and serves as a thermal shield and also as a protection against meteorites.

EXPERIMENTAL BACKGROUND

The explosive reaction that destroys the RCS engines has always been observed to occur at the time of engine ignition and is apparently due to either the detonation of the heterogeneous constituents of the rocket engine, consisting primarily of unreacted propellant droplets and vapors,

³Reference to specific brands, equipment, or trade names in this report is made to facilitate understanding and does not imply endorsement by the Bureau of Mines.

⁴Primacord is a trade name of the Ensign-Bickford Co. (Simsbury, Conn.) for their detonating fuses, used primarily for initiating commercial explosives. Primacord consists of a central core of PETN encased in textile braid and coated with various coats.

and/or the detonation of explosive materials accumulated on the engine walls from previous pulses. The latter mechanism could be one of two types; that is, the propagation of a detonation through the condensed-phase materials in situ on the engine wall, or the propagation of a detonation through these materials after they have been forcibly removed from the engine wall and dispersed in the combustion chamber, usually by means of a shock wave. For the sake of discussion, these latter two types of detonation phenomena will be referred to as film detonation and disrupted film detonation, respectively.

It has been established that the materials on the internal wall of the rocket engine contain, in addition to unreacted propellants, substantial proportions of explosive materials such as hydrazine nitrate, ammonium nitrate, and possibly hydrazoic acid. There is ample combustible available for supporting an explosion. In view of the possible occurrence of these two explosion mechanisms, an investigation was conducted to reproduce these mechanisms as closely as possible.

The gas-phase detonation was chosen to simulate the pressures and combustion dynamics of the heterogeneous detonation and the disrupted film detonation, and the explosion of a thin layer of explosive was intended to simulate the explosion of material accumulated on the wall. During these experiments, peak gas pressures immediately behind the detonation front, of typically 8 to 10 kilobars were measured in film detonation tests, while approximately 7.5 kilobars were measured in disrupted film detonation tests.

To determine the relationship between explosions--via the film or disrupted film detonation--and resultant fragmentation, it was necessary to correlate actual engine damage with explosion parameters. Since the only obvious criterion was fragment size, it was assumed that if the size of the fragments produced experimentally from molybdenum engines exploded in laboratory experiments would be similar to the size of those obtained from the exploded TMC and MSC engines then the destructive forces would be similar.⁵ It also was assumed that the fragments of the MSC and TMC engines used as a criterion of size were not further fragmented by collision with their surroundings. The fragments from the exploded engines were observed with a high-speed motion camera. In the tests with pre-assembled, sectioned engines, the pre-cut sections and/or the blowout plugs, when used, were hurled in all directions by the force of the explosion. The velocities and rotations of these sections were measured from movie film records.

⁵The shattering or fragmenting power (Brisance) of an explosive has been shown in general to be linearly related to its rate of detonation.

On the Apollo Service Module, clusters of four molybdenum RCS engines are positioned 90 deg apart on a panel mount. Early engines had a molybdenum diffuser section; the molybdenum engine, without diffuser, can be seen in figure 1. In the MSC qualifying tests, the clusters contained both SS and molybdenum engines. In one of MSC's tests, an explosion occurred in a SS engine. While the explosion did not destroy the SS engine, it did damage the diffuser of the molybdenum engine positioned opposite to it. As a result of this accident, all diffusers are now made of SS. As part of this study, it was desired to ascertain if an explosion occurring in a molybdenum engine, although not strong enough to destroy the engine, might have sufficient impulse to loosen the mounting connectors or damage the mounting panel. Either case could adversely affect the performance of the specific engine. It was thus decided to measure the total impulse, in the direction of the thrust, due to an explosion in the engine. Total impulse is the combined effect of the reflection of the blast wave from the injector face of the chamber and the exhaust of the product gases out the throat; the former effect apparently accounts for most of the total thrust. In these studies, the total impulse was measured by means of a ballistic mortar.

PROCEDURES AND RESULTS

Set I. Deformation Experiments

Engine Deformation Experiments

For the initial engine deformation experiments, combustion chambers were machined from No. 347 SS, the same material used for engines in the MSC qualifying studies. The engines in this study were also very similar in geometry to the MSC engines. Figure 2 shows a prototype Apollo attitude control engine used by MSC in their qualifying tests, while figure 3 shows a scaled drawing of the combustion chambers used in this study. The explosive used was tetryl; 3, 6, and 7.5 g of tetryl, in the form of pressed pellets, were placed in various locations in the combustion chambers and were fired with a No. 8 Du Pont electric detonator. Figure 4 shows a cross section of the complete motor (engine) assembly, including the detonator and tetryl pellet. A scaled drawing of the various charge locations is shown in figure 5. The complete assembled experimental setup is presented in figure 6.

Six experiments were conducted with various charge sizes and locations. Of these, five were conducted at atmospheric pressure and the sixth in a low pressure environment. The apparatus was assembled in a bombproof and the charge was fired remotely. Engine deformation was observed visually, as well as physically, by measuring the change in internal volume of the combustion chamber, and by measuring the change in outside dimensions of the engines. Pien marks on the exterior surface of the engine were used to measure the eccentricity of deformation of the engines.

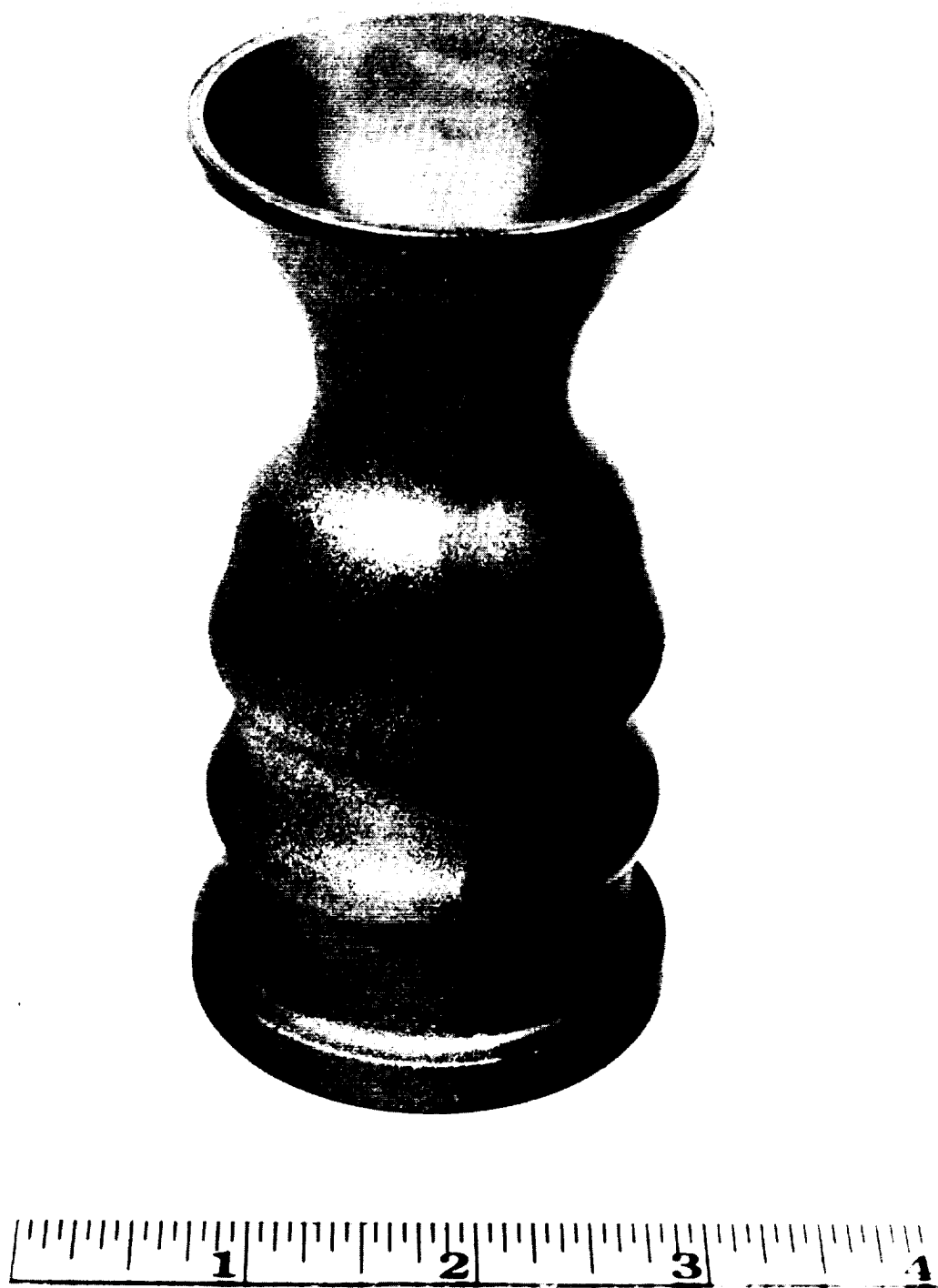


FIGURE 1. - RCS Molybdenum Engine .



FIGURE 2. - Stainless Steel Prototype Apollo Attitude Control Engine
Used by the MSC in Their Qualifying Tests.

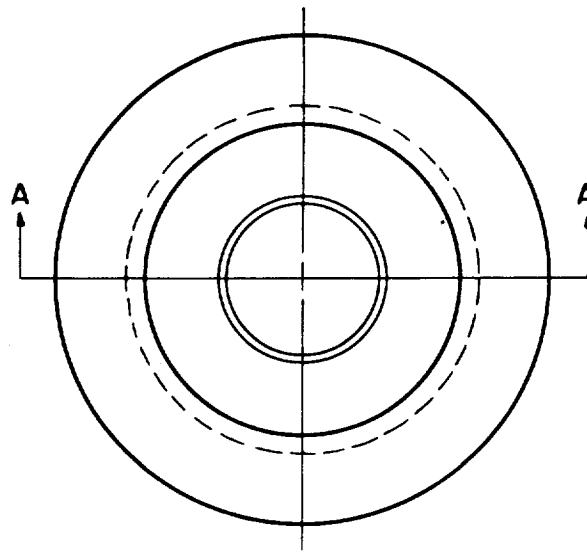
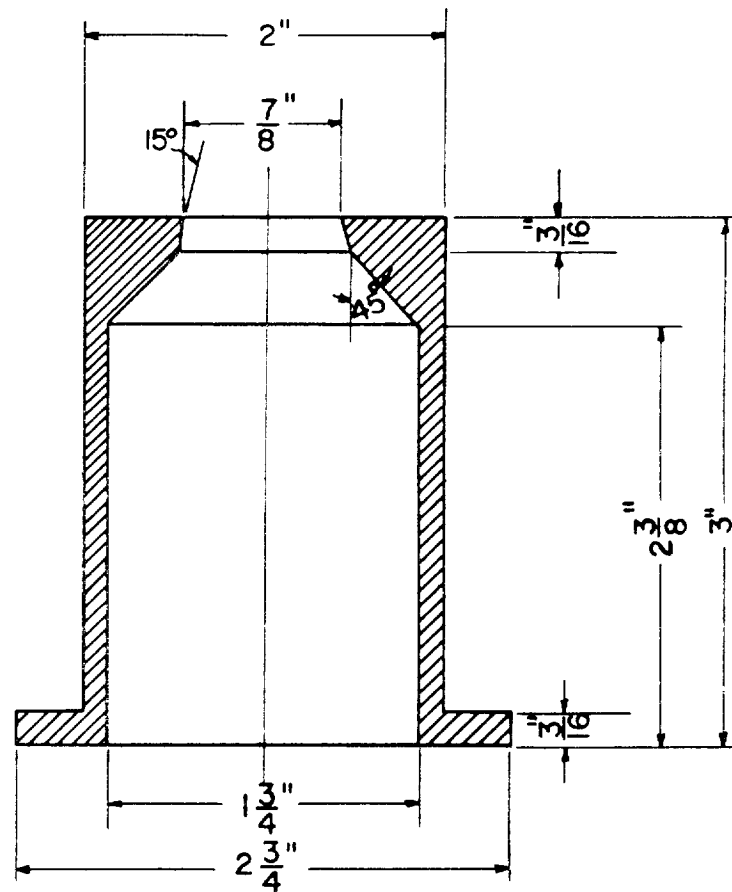


FIGURE 3. - Drawing of Simulated Rocket Engine Combustion Chamber.

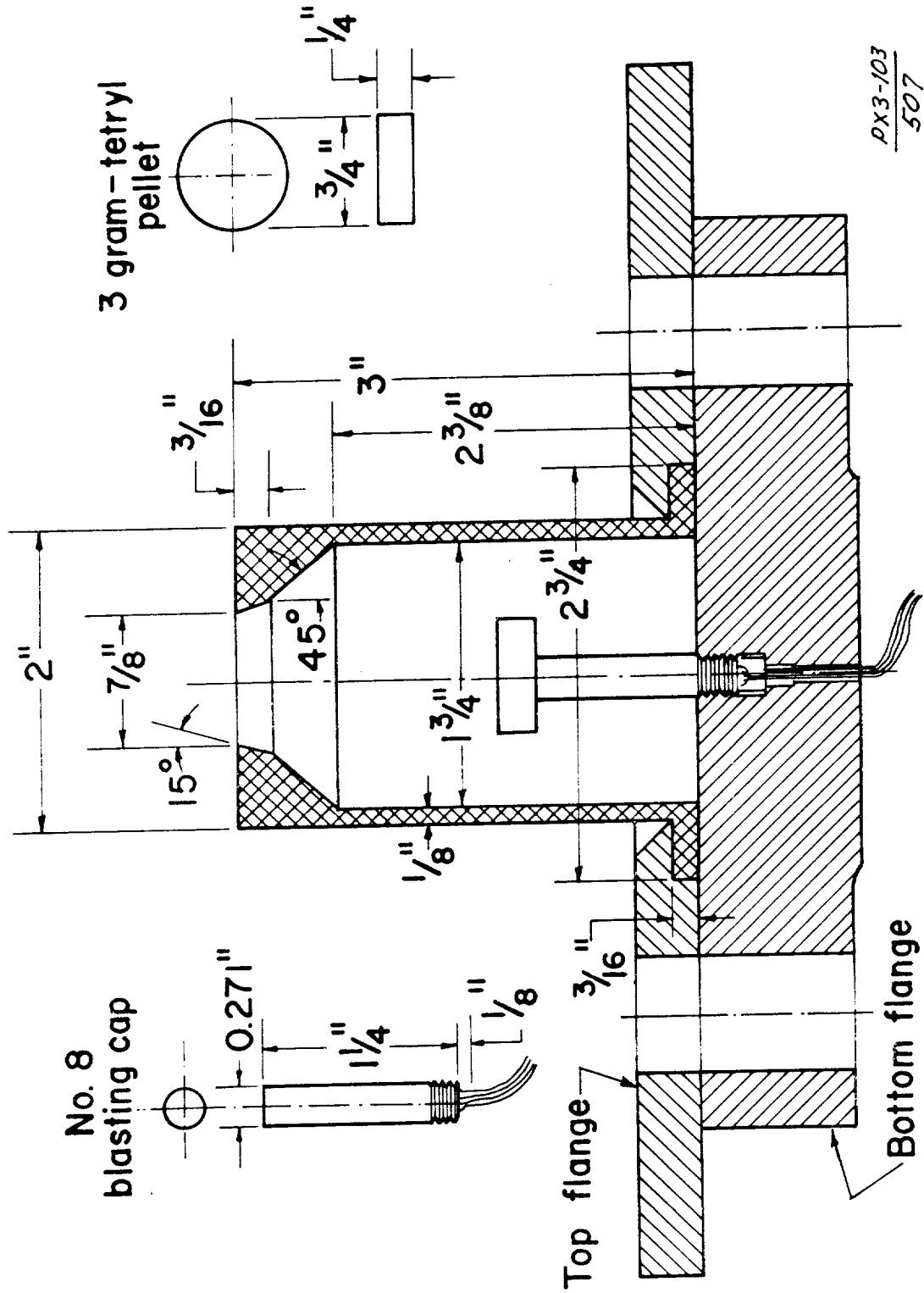


FIGURE 4. - Scaled Drawing of the Assembled Components Used in the Destruct Experiments With the Simulated Combustion Chambers.

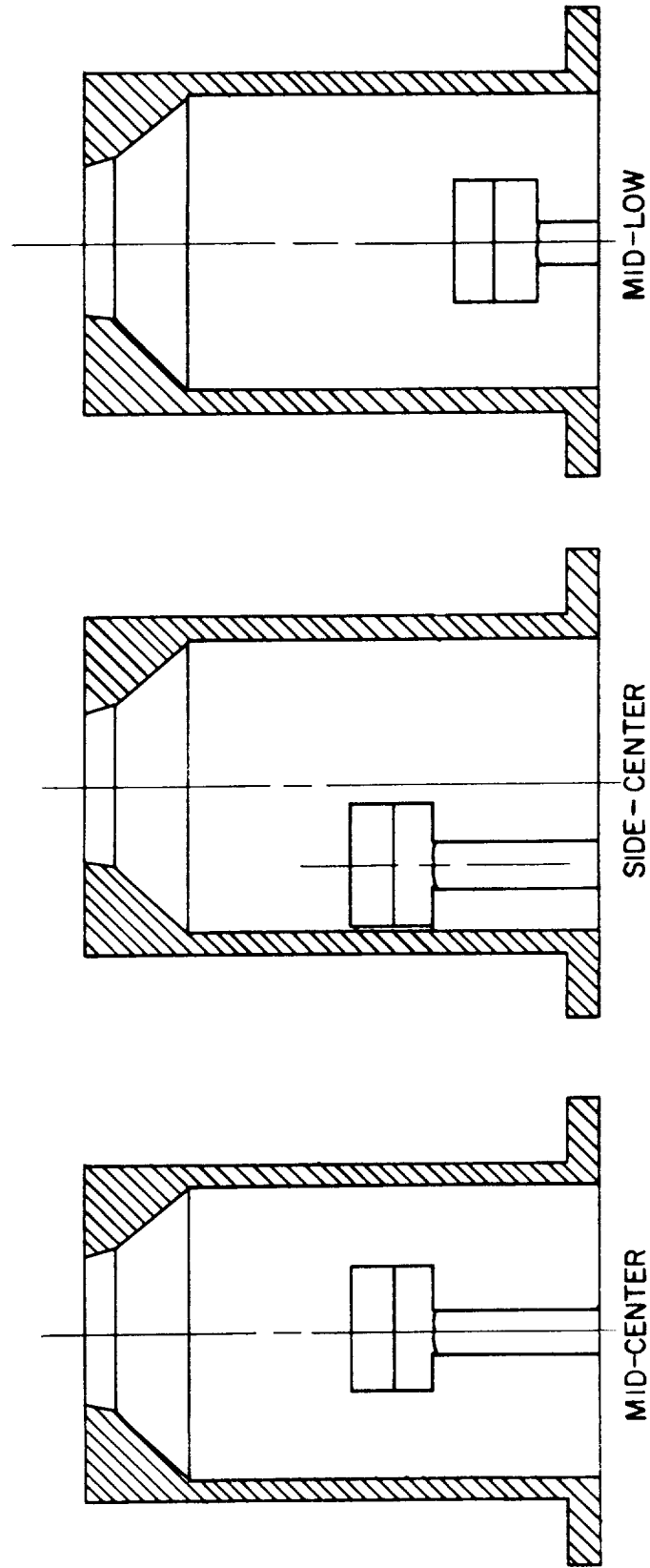


FIGURE 5. Drawing Showing the Three Charge Locations Used in the Destruct Experiments.

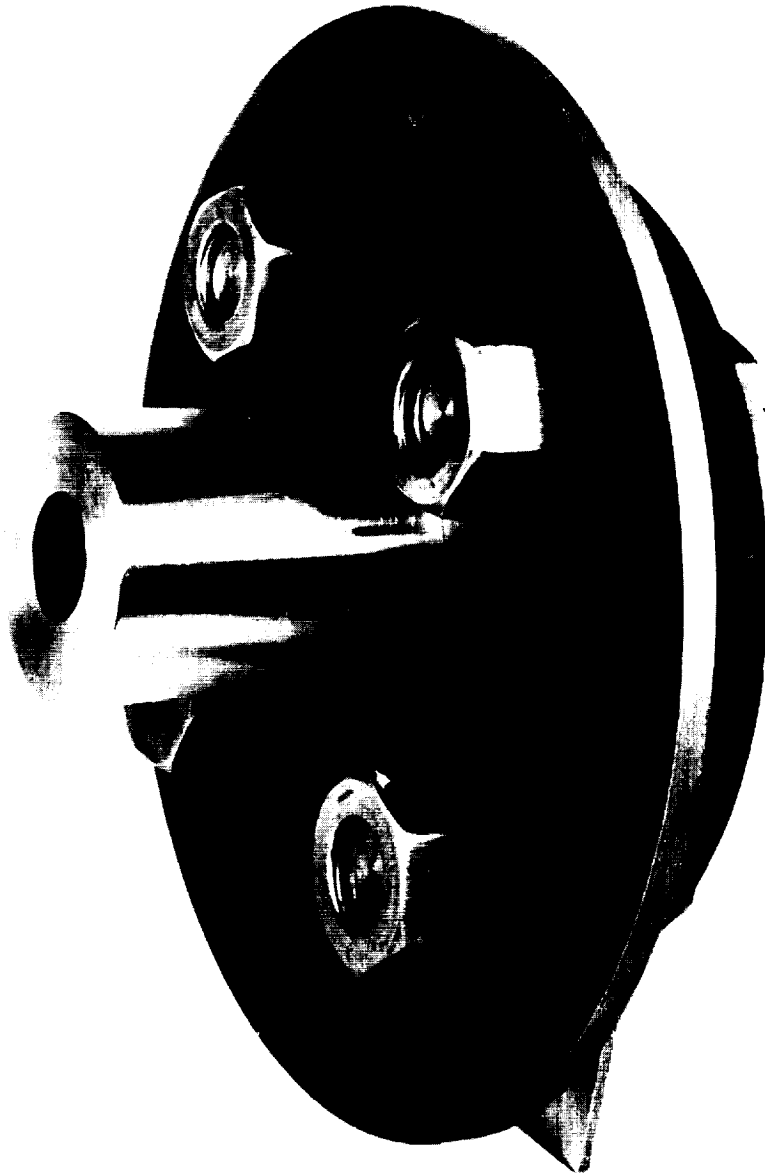


FIGURE 6. - Engine Destruct Test Assembly.

The results of these experiments are shown in table 1, which gives the percent increase in the motor's maximum diameter and volume for each of the tetryl charge sizes used and for all charge locations. The increase in volume for 3 g of explosive was approximately 5 pct; for 6 and 9 g, the change in volume was 11 and 20 pct, respectively. The respective changes in diameter for the same charges were 2.5, 13.5, and 20 pct. The percentage increase in the maximum diameter of the engine is plotted as a function of the charge weight for the mid-center position (fig. 7). Since a single experiment was conducted for each charge size and position, no estimate of the experimental error was obtained.

TABLE 1. - Results of simulated engine experiments. Percent change in volume and maximum diameter of simulated engines resulting from the explosion of various weights of tetryl in the various locations of the combustion chambers

Experiment No.	1/ Charge weight, g	Charge location	Volume, cm ³		Volume change, pct	Maximum diameter, cm		Diameter change, pct
			Before	After		Before	After	
1	3	Mid-center	105.7	110.9	4.92	5.08	5.207	2.50
2	6	do	105.7	117.5	10.7	5.08	5.712	12.45
3	7.5	do	106.5	127.0	19.1	5.08	6.101	20.10
4	6	Side-center	106.8	2/	-	5.08	-	-
5	6	Mid-low	106.0	115.5	9.05	5.08	5.733	12.85
6 ^{3/}	6	Mid-center	105.7	119.1	12.7	5.08	5.842	15.00

1/ Weight of pressed tetryl pellets exclusive of Du Pont No. 8 detonator.

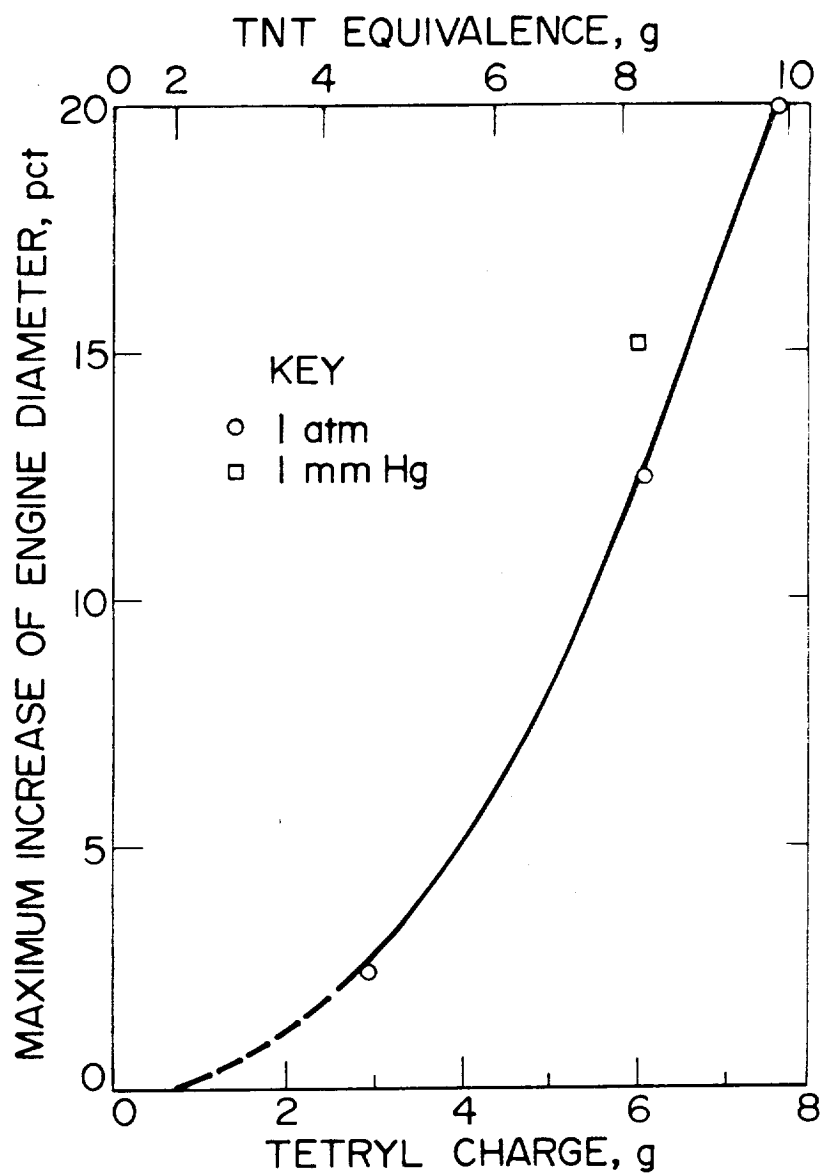
2/ Engine No. 4 exhibited a weight loss of 9.3 g.

3/ Fired in an environmental pressure of approximately 1 mm Hg.

Figure 8 illustrates the relative deformation of the three engines after firing in ambient atmospheres, 3, 6, and 7.5 g of tetryl charges, respectively, at the mid-center location. Figure 9 shows a cutaway view of the engine fired with the 7.5-g charge. The pitting effect near the flanged end is due to the high velocity fragments from the No. 8 detonator. These fragments in no way contributed to the main deformation. As shown in table 1, the results of a charge exploding in a low pressure (1 torr) environment (experiment No. 6) when compared to the results obtained from an equal charge, fired in an ambient atmosphere, are not sufficiently different to suggest an effect of the surrounding gas on the deformation.

Since MSC's engine damage, in an accident that occurred in their qualifying test series (1)⁶ amounted to about 18 pct increase in their 347-SS engine's diameter, figure 7 shows it to be the result of an explosive equivalent to 7.2 g of tetryl, exclusive of the No. 8 detonator, or to 10.1 g of TNT (inclusive of the No. 8 detonator), or to at least 6.0 g of an A-50/NT0 mixture (based on a maximum TNT equivalent of 168 pct for this mixture; see volume II of this report).

⁶Underlined numbers in parentheses refer to items in the list of references at the end of this report.



PAH-73
534

FIGURE 7. - Percent Increase in Engine Diameter as a Function of Tetryl Charge (exclusive of detonator) and TNT Equivalence (inclusive of detonator).

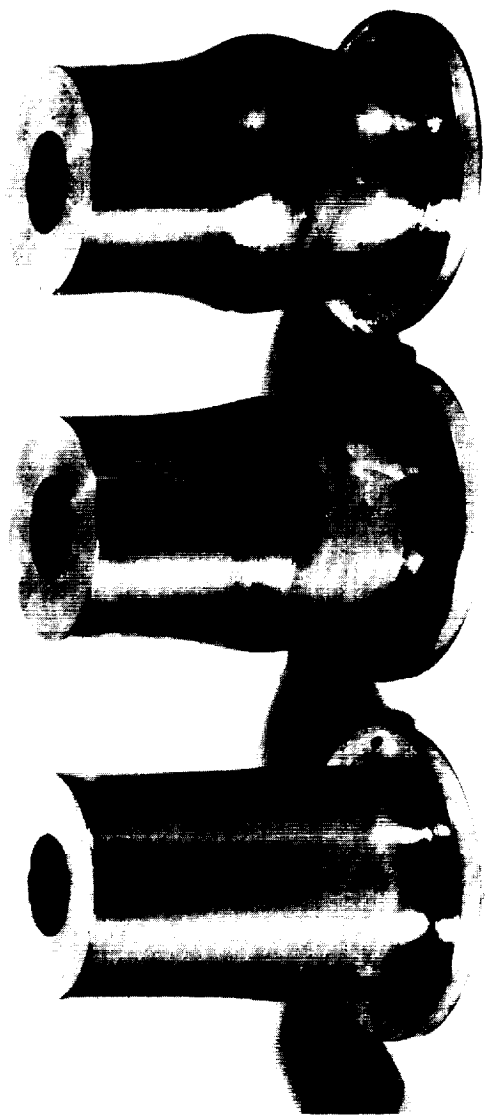


FIGURE 8. - Simulated Engine Deformation Resulting from the Explosion of 3.0, 6.0 and 7.5 g of Tetryl Located at the Center of the Engine.



FIGURE 9. - Cross Section of the Deformed Combustion Chamber Resulting from the Explosion of 7.5 g of Tetryl Located at the Center of the Combustion Chamber.

Furthermore, based on the yield strength of 347 SS of 2,000 to 8,000 atm, (30×10^3 to 120×10^3 psia) and utilizing Loving's empirical formula (2) which relates explosive pressures to vessel volume and weight of explosive, it is found that 0.73 to 2.91 g of TNT should be the minimum amount of this explosive capable of permanently deforming the MSC SS engines; that is, of surpassing the elastic limit (3) of the engine. When the results of this calculation are compared to the Bureau's extrapolated experimental results, as shown by the dashed section of curve in figure 7, it is apparent that Loving's formula does give realistic values for the minimum quantity of explosives that will cause permanent change, as it is in this charge range that permanent engine deformation first seems to occur.

Experiments 2, 4, and 5 (table 1) were conducted with 6 g of tetryl. In each experiment, the location of the charge was different; the purpose was to investigate the effect of charge location on damage. Figure 10 shows the effect on the engines from these shots. It can be seen that moving the charge off the axis of the motor has a pronounced effect on the resulting damage; the engine was actually ruptured when the charge was near the wall at mid-height. In general, the percent volume change for the mid-low (experiment 5) and mid-center (experiment 2) was not significantly different. The percentage change in volume for the mid-low shot was smaller than for the mid-center shot, but the corresponding change in maximum diameter was smaller, indicating that the contour of the deformed surface in the mid-low test is more sharply tapered, apparently due to the restraining effect of the flange near the deformed area.

Since explosives close to the wall are more damaging, it seems that accumulation of potential explosives on the engine walls should certainly be avoided.

Impulse Measurements

In these experiments, the ballistic mortar was used to measure the impulse delivered to the RCS engine mounting when an explosive reaction occurred within the engine. In order to avoid the possibility of deformation of the engine, a thick-walled facsimile RCS engine was machined from cold rolled steel so as to fit snugly in the mortar from which its own firing chamber had been removed. The projectile normally used in the ballistic mortar tests was not needed in these series of tests, since the purpose was to measure the thrust imparted to the mortar by both the explosion products escaping from the engine and the blast wave reflected from the engine's injector face. Three, six, and nine g of tetryl were used in the experiments as the explosive charge. The tetryl pellets were glued to the top of a No. 8 detonator and this assembly was positioned inside the engine. Figure 11 shows a detailed drawing of the engine used in these tests. In the experiments, the vertical lift of the mortar was measured, and a simple calculation converted the vertical lift of the mortar to total impulse. The results of this calculation are shown in figure 12 where the weight of the explosive charge, including the detonator, expressed in equivalent weight of TNT is plotted against the total impulse. Since only a single experiment was conducted at each of these data points, the extent of experimental error is not known.

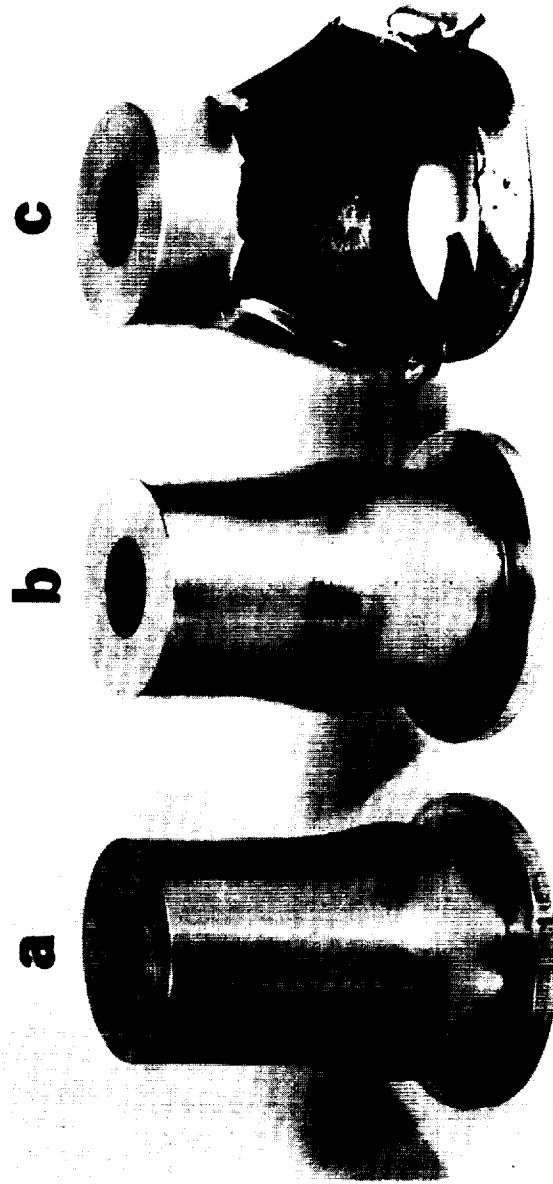
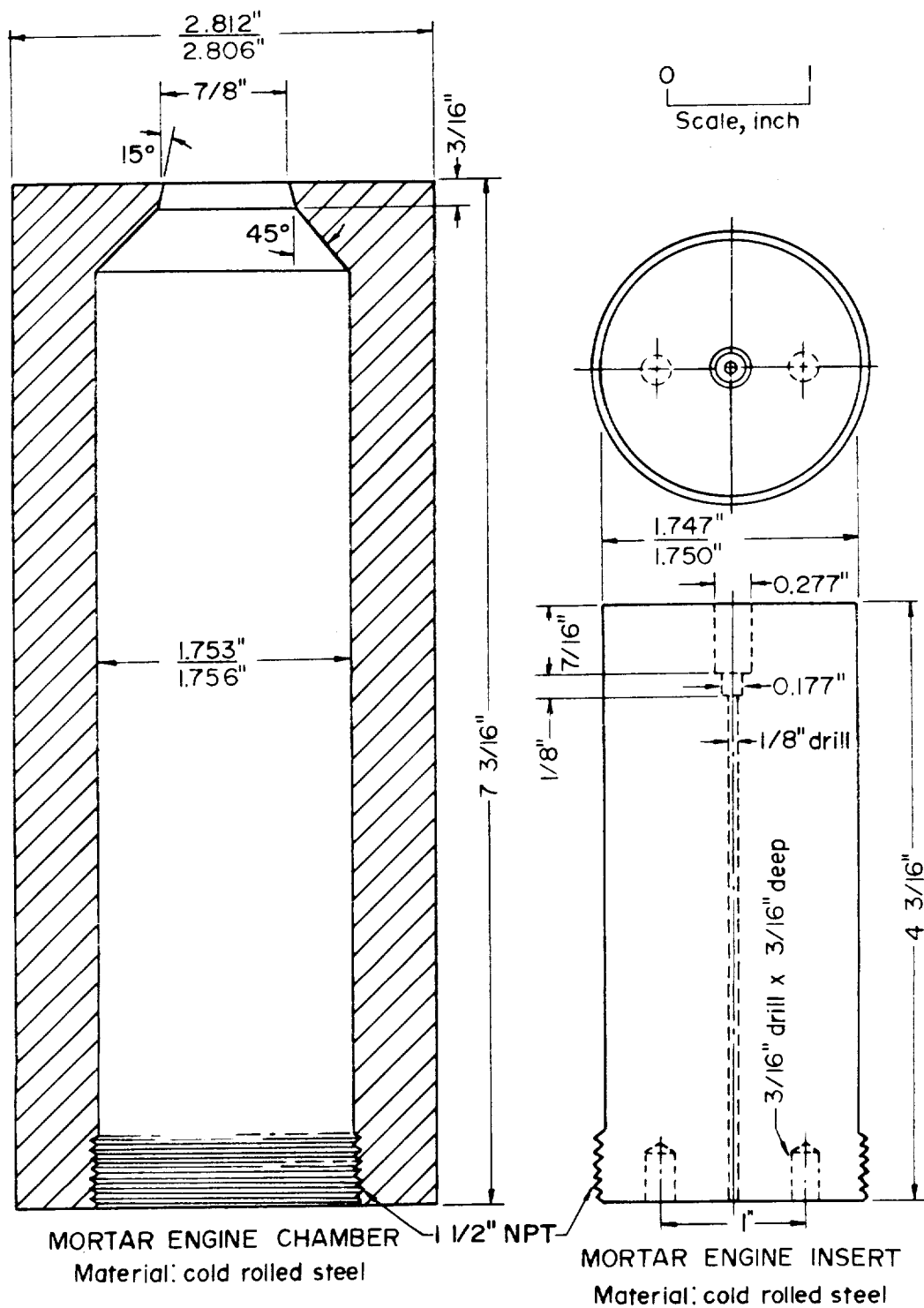


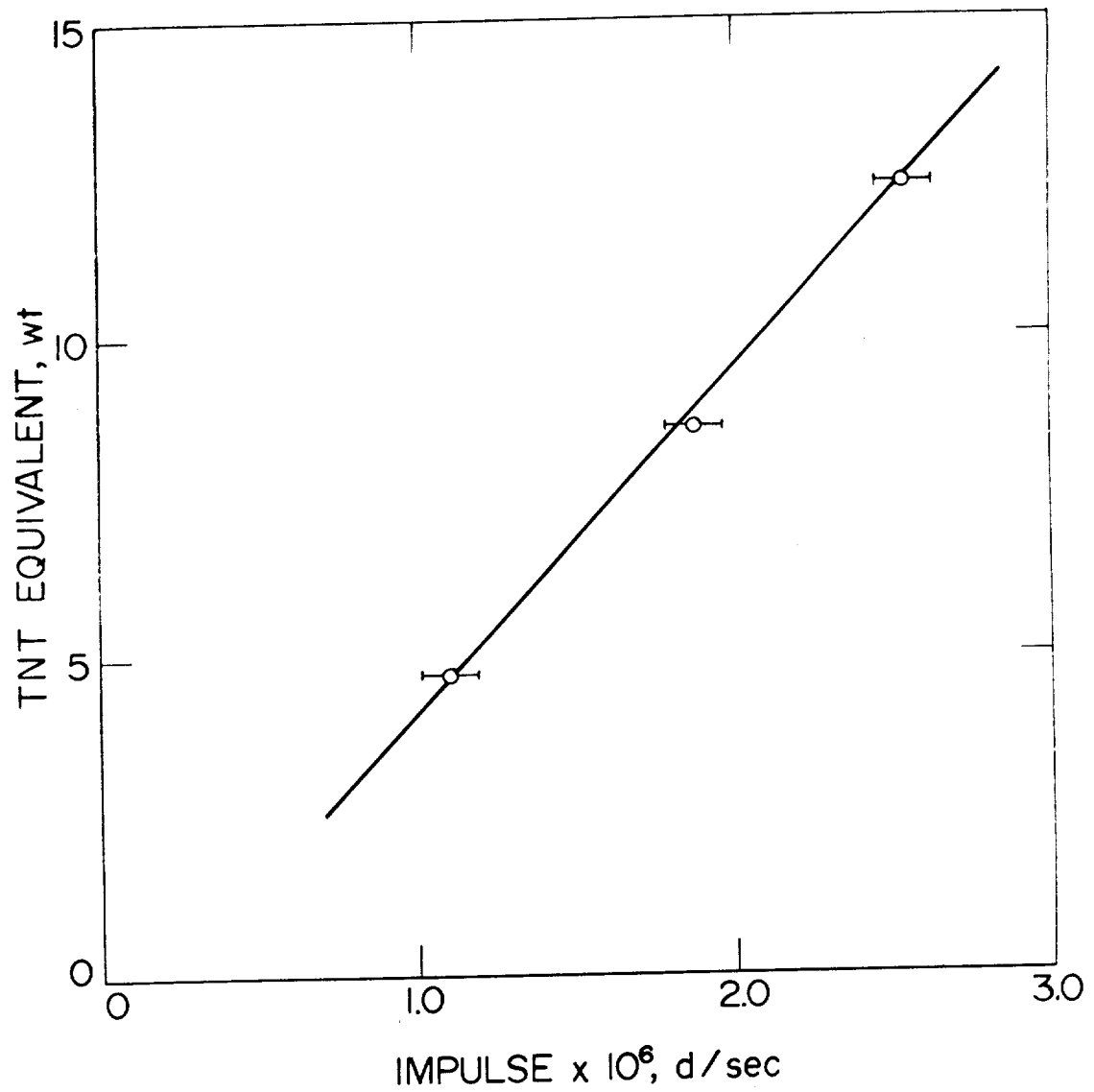
FIGURE 10. - Deformed Simulated Engines Resulting from the Explosion of 6 g of Teteryl
Fired in an Air Environment with the Charge Located (a) on the Engine's
Axis Near the Injector; (b) at the Engine's Center, and
(c) at Mid-height Near the Engine Wall.



PM-73
531

FIGURE 11. - Scaled Drawing of the Simulated Mortar Engine.

An explosion in the reaction chamber of the rocket engine generates a blast wave (except under vacuum conditions), one part of which travels out of the rocket nozzle while another part is reflected off the injector face. Since the blast wave striking the injector imparts a forward motion to the engine while the part of the blast wave leaving the nozzle contributes only a negligibly small rearward thrust, the blast wave per se contributes a net measurable forward thrust to the engine. As the blast waves continue to reflect from the engine's internal surfaces and interact with one another, the chamber pressure approaches a uniform value. It can be shown that the time necessary for pressure equalization in these chambers is of the order of 20 μ sec. When the pressure is equalized, the hot compressed product gases escaping from the nozzle provide an added thrust. This thrust has been calculated using Rodean's transient rocket thrust equations (4). For a gas product chamber temperature of 3,000° K, Rodean's equation shows that the chamber pressure drops 90 pct of its initial value within 0.5 msec. Therefore, pressure equalization is approximately 25 times faster than the product gas exhaust process; this difference in time justifies the partitioning of the engine thrust into these two segments. To calculate the thrust imparted to the engine by escaping product gases, it is necessary to know the initial pressure in the combustion chamber following pressure equalization. This was obtained from ballistic mortar experiments. Utilizing results from tests conducted by the Bureau for the purpose of calibrating the mortar with TNT and additional necessary information, an initial effective explosion pressure of about 340 atm is obtained for the explosion of 9 g tetryl in the rocket engine. Using this value for the initial explosion product gas pressure and Rodean's (4) transient thrust relations, the impulse due to the escape of the combustion product gases is approximately 200 g-sec. Since the experimental value given in figure 12 shows that the measured total impulse is approximately 2,720 g-sec (or 2.6×10^6 dyne-sec) for 9 g of tetryl, the difference between these two values, 2,520 g-sec, is apparently due to the reflection of the blast wave from the injector face.



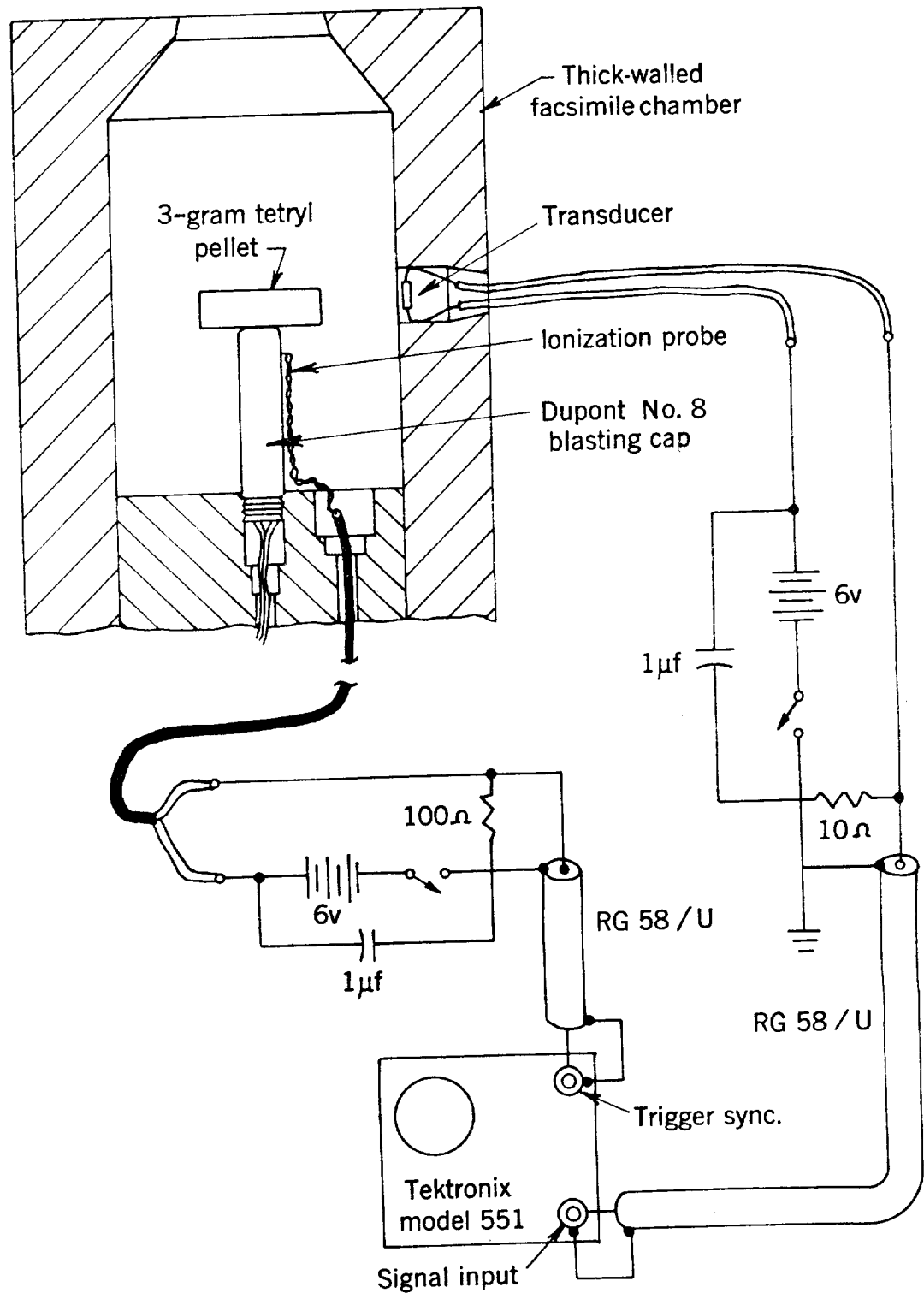
R64-73
533

FIGURE 12. - Impulse Resulting from the Explosion of Various Amounts of Tetryl Fired in the Simulated Mortar Engine.

Explosion Pressure

The same thick-walled facsimile engines that were used to measure the total impulse also were used in the experiments in which explosion pressures in the engine were measured. Figure 13 shows a drawing of the thick-walled engine, modified to include a high pressure resistive transducer. The transducer itself is depicted in figure 14. Although the rise time of this transducer is believed to be of the order of magnitude of the time required for the shock wave to transverse the diameter of the resistor, the initial pressure peak measured represents usable information.

These experiments were conducted in very much the same manner as the engine deformation experiments described previously. Two camera-equipped oscilloscopes recorded the transducer signals. In these experiments, the explosive charge was positioned in the middle of the engine chambers, directly opposite the flush-mounted pressure transducer. Three, six, and nine grams of tetryl were fired with a No. 8 detonator. Figure 15 shows an oscilloscope record of the transducer output for one of the 9-g shots. Since only the first peak shock pressure in the oscillograms represented usable information, the remaining portion of each has been ignored. Table 2 gives the measured peak reflected shock pressures obtained from such oscillograms for the various shots (the confidence intervals represent 90 pct values). Also shown in this table are effective design pressures obtained from Loving's empirical formula (2). It is not surprising that Loving's effective pressure values are lower than the peak shock pressures, which vary between 6,000 and 9,000 atm for the various explosive charges, as the relative magnitude of these two values depends on the duration of the pressure load and the mechanical response of the chamber wall. It would appear that Loving's relation gives reasonably conservative values for the explosion pressures developed within these engines. Furthermore, it is assumed, as shown in the section titled "Impulse Measurements," that the blast wave from the explosion of 9 g of tetryl accounts for 2,520 g-sec (2.47×10^6 dyne-sec) of impulse. Using this value and an average peak pressure of 3,400 atm, the effective duration of the blast wave is about 100 μ sec, not an unreasonable value.



PX3-103
553

FIGURE 13. - Electronic Circuitry Used in Conjunction with the Resistor Pressure Transducer for Recording Explosion Pressures.

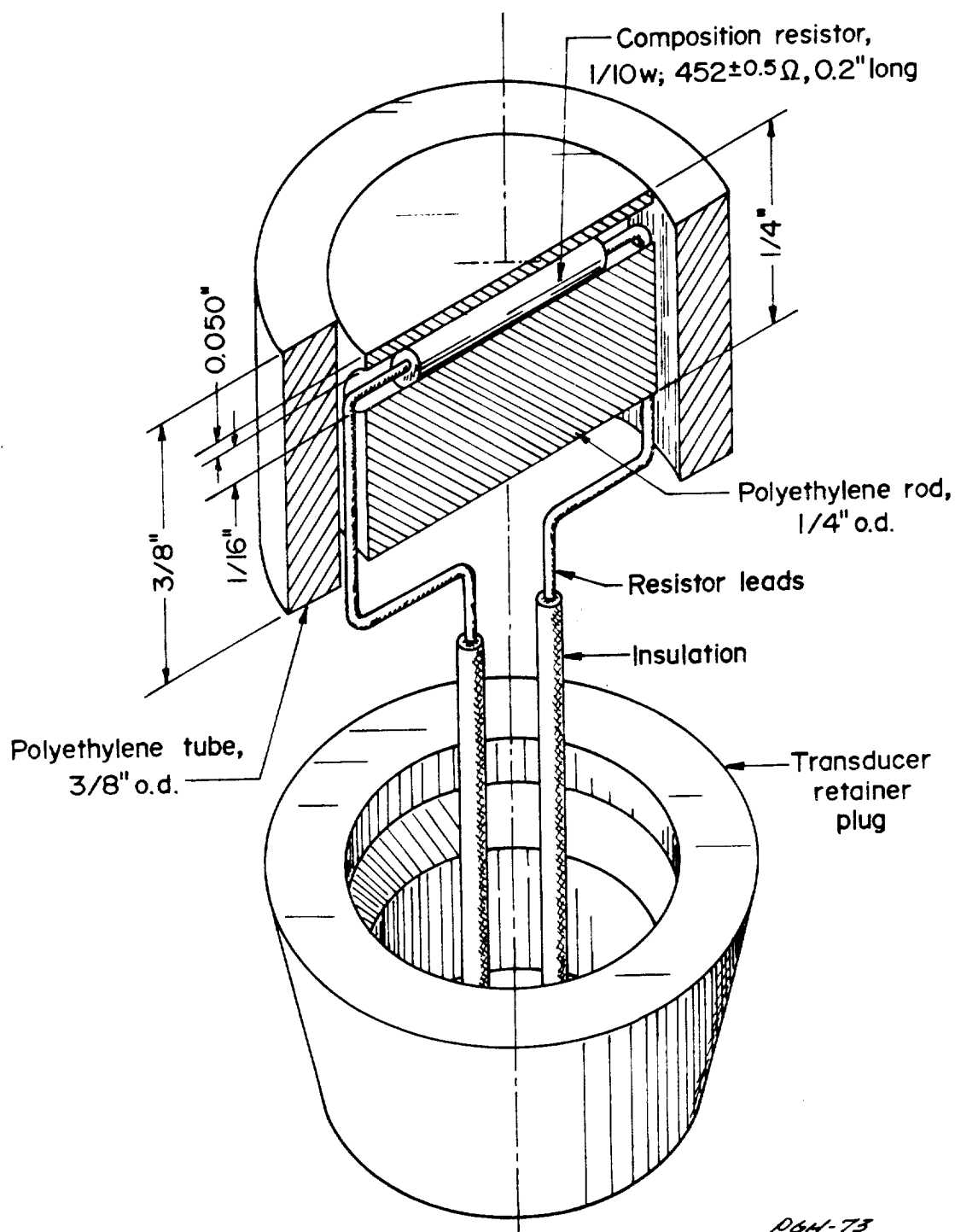


FIGURE 14. - Resistor Pressure Transducer Used for Recording Peak Explosion Pressures at the Chamber Wall.

DGH-73
523

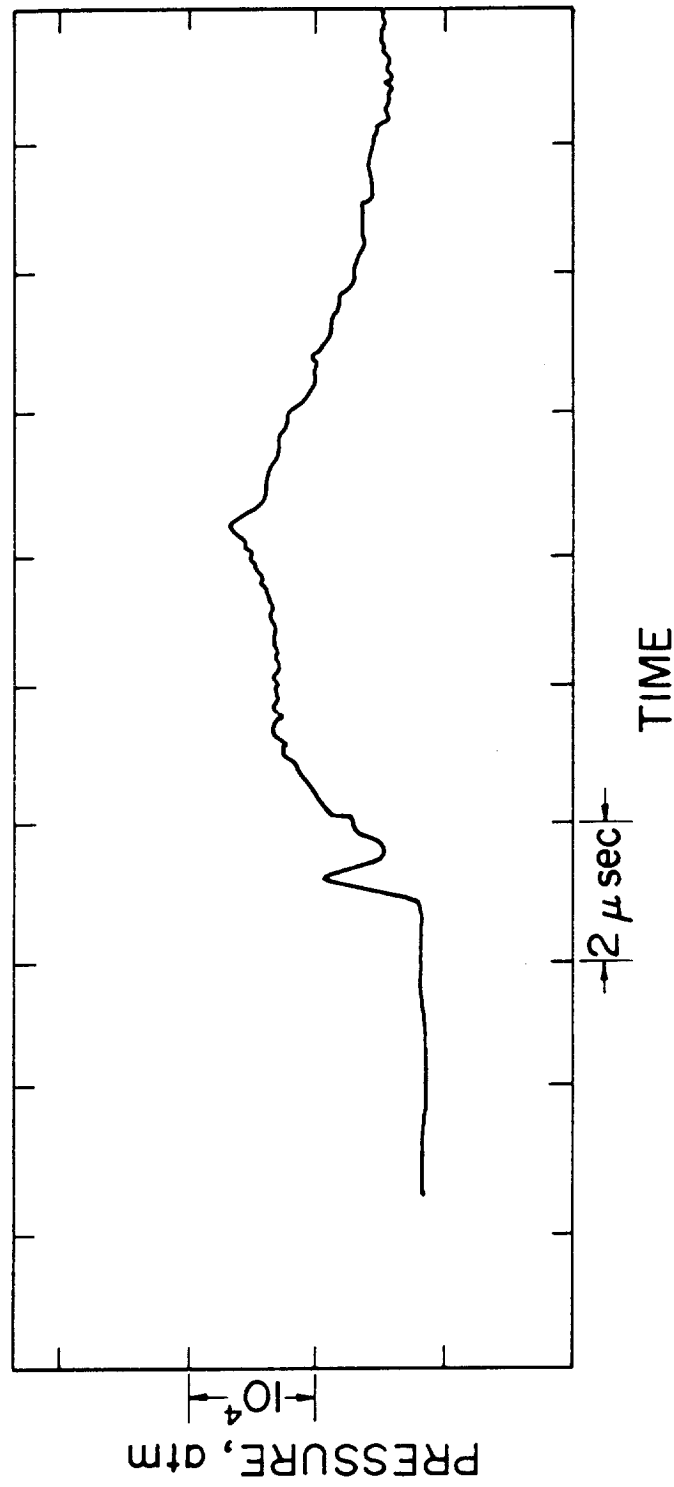


FIGURE 15. - Resistor Pressure Transducer Record Obtained at the Wall Opposite a 9-g Tetryl Charge Located at the Chamber's Mid-Center Position.

TABLE 2. - Peak shock pressures resulting from the explosion of various weights of tetryl located at the center of the combustion chamber and striking the wall adjacent to the charge center

Tetryl charge weight, g	<u>1</u> /Total charge weight, equiv. TNT, g	Number of trials	Peak reflected shock pressure, ($\times 10^3$ atm)	<u>2</u> /Effective design pressure, ($\times 10^3$ atm)
3	4.75	6	5.8 \pm 0.9	2.4
6	8.59	3	6.9 \pm 2.1	4.8
9	12.43	2	8.8 \pm 1.3	7.2

- 1/ Combined weight of tetryl pellet and No. 8 detonator expressed in TNT equivalent weight. The TNT equivalent weight of the No. 8 Du Pont detonator was calculated to be approximately 0.91 g. The TNT equivalent percent of tetryl is 128.
- 2/ Calculated from Loving's (2) equation assuming a value of $K = 2 \times 10^4$.

Set II. Destruct Experiments

SS Engine Fragmentation Experiments

In addition to the SS engine deformation experiments, preliminary SS engine fragmentation experiments also were conducted. The engines, loaded with tetryl and detonators, were placed inside a circular barricade of wax blocks used to measure fragment velocities, via amount of penetration into wax.

In the first experiment, a tetryl charge of 23.3 g (1.9 cm in diameter and 5.1 cm long) was fired with a No. 8 detonator. In the second experiment, the tetryl charge weighed 10.5 g (1.3 cm in diameter and 5.1 cm long). Due to the length of the tetryl explosive charge, only 0.95 cm of the detonator's length extended into the chamber. The charges were centrally located.

A third experiment was designed to simulate the damage (deformation) incurred by an engine explosion at MSC, Houston, Tex., mentioned previously (1). On the basis of results discussed in the engine deformation section, measurements from the MSC engine, and the results in figure 7, a cylindrical, centrally located, tetryl charge, 0.95 cm in diameter by 5.1 cm long, and weighing 7.3 g was used.

The engine that was fired with the 23.3-g charge shattered into many pieces. Sixty-five pieces were recovered on the floor outside the circular wax barricade, on the floor inside the barricade, and in the wax blocks themselves. The two largest segments were the nozzle section weighing 160 g, and the flange section weighing approximately 100 g.

The total recovered fragment weight distribution is given in table 3. The fragment penetration in the wax blocks is given in table 4. The total weight recovered was 449.6 g. The average weight of these engines is 458.6 g. Thus, recovery was nearly complete.

TABLE 3. - Fragment weight distribution

Fragment weight range, g	Number of fragments	Total weight of fragments, g	Percent of the total weight
<0.1	19	0.12	0.03
0.1-1.0	10	3.54	.79
1.0-5.0	21	63.13	14.04
5.0-10.0	9	61.32	13.64
10.0-100.0	4	53.24	11.84
>100	2	268.25	59.66

TABLE 4. - Fragment penetration distribution in the
wax blocks

Fragment penetration range, cm	Number of fragments	Percent of fragments
<0.32	17	41.4
0.32-1.27	5	12.2
1.27-2.54	4	9.7
2.54-5.08	2	4.9
5.08-7.62	8	19.5
>7.62	5	12.2

Due to the configuration of the SS engine with flange and thick-wall nozzle area, these two areas did not break into many segments. It is only the central portion of the engine that broke into segments ranging in weight from less than 1 g to 100 g. A large number of the fragments (75 pct) weighed less than 5 g, while 85 pct of the weight consisted of fragments heavier than 5 g. Most of the fragments possessed enough energy to move a distance of up to 185 cm (the distance to the farthest wall), or to traverse at least 10 cm of wax.

The engine, which was charged with 10.5 g of tetryl, was broken into few fragments, indicating that this weight of tetryl is just sufficient to break a SS engine of this design. Only three large fragments were recovered; their combined weight was 468.3 g (393.3, 52.4, and 22.6 g), essentially a complete recovery. The major part of the engine remained in the retaining flange used in these experiments (fig. 6).

The deformation produced in the third engine was very similar to that of the SS engine deformed at MSC (1). The engine diameter increased 17 pct in the Bureau test; a corresponding increase of 18 pct was found in the MSC engine. A pressure record obtained from this last engine is shown in figure 16.

The weights of tetryl used in the two panel-engine destruct experiments described in the next section, were selected on the basis of these test results.

Panel-Engine Destruct Experiments

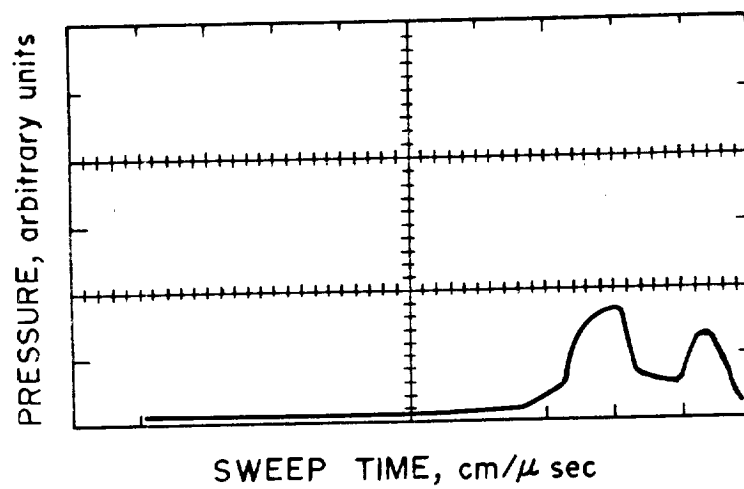
With the results obtained from both the engine deformation and engine destruct experiments, explosive charge sizes were selected to fragment the molybdenum engines into appropriate fragment size distributions. The chosen charge sizes were used in the two succeeding experiments to determine the extent of damage to the panel from an engine explosion.

The specific section of the module used was the Apollo AFRM 001 Service Module Reaction Control System Panel B, fabricated of honey-combed aluminum; it houses a helium pressure vessel and associated feed lines and electrical lines.

In actual Apollo tests, four engines, 90 deg apart, are mounted on the outside of the module. For the Bureau tests only one molybdenum engine at a time was exploded. Two panels were used, each with a single molybdenum engine. The molybdenum engines with the diffuser removed were loaded with tetryl and detonated with a No. 8 detonator.

Since the resultant fragments were needed for analysis, those which traveled away from the panel were collected in a semicircle of paraffin blocks stacked in five sections three layers deep. The depth of penetration of the fragments in the wax could be used to calculate the energy and velocity of the resultant fragments. The paraffin barricade was supported firmly in place, so as not to be moved by the impact of the flying fragments hitting it. A sheet metal barricade, 0.08 cm thick, was placed 30 cm back of the panel to stop any particles which penetrated the panel.

For the first panel, a tetryl charge of 23.3 g (1.9 cm in diameter and 5.1 cm long) was placed in the center of the engine with the aid of a spacer. The tetryl explosive charge for the second panel weighed 7.3 g (5.1 cm long and 0.95 cm in diameter). In this latter experiment, special timing grids were located in front and on either side of the engine for measuring the fragment velocities. Figure 17 shows the test setup which was similar for the two experiments with the panels.



PGH-73
525

FIGURE 16. - Resistor Pressure Transducer Record Obtained with
10.5 G Teteryl at the Center of the Engine.

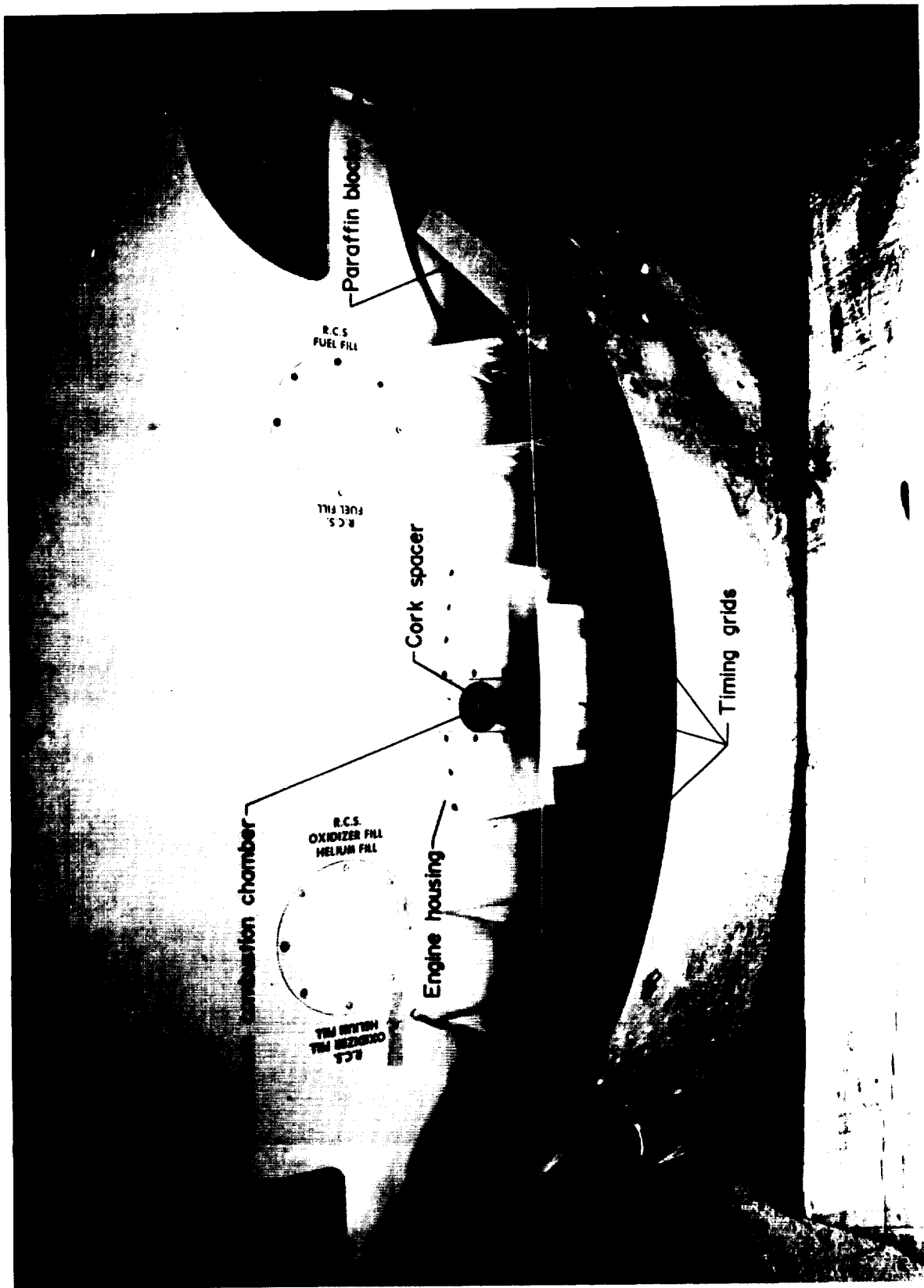


FIGURE 17. - Panel-Engine Destruct Test Assembly.

The molybdenum engine containing the 23.3 g of tetryl fragmented into hundreds of fragments. Almost 700 fragments of various sizes were recovered. Many others were embedded in the panel. The area of the panel, immediately adjacent to the engine mount, is covered with a cork pad. A cursory inspection of this area revealed no penetration marks, but more careful inspection of the module with the cork pad removed showed that a large number of small fragments penetrated the aluminum skin. A few fragments penetrated the panel; numerous fragment holes and spalling effects could be noted on the back of the panel. The helium pressure tank, at the upper portion of the panel, was not affected. One fragment passed through the module with enough energy to produce a deep indentation in the sheet metal behind the panel back. Detailed photographs of the results of the first panel test are not available, but photographs of the second panel test show the same general picture (fig. 18 and 19). The interior of the panel was not inspected. The damage to fuel lines, electrical connectors and cables, and other parts appeared to be minor.

Tables 5 and 6 contain the weight range and penetration into the wax blocks of the recovered fragments from the molybdenum engine used in panel shot No. 1.

TABLE 5. - Fragment weight distribution,
panel shot No. 1

Fragment weight range, g	Number of fragments	Total weight of fragments, g	Percent of total weight
<0.1	416	7.73	3.0
0.1-1.0	201	91.82	35.9
1.0-5.0	73	137.01	53.5
5.0-10.0	3	19.47	7.6

TABLE 6. - Fragment penetration in the wax blocks,
panel shot No. 1

Fragment penetration range, cm	Number of fragments	Percent of total particles
<0.3	<u>1</u> /368	69.6
0.3-1.2	17	3.2
1.2-2.5	16	3.0
2.5-5.0	57	10.8
5.0-7.5	52	9.8
>7.5	19	3.6

1/Includes surface particles.

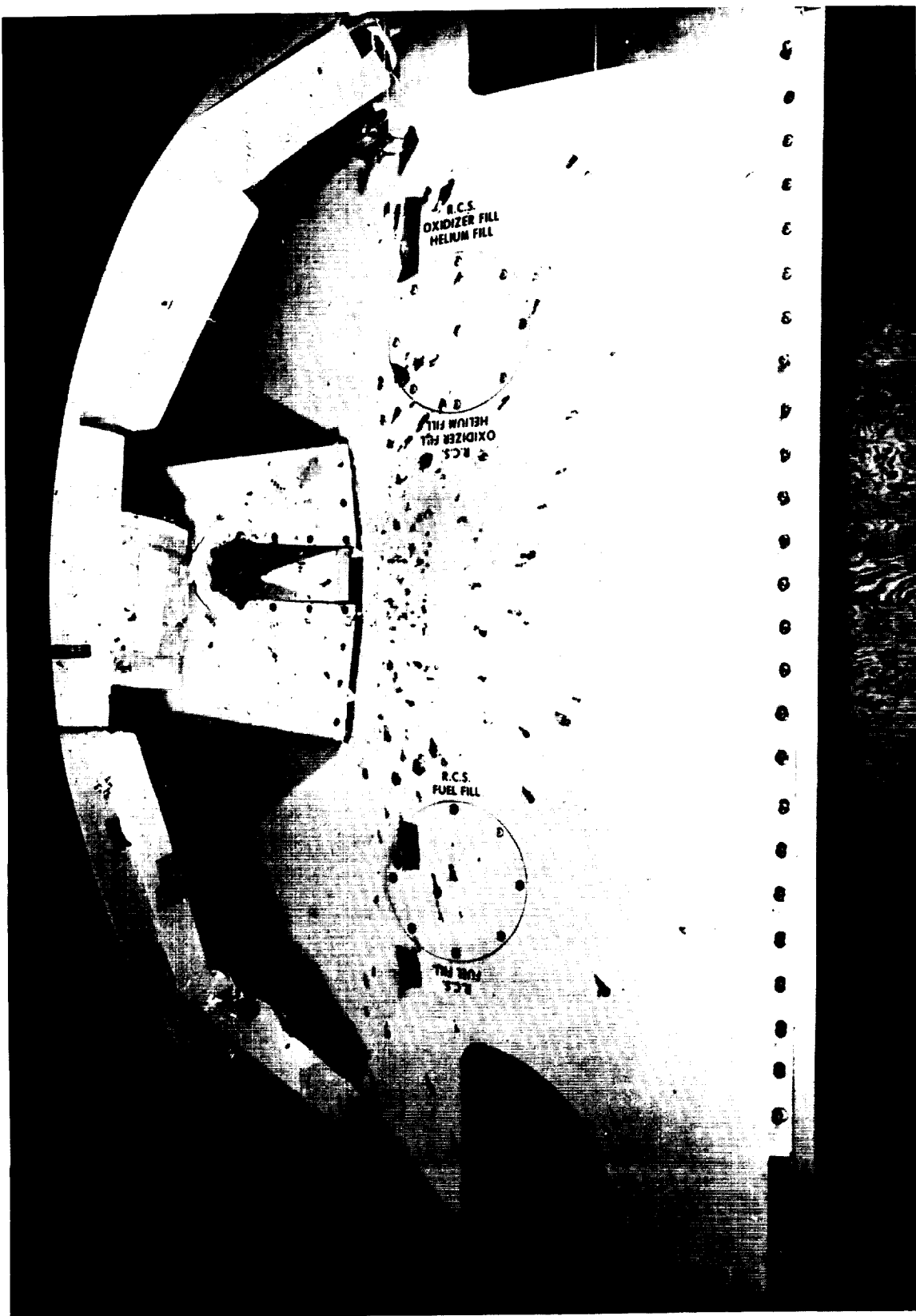


FIGURE 18. - Resultant Damage to the Outer Surface of the RCS Panel by the Explosively Destroyed Molybdenum Combustion Chamber.

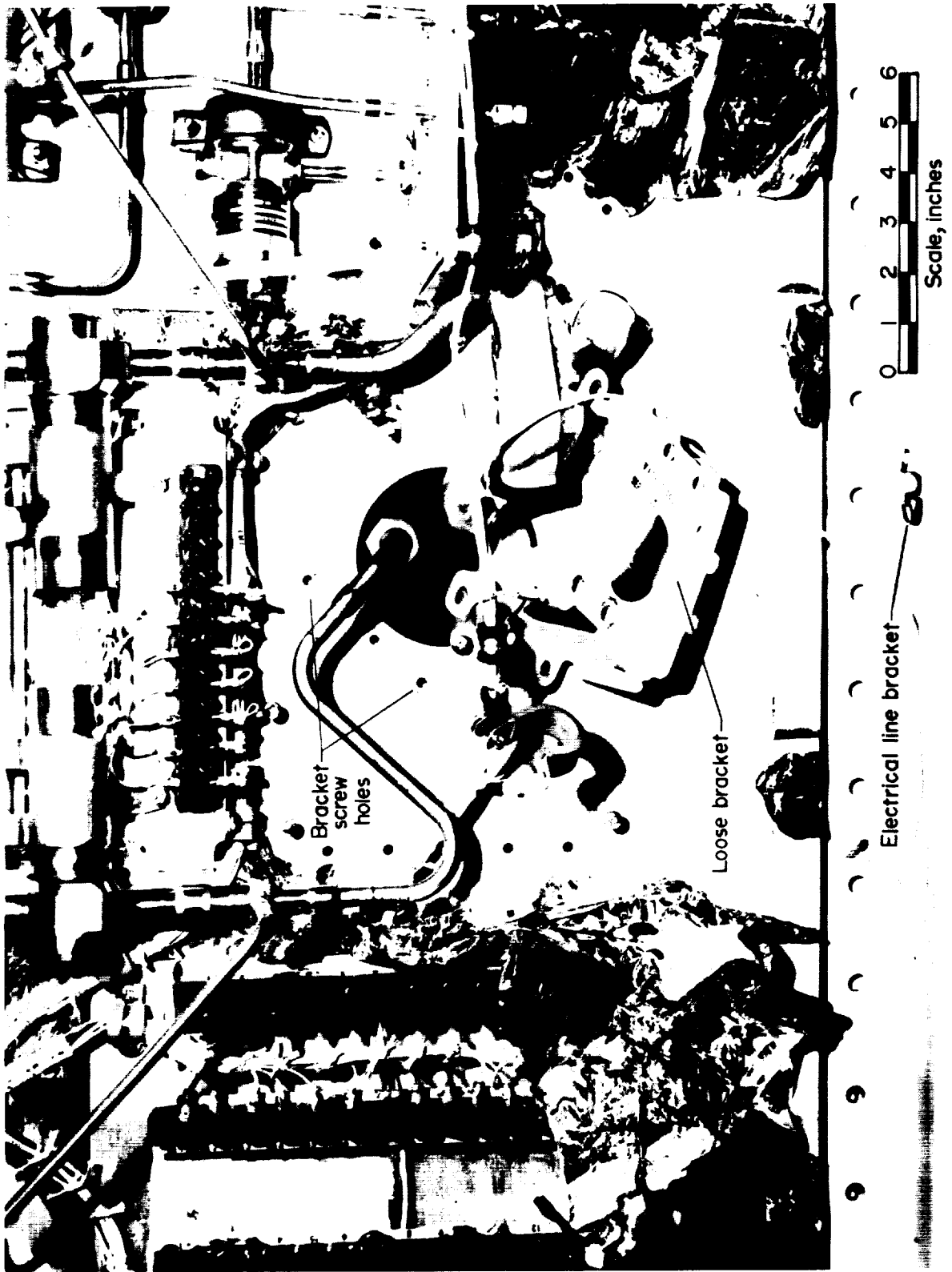


FIGURE 19. - Resultant Damage to Inner RCS Panel

In the second panel shot, in which 7.3 g of tetryl were used, the molybdenum engine was also completely fragmented by the explosion. The recovered fragments and parts, exclusive of those embedded in the panel, are shown in figure 20. The holding ring was broken into large segments at the six holding ring bolt positions, and the holding ring bolts had sheared. The blank injector face was bowed inward by the downward force of the detonation, and the injector face was pushed down into its housing. The cork insulation in the vicinity of the engine mounting was cracked. The cork insulation just above the side of the engine housing was perforated by fragments, but no visible penetration of the honeycombed aluminum panel was evident from the rear of the panel. Figure 19 shows that the back of the panel (inner section) was only slightly damaged; three screws holding a bracket over the tank feed line hole were sheared. The bolts of one of the electrical line brackets were sheared. None of the panel components were removed or inspected for hidden damage; the panel was returned to MSC for their inspection.

The molybdenum engine weighed 470 g before the experiment, and 309 g (66 pct) were recovered as fragments exclusive of those embedded in the panel. A total of 433 fragments were recovered for an average fragment weight of about 0.7 g. Table 7 gives a more detailed description of the recovered fragments.

TABLE 7. - Distribution of total fragment weight and number as a function of engine component

Molybdenum engine component	Total number of fragments recovered	Total weight recovered, g	Average weight per fragment, g
Engine base ring...	20	55.46	2.76
Engine body.....	371	206.00	0.55
Engine diffuser....	42	47.70	1.14

The velocity of fragments that lodged in the paraffin blocks can be calculated with the aid of the following equation:

$$v_t^2 = v_o^2 e^{-\left(\frac{\sigma_t \cdot A_f \cdot d}{M_f}\right)} + \frac{2K}{\sigma_t} \left[e^{-\left(\frac{\sigma_t \cdot A_f \cdot d}{M_f}\right)} - 1 \right] \quad [1]$$

where

σ_t = target density, g/cm³

A_f = fragment cross section, cm²

M_f = fragment mass, g

d = fragment penetration depth, cm

K = target penetration strength coefficient, (cm/sec)² (g/cm)³

V_o = initial fragment velocity, cm/sec

V_t = fragment velocity in target, cm/sec

e = base of natural logarithm

A representative sample of 24 fragments was selected from those that penetrated into the paraffin.

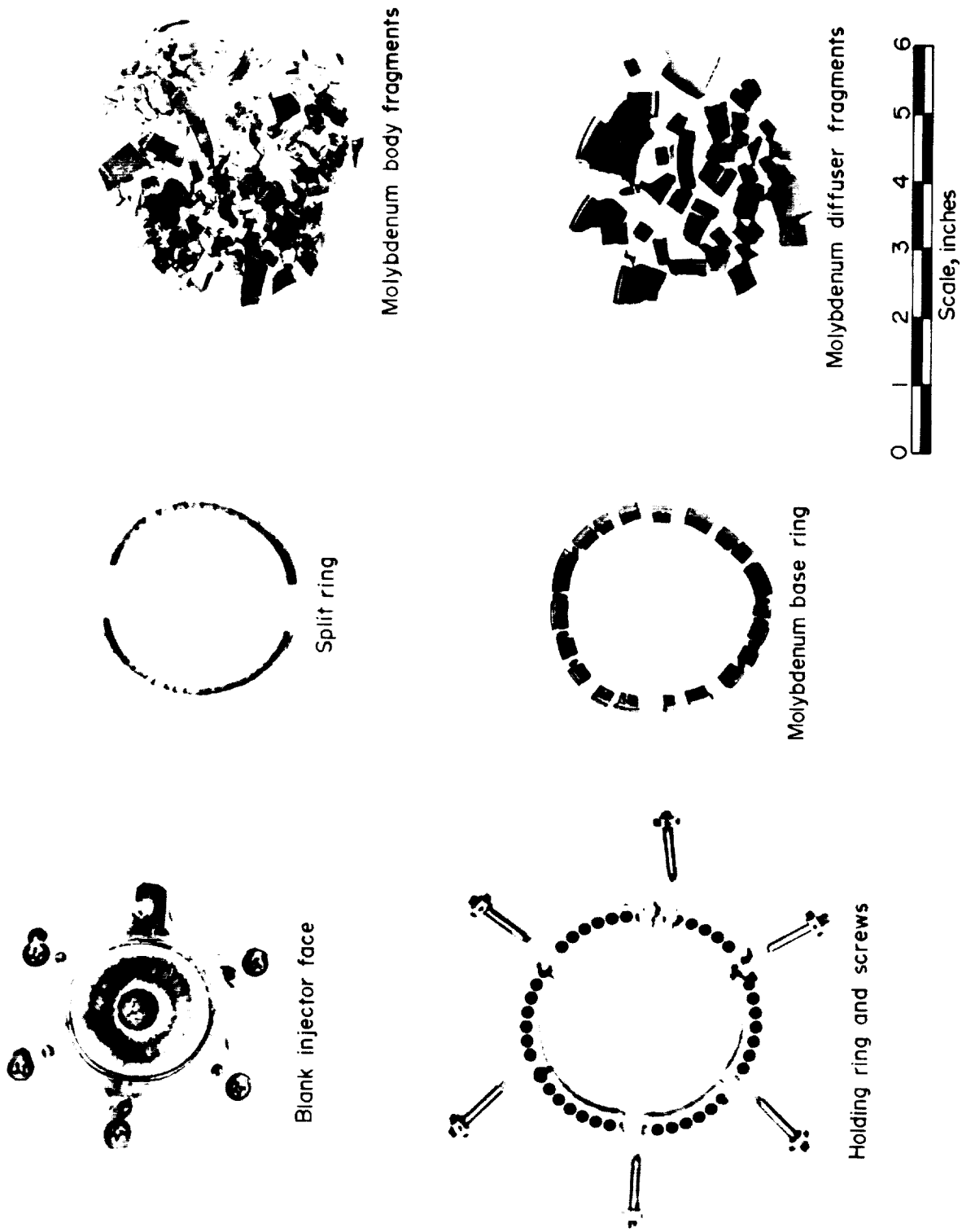


FIGURE 20. - Recovered Molybdenum Combustion Chamber

The initial fragment velocity, V_0 , is obtained from this relation by setting the fragment velocity in the target, V_t , equal to zero and inserting in the above equation the experimentally obtained values of the fragment's mass, cross section, and depth of penetration in the paraffin. A value of 0.9 gm/cm^3 was used for the target density (paraffin wax). The target penetration coefficient, K , experimentally determined by measuring the penetration depth into the wax of projectiles with known initial velocity, was found to be $2.78 \times 10^8 (\text{cm/sec})^2 \cdot (\text{g/cm}^3)$. Substituting these values into equation 1 yields:

$$V_0 = 2.48 \times 10^4 (e^{-\tau} - 1)^{1/2} \quad [2]$$

$$\text{where} \quad \tau = \frac{\sigma_t \cdot A_f \cdot d}{M_f} \quad [3]$$

Equation 2 was used to calculate the average initial fragment velocity for the representative sample of 24 fragments from the 7.3-g charge; the velocity calculated was 130 m/sec.

The highest and lowest calculated fragment velocities were 207 and 50 m/sec, respectively. No information was obtained from the fragment velocity grids due to equipment malfunction.

As expected, the damage to the second RCS panel from the explosion of 7.3 g of tetryl in a molybdenum engine was not as severe as in the first experiment using 23.3 g of tetryl. Velocity estimates in the first experiment gave fragment velocities of the order of 460 m/sec while the second experiment indicated average fragment velocities of 130 m/sec. This suggests a direct proportionality between charge size and fragment velocity. From the results of the panel damage obtained in the first experiment, it appears that about 23 g of tetryl (30 g of equivalent TNT) represents the minimum amount of explosive necessary for the resulting molybdenum fragments to penetrate the honeycombed aluminum panel. These latter experiments also suggest that there may be a preferred fragment trajectory angle relative to the panel normal, for fragment penetration of these honeycombed structures; however, this concept was not pursued.

Set III. Fragmentation Studies

Fragment-Kinematics

The Lunar Module (LM) vehicle has at least two areas that are vulnerable to fragment damage and to fragment penetration; these are the Vycor windows and the blanket cover (which serves as a meteorite and thermal shield). In order to prevent damage to these areas, a knowledge of the degree of vulnerability is a first requisite. This group of experiments was designed to answer some of the related questions.

As was mentioned earlier, the molybdenum engines were scarce and SS engines were used throughout this task, except for the two molybdenum engines at the beginning of the test series and for three molybdenum engines at the end of the test series. Although SS differs from molybdenum in many of its mechanical properties, it is as satisfactory as molybdenum for tests in which the fragment-kinematics, rather than the fragmentation phenomena itself, is of major interest.

Both molybdenum and SS engines were used in the experiments. The SS engines were identical to those used in the earlier engine deformation studies. These engines were quartered or halved lengthwise, and some of the sections were fitted with cylindrical blowout plugs, ranging in size from 0.32 to 2.54 cm in diameter. The sectioned engines were assembled prior to each experiment and sealed with silicone grease. The molybdenum engines were not sectioned. The sections and plugs provided fragments of known size and geometry; they were easier to study and results were more easily compared with theoretical values.

The experimental procedures described here were identical for both the molybdenum and SS engines. Figures 21 and 22 show photographs of the sectioned SS engines with the cylindrical SS plugs in place. Instead of using tetryl as the explosive charge, gas-phase explosions and thin layer detonations were utilized because they are more representative of the possible conditions during actual engine operation; thin layers of liquid containing potentially explosive material were found on the engine walls. For the gas-phase detonation, a stoichiometric ethylene-oxygen mixture was chosen. This system was chosen because it has been extensively studied and its detonation characteristics are well known. The stoichiometric ethylene-oxygen detonation has a maximum detonation pressure of approximately 34 atm, a velocity of 2.2 mm/ μ sec, and a constant volume combustion pressure of 16.1 atm. An exploding wire ignition source was selected, primarily to insure creation of a stable detonation within a fraction of a millimeter of the wire's surface. A high-speed (6,000 frames/sec) camera recorded the events during and immediately following the explosion. Two copper tubes (0.32-cm-id) served both as purge lines for the gas and as electrodes for the exploding copper wire. The engine was placed on a thick plastic base through which the copper tubes extended into the engine, and in which was mounted a Kistler⁷ pressure transducer, flush with the base, and centered between the two tubes. The gases were mixed prior to entering the engine.

The open top of the engine was covered with aluminum foil coated with silicone grease. The engine was gently purged with the gas mixture, using a quantity of gas equal to approximately 20 times the engine volume, to assure removal of air. At this time, the flow of gas was stopped and the wire was exploded.

⁷See footnote 3 on page 7.

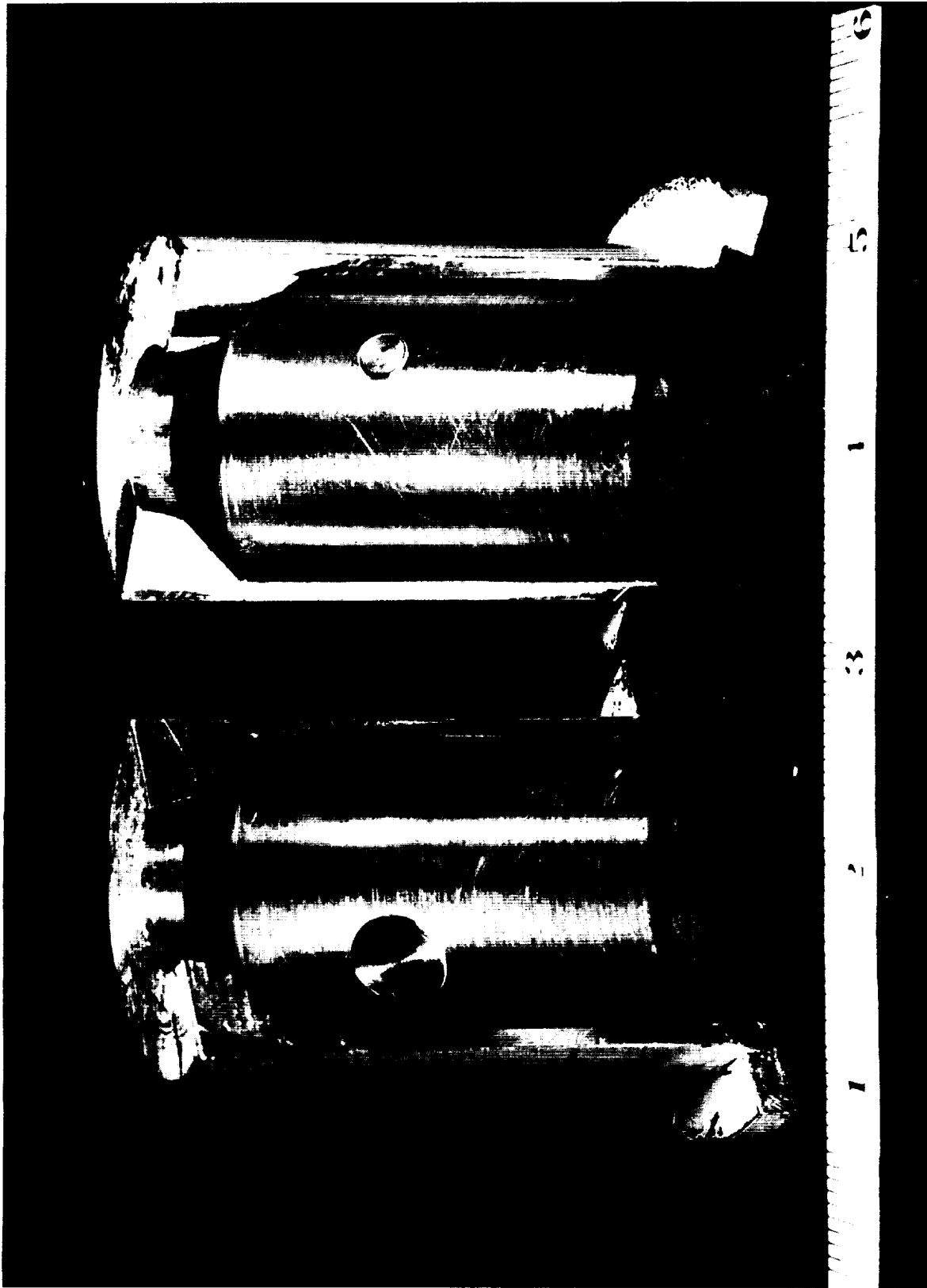


FIGURE 21. - Stainless Steel Engine Halves Containing 1.3- and 0.6-cm Diam Blowout Plugs.

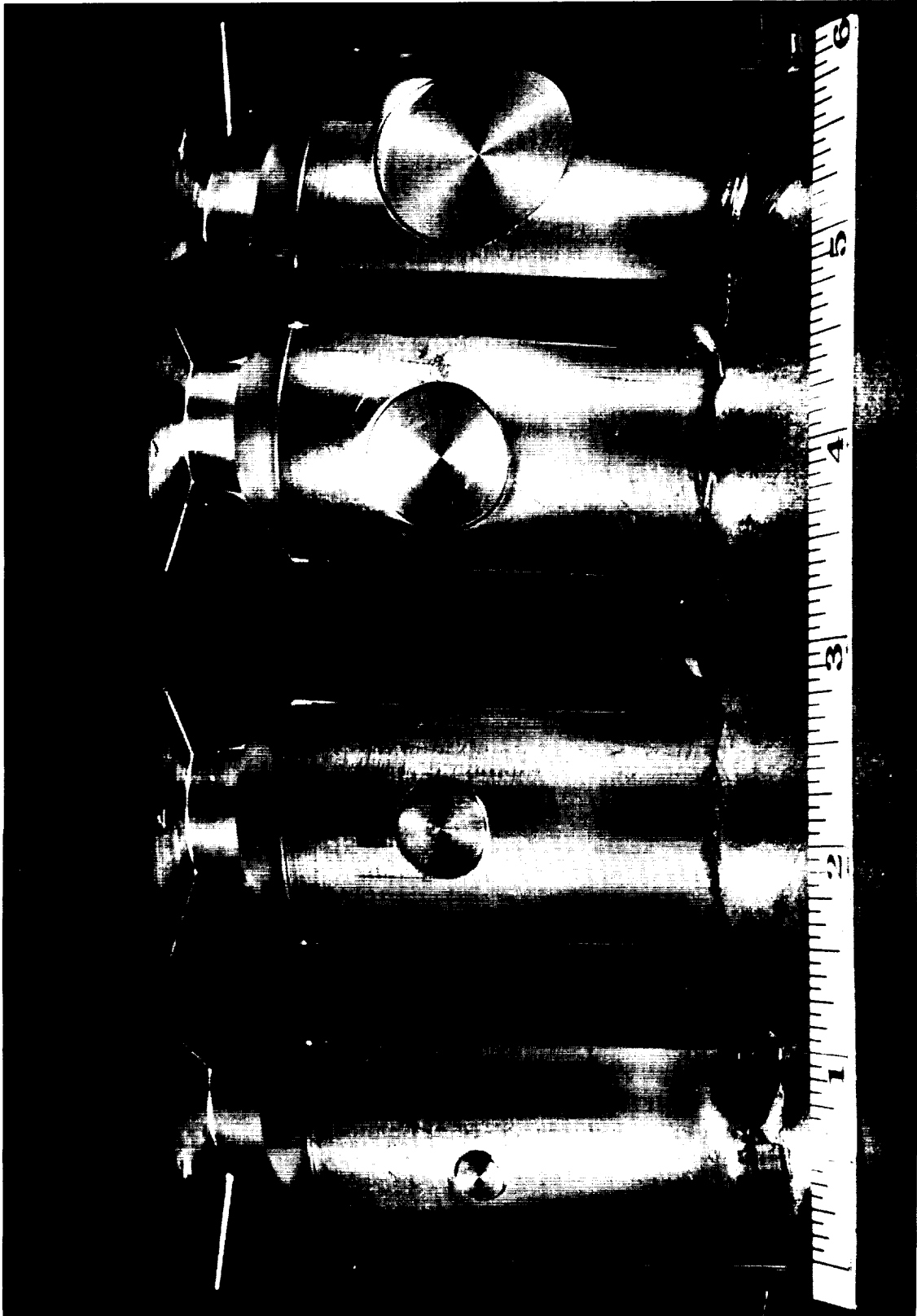


FIGURE 22. - Quartered Stainless Steel Engines Containing 0.6-, 1.3-, 1.9- and 2.5-cm-diam Blowout Plugs.

This same experimental setup also was used in the experiments in which the source of explosion was a thin layer detonation, except that the copper tubes and exploding wires were not required. The pressure transducer also was not used since the pressures generated in these experiments could seriously damage the sensing unit. Two explosive systems were used. The first consisted of lens tissue having an average thickness of 2.5 mils, wetted with various amounts of a 50:50 NG-EGDN solution. A cellulose wick was prepared of the same lens tissue and wetted with the same solution. The wick was placed in contact with the lens paper covering the inside walls of the engine, and the composite was detonated by a length of Primacord initiated by a detonator. Figure 23 shows the setup complete with explosive train.

The weight of lens paper used inside the engine and in the portion of the wick extended into the engine was kept constant, so that its contribution and that of the solution which wetted the wick could be assessed; the amount of the NG-EGDN to wet the lens paper inside the engine was carefully weighed.

After the wetted tissue was applied to the walls of the engine section, the engine was assembled. A Fastax⁸ camera recorded the trajectories of the fragments.

A few experiments were conducted, but it proved difficult to reproduce the exact amount of explosive contained in these films, and the technique was abandoned. Still, the data obtained from the experiments was useful and is included in the results. The new explosive system chosen was Primacord. The Primacord, 0.32 cm in diameter, and containing approximately 86.4 mg of pentaerythritol tetranitrate (PETN) per 10 cm was coiled down the wall of an engine segment and secured with cellulose acetate cement. A 20-cm portion extended out the throat and was initiated with a No. 8 detonator. This system proved quite satisfactory.

The assembly used to clamp the molybdenum engine in place was the same as the one used to clamp the SS engines and is shown in figure 6. The side of the engine covered with explosive was painted with aluminum paint for identification after the shot. A 0.63-cm thick, cold-rolled steel plate, and a wax slab, 5-cm thick, were positioned on either side of the molybdenum engines, and approximately 30 cm away. These materials were used to obtain information concerning the effects of the molybdenum fragments on impacting hard and soft surfaces.

⁸See footnote 3 on page 7.

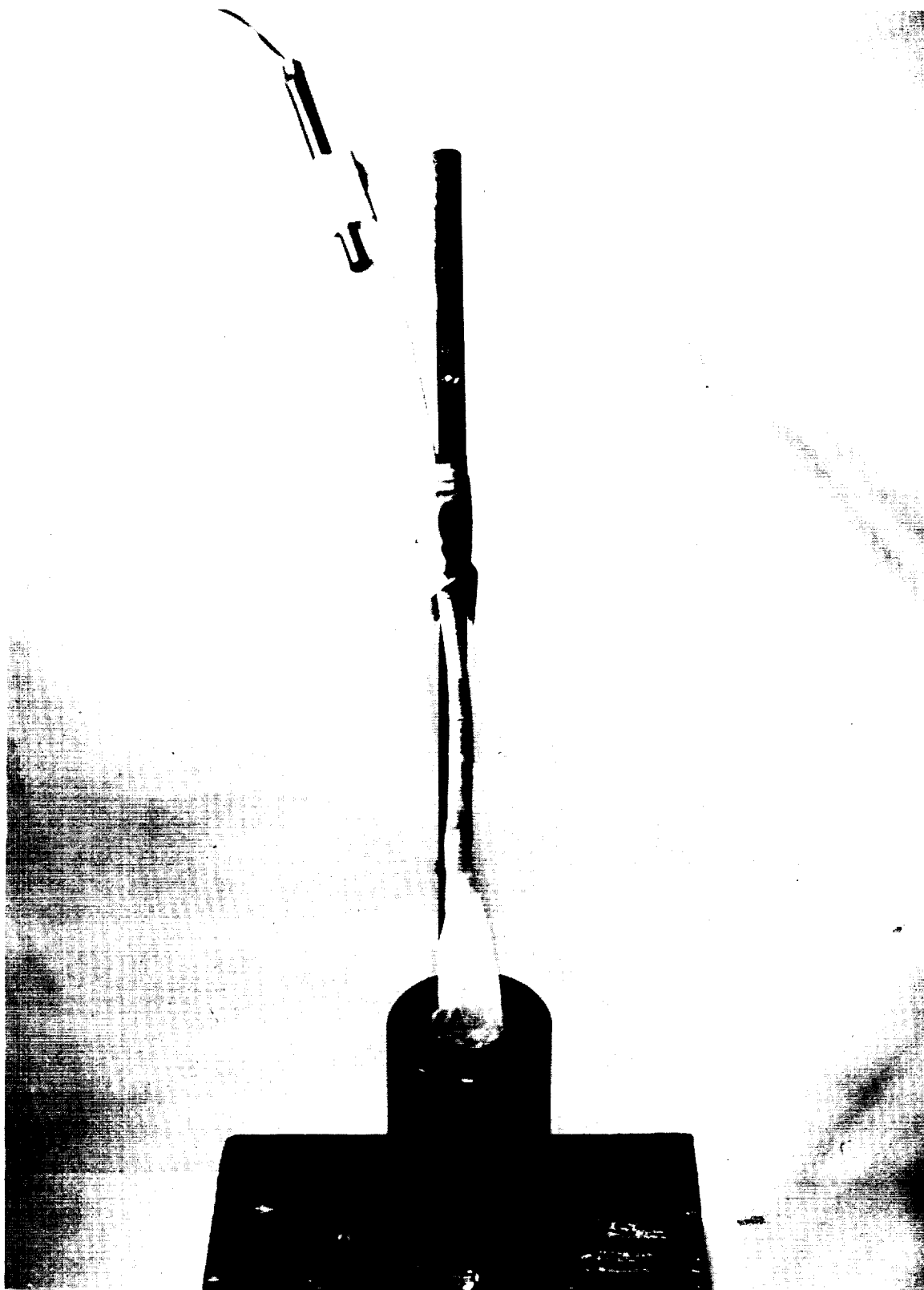


FIGURE 23. - Assembled Stainless Steel Engine Including Explosive Train Containing NG-EGDN-Cellulose Wick. Primacord and detonator also were used in the thin film detonation study.

It was desirable to fragment the molybdenum engines in a manner that would yield fragments, the number and size of which would be as close as possible to those fragments found in molybdenum engines that were destroyed in qualifying tests at MSC and TMC. Photographs of the destroyed engines from the MSC and TMC tests are presented in figures 24 through 31, inclusive. Figures 24 and 25 show the reassembled MSC engine. Figures 26 through 31 show the reassembled TMC engines. It can be seen that the fragment sizes in these MSC and TMC engines differ by a factor of two to three, suggesting that the corresponding explosion energies differ by about the same factor. Engines were not destroyed in the Bureau experiments in which ethylene-oxygen gas-phase detonations were initiated in the molybdenum engines. Although the detonation pressure was high, its velocity also was large and as a result the total impulse delivered to a unit wall area by the high pressure zone following immediately behind the detonation front was only 77 dyne-sec. Due to the brittle nature of molybdenum under high rates of stress loading (6), even a small impulse might be capable of damaging the engine. Furthermore, even if the impulse is small and the engine is not visibly damaged, repeated explosions will eventually impair engine performance.

In the experiments using the thin layer explosive, the first molybdenum engine was exploded with a 3-mil thick sheet of lens paper wetted with the NG-EGDN solution. An arrangement of paper saturated with the explosive solution and applied to half a SS engine, in a similar fashion, can be seen in figure 32.

The second molybdenum engine was fired with Primacord; an arrangement of Primacord in a SS engine section is shown in figure 33. In both these experiments only half the molybdenum engine wall was covered with explosive, thus making it possible to distinguish between the fragmenting ability of the explosive layer per se and that due to pressurization by the explosion product gases. In the first experiment using 0.75 g of explosive (NG-EGDN-cellulose), the engine fragments were considerably smaller than those from the MSC or TMC engines (fig. 34). The average weight of the fragments from the covered half was 0.8 g; the respective weight from the uncovered half was 1.5 g. The average weight of fragments from damaged TMC engines was 3.94, 6.96 and 12.4 g, respectively. Therefore, 0.5 g of explosive (Primacord) was used in the second experiment. The fragments produced in this experiment and shown in figure 35, varied from an average weight of 6 g for the covered half to 44 g for the uncovered half. The smaller fragments are within the size range of fragments obtained from the damaged TMC engines. The results, detailed in table 8, demonstrate that the presence of the explosive layer contributed to the fragmentation. From a comparison of fragment sizes of the engines exploded at the Bureau and those of TMC and MSC, it was concluded that an explosive charge equivalent in power to 0.5 to 0.75 g of PETN caused the damage in the MSC and TMC engines. Unfortunately, two molybdenum engine explosions were not sufficient to establish the absolute significance of the layer detonation in destructing engines. Thus, additional experiments were conducted using 10 SS engines. The engines were either halved or quartered and some contained cylindrical blowout plugs.



FIGURE 24. - Front Half of the Destroyed MSC Engine.



FIGURE 25. - Rear Half of the Destroyed MSC Engine.

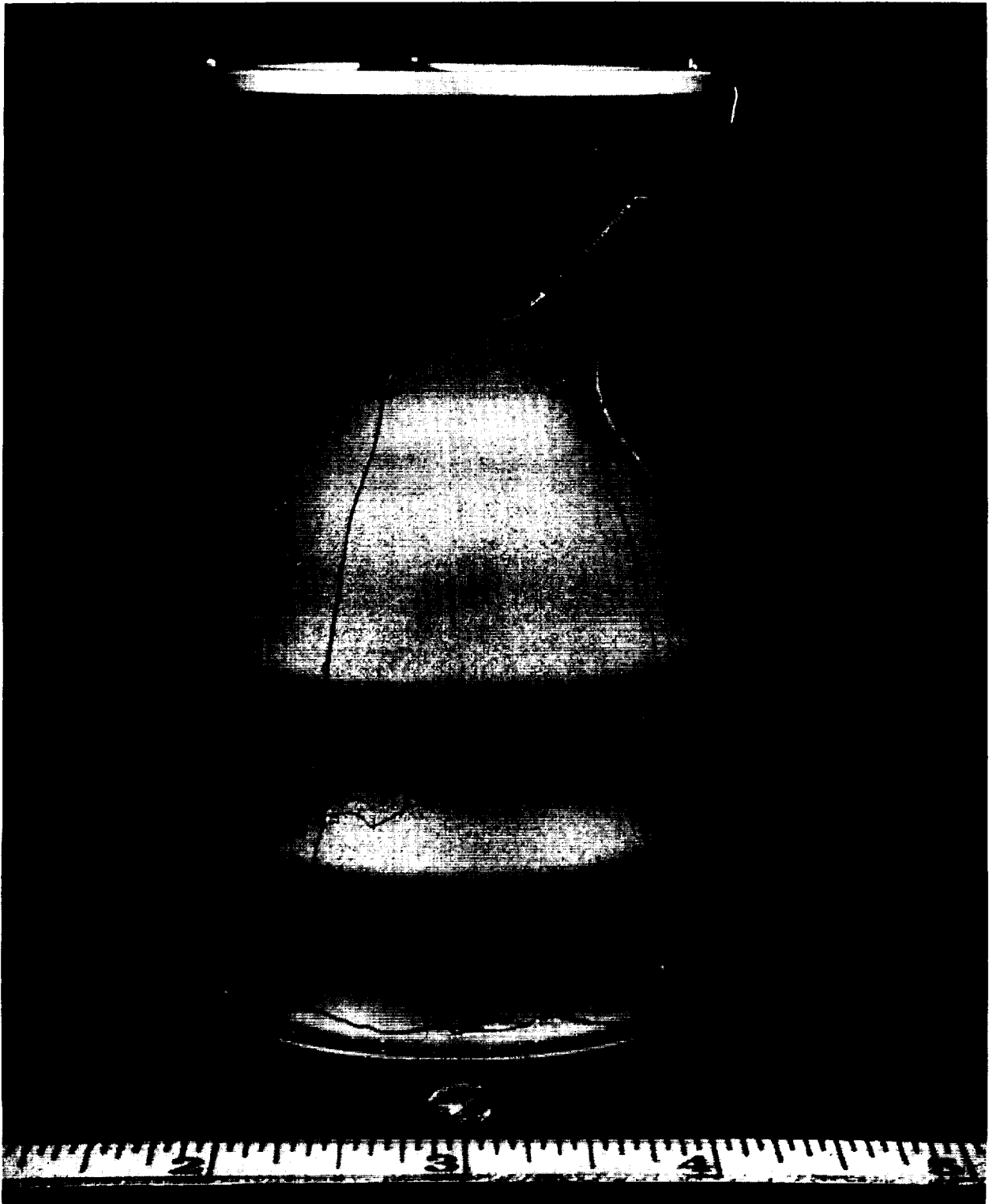


FIGURE 26. - Front Half of the Destroyed TMC Engine (042).

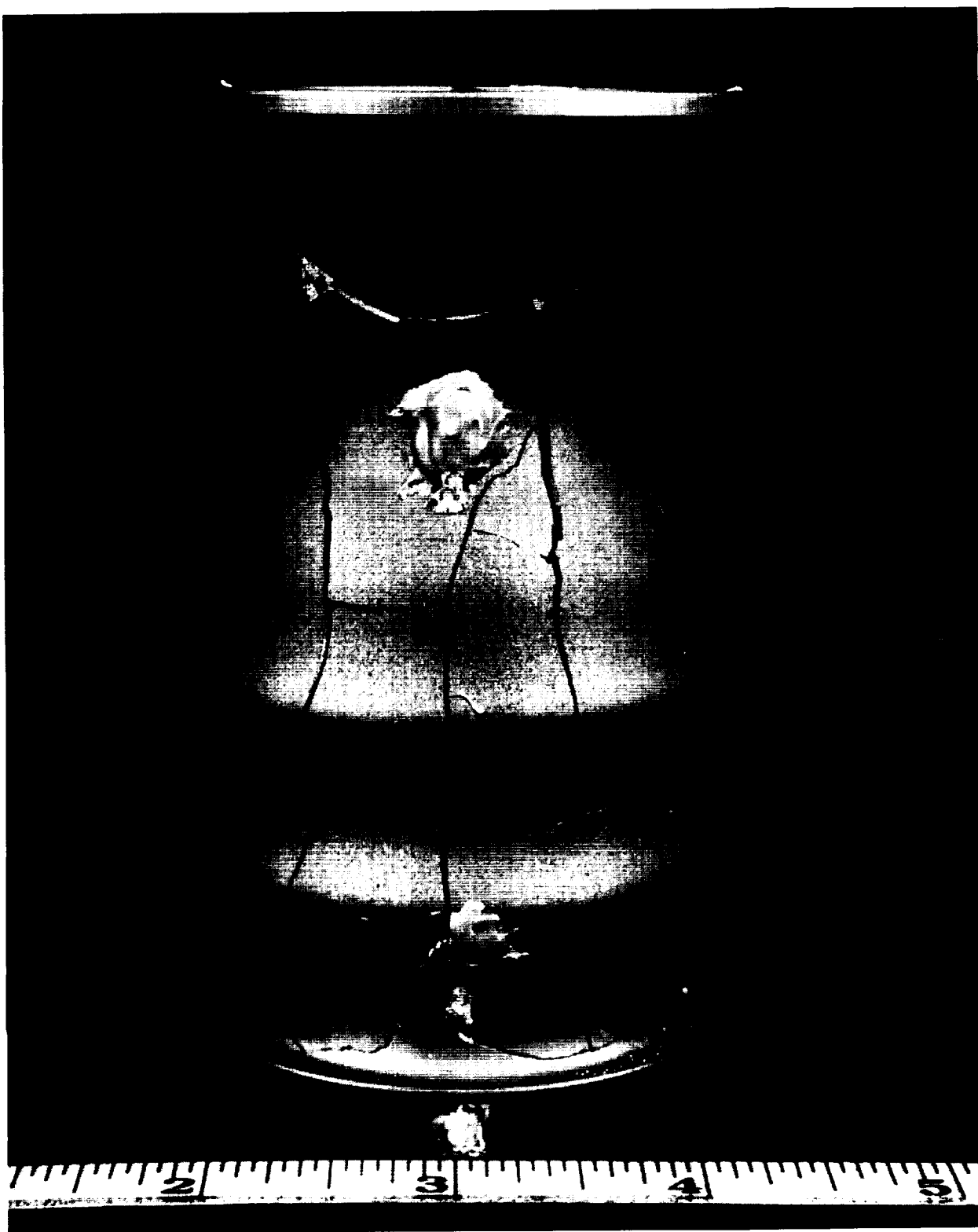


FIGURE 27. Rear Half of the Destroyed TMC Engine (042).

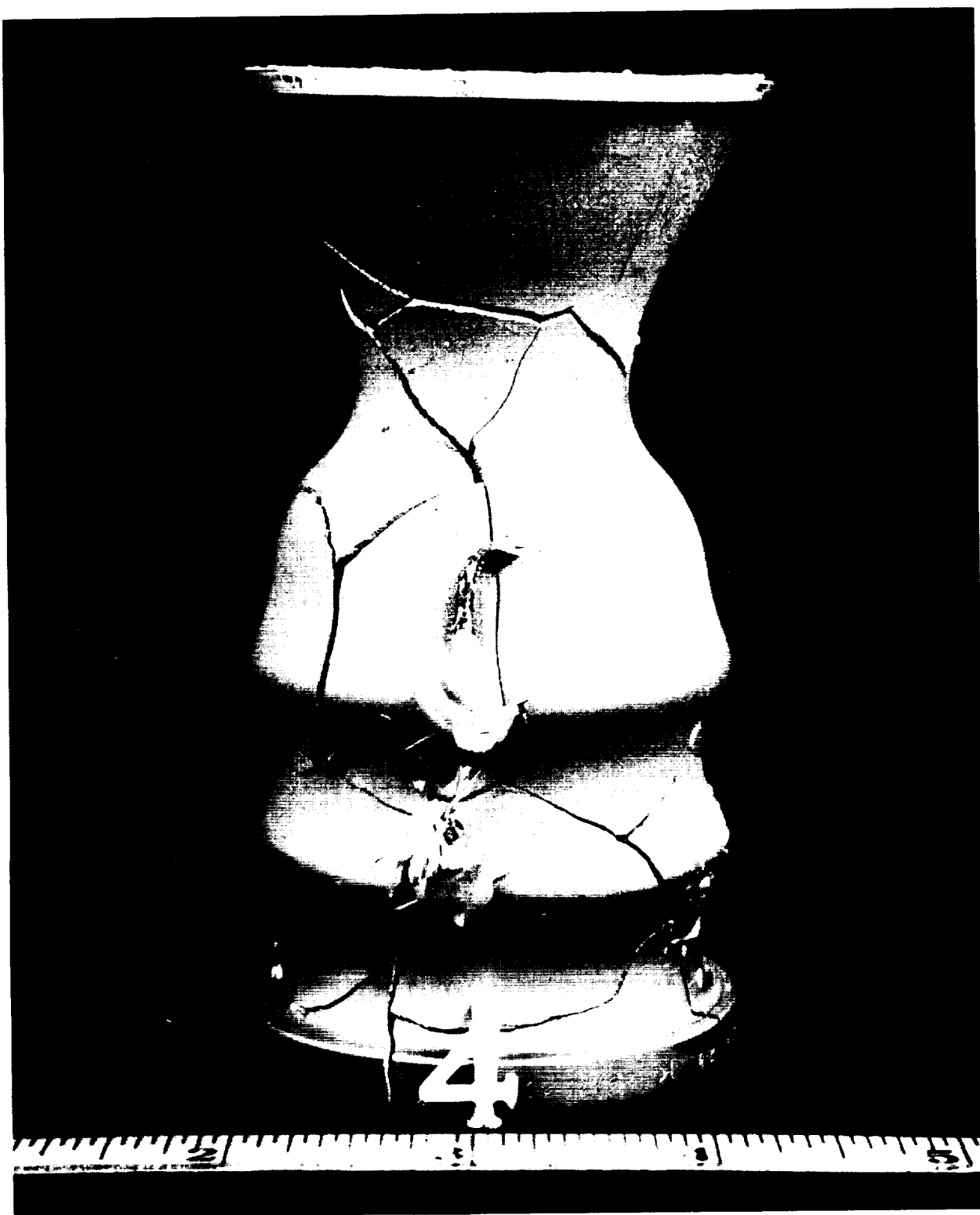


FIGURE 28. - Front Half of the Destroyed TMC Engine (379).

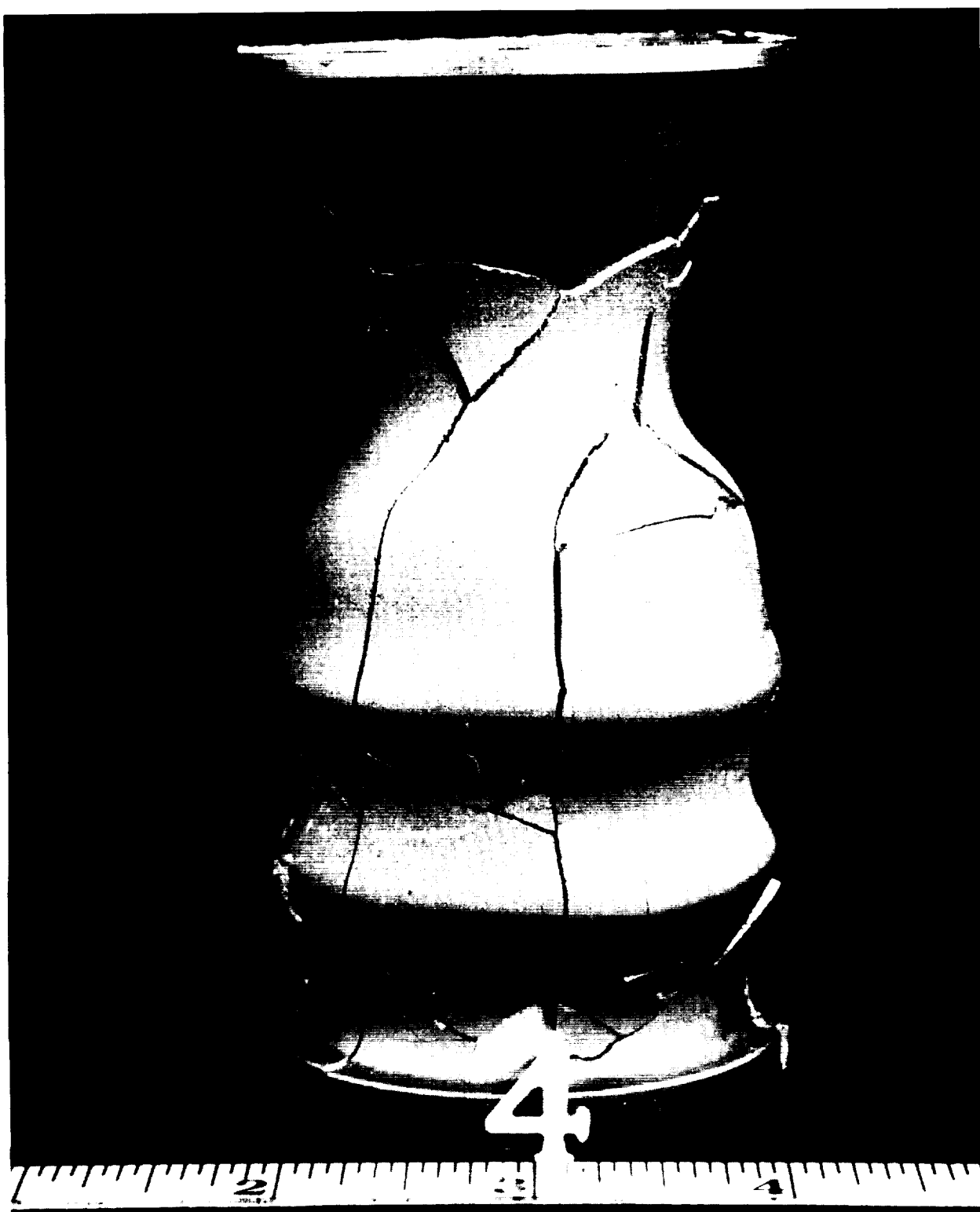


FIGURE 29. - Rear Half of the Destroyed TMC Engine (379).

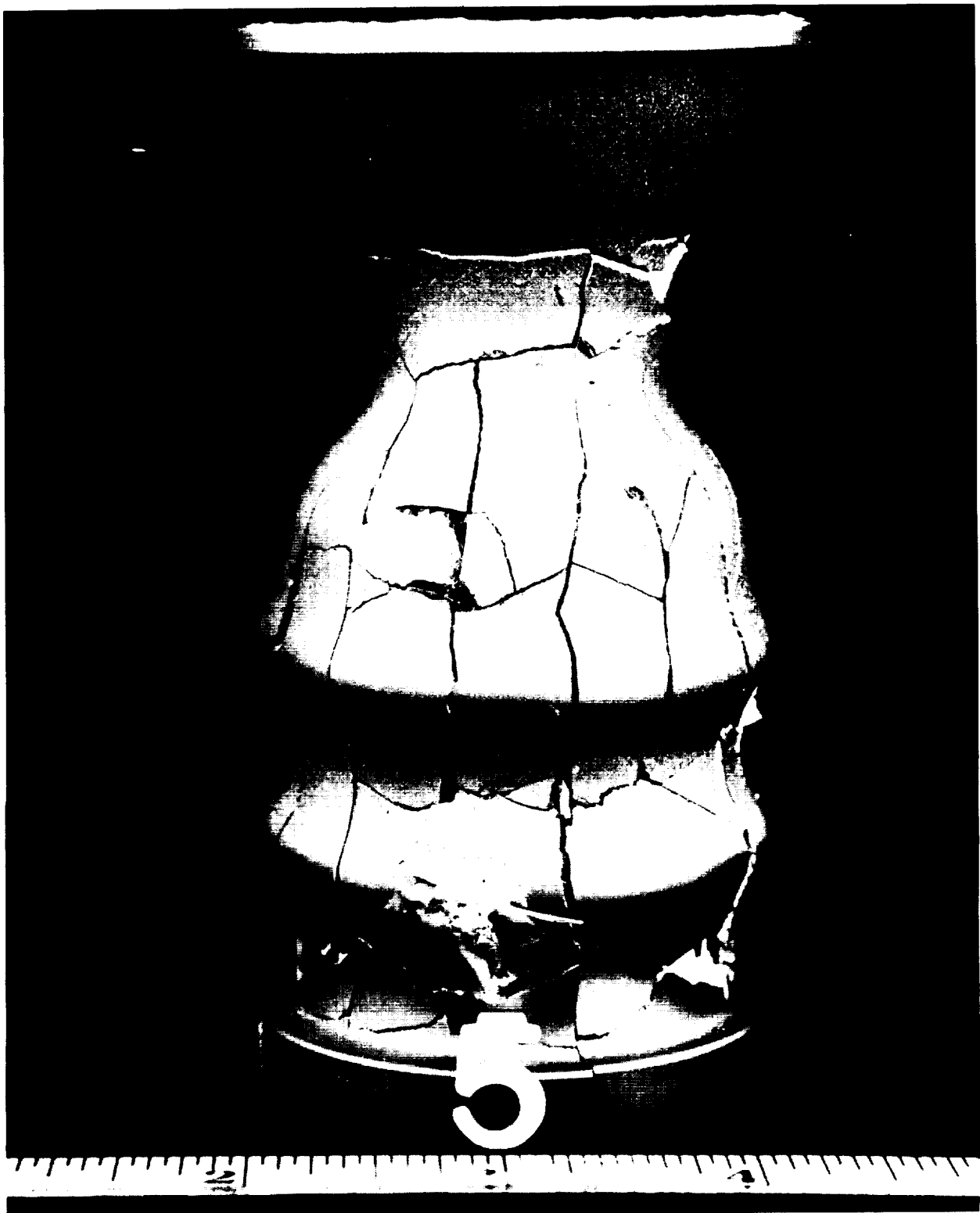


FIGURE 30. - Front Half of the Destructed TMC Engine (542).

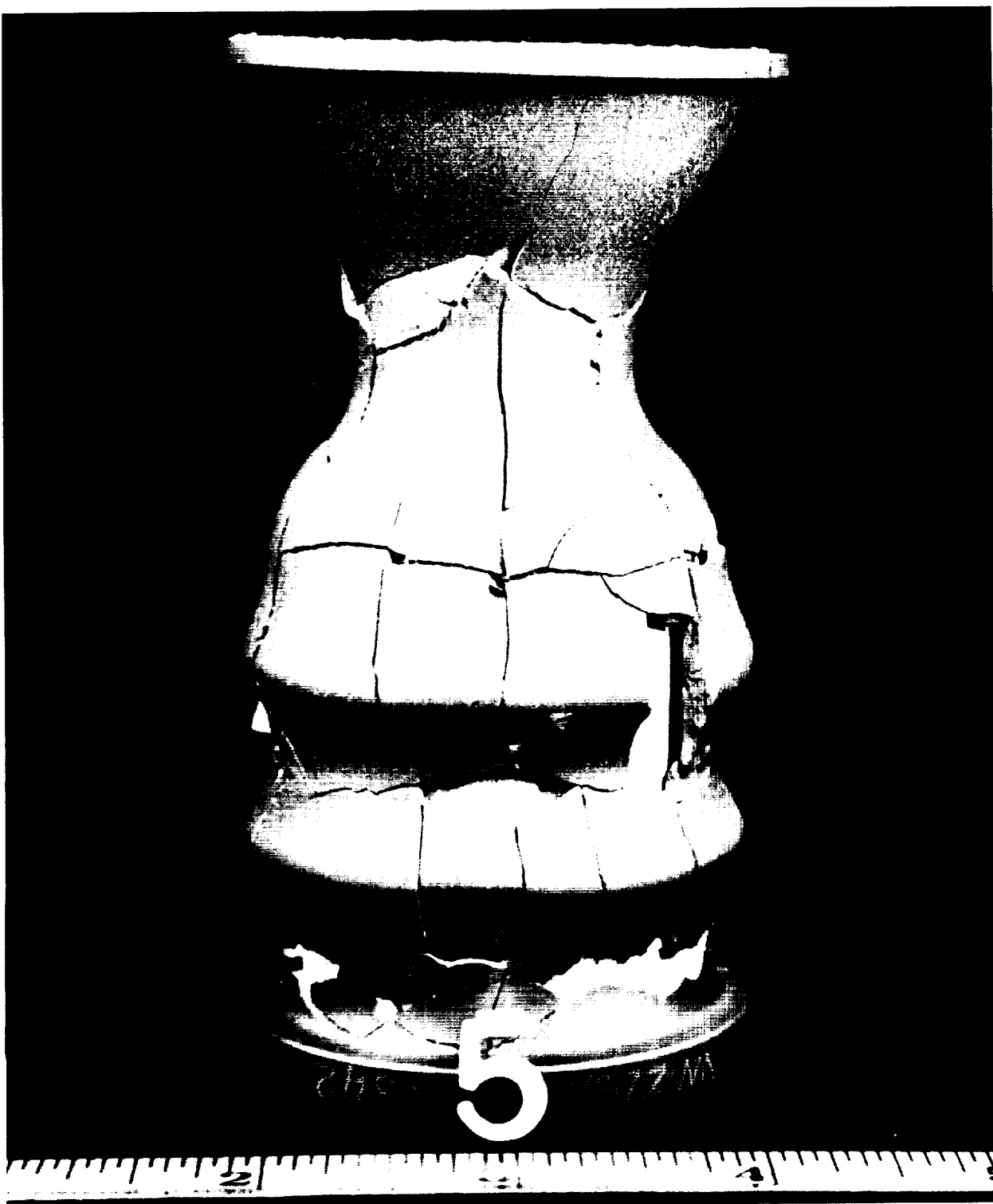


FIGURE 31. - Rear Half of the Destroyed TMC Engine (542).

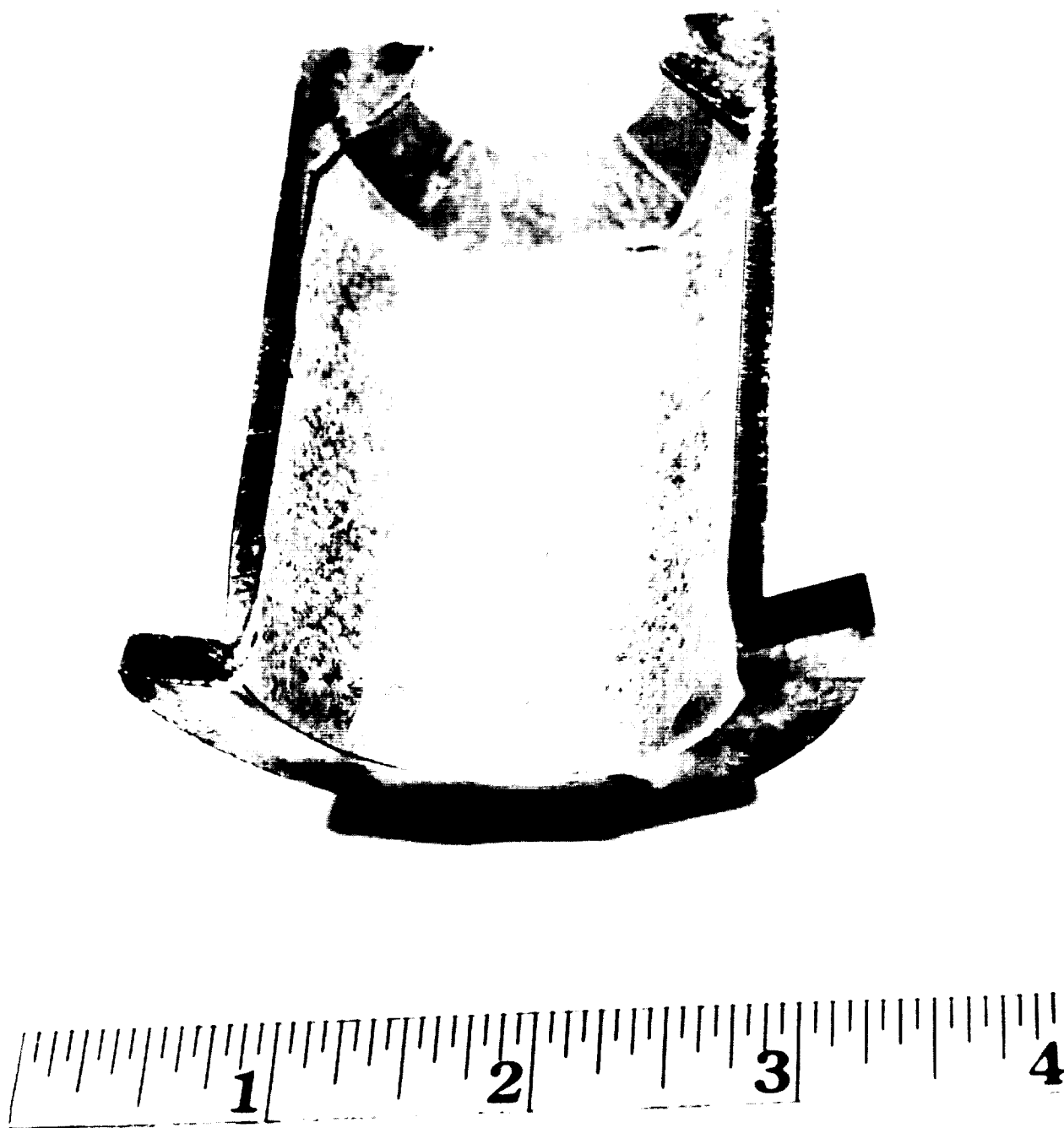


FIGURE 32. - Stainless Steel Engine Section Loaded with a Single Layer of the NG-EGDN-Cellulose Explosive Film.

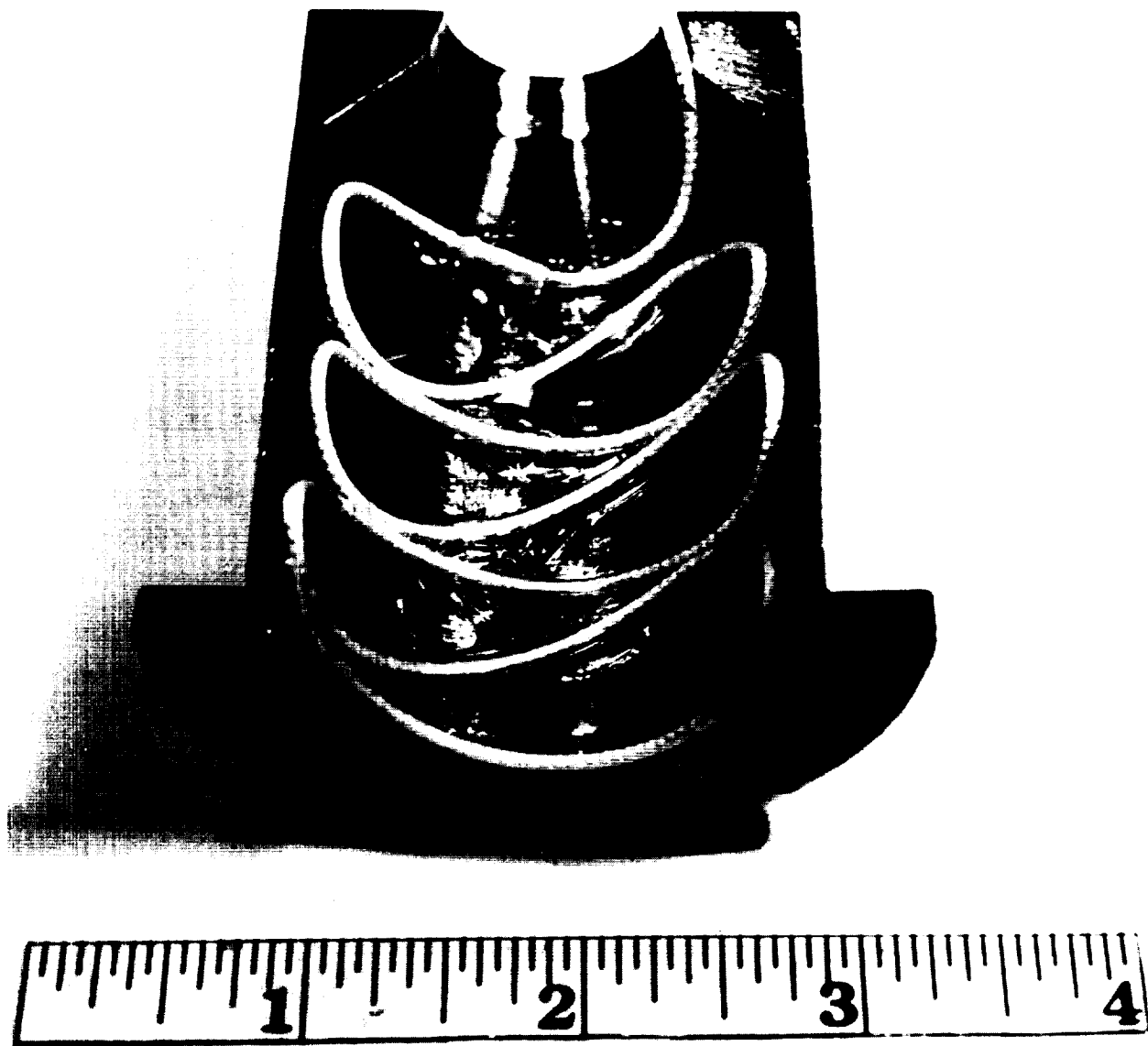


FIGURE 33. - Stainless Steel Engine Section Showing Primacord Loaded on the Engine Wall.

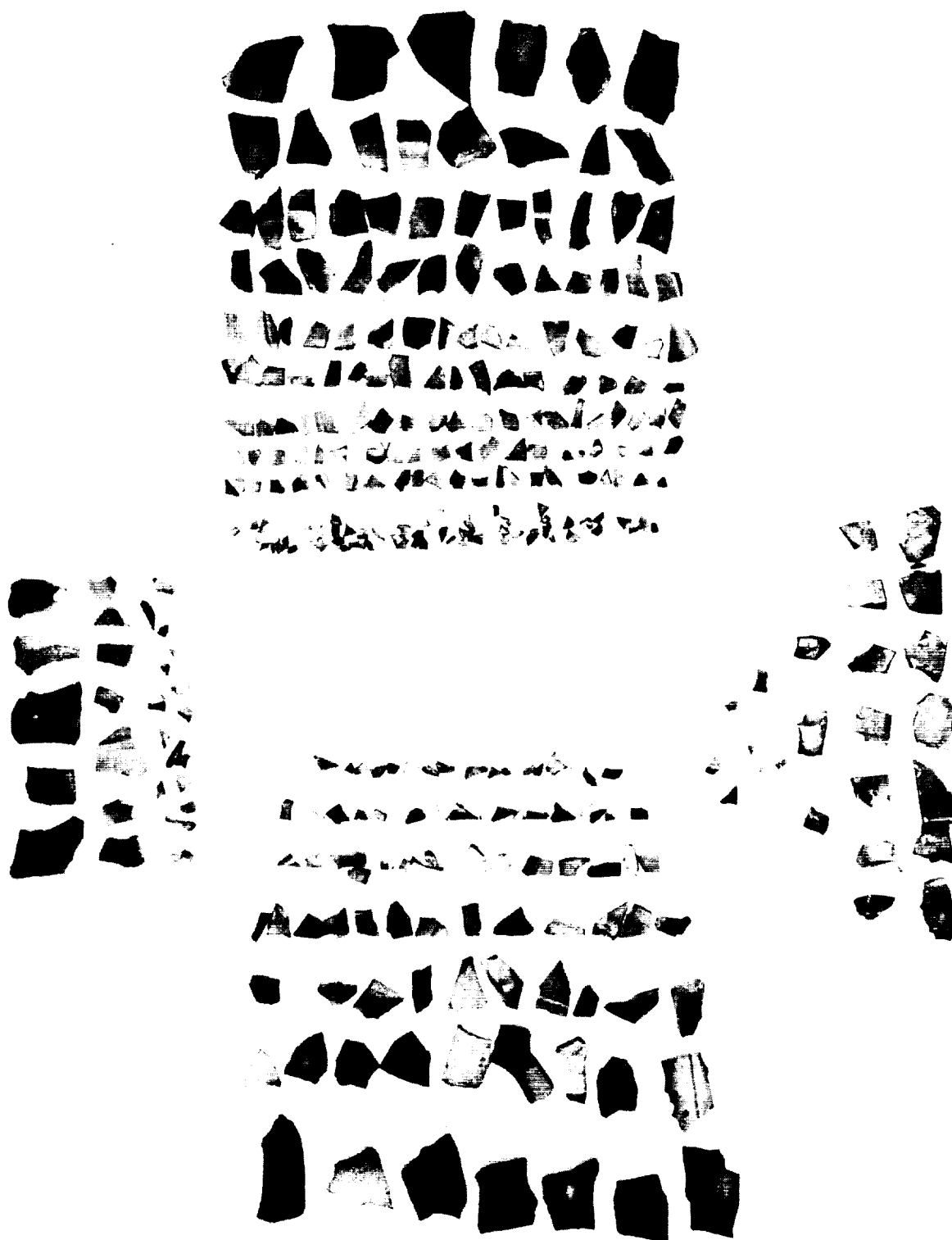


FIGURE 34. - Molybdenum Engine Fragments Resulting from the Explosion of 0.75 g of Explosive Film (NG-EGDN-Cellulose) Covering Half the Engine Internal Surface.



FIGURE 35. - Molybdenum Engine Fragments Resulting from the Explosion of 0.5 g of PETN (Primacord) Covering Half the Engine Internal Surface.

TABLE 8. - Recovered fragments from the destructed molybdenum engines and their average weight and velocity range

I. Bureau Tests

Weight of explosive, g	Loaded half of engine			Unloaded half of engine			² /Velocity range, m/sec
	Number of fragments	Average weight of fragments, g	¹ / σ , g	Number of fragments	Average weight of fragments, g	σ , g	
0.75 ³ / ₄	207	0.8	2	76	1.5	2.5	21-30
.50 ⁴ / ₄	31	6.0	8	5	44.0	63.0	6-9

II. TMC Tests

Engine	Total number of fragments	Total weight of fragments, g	Average weight of fragments, g
TMC (375)	48	334.0	6.96
TMC (542)	84	330.8	3.94
TMC (042)	26	328.8	12.4

¹/ The 90 percentile standard deviation.

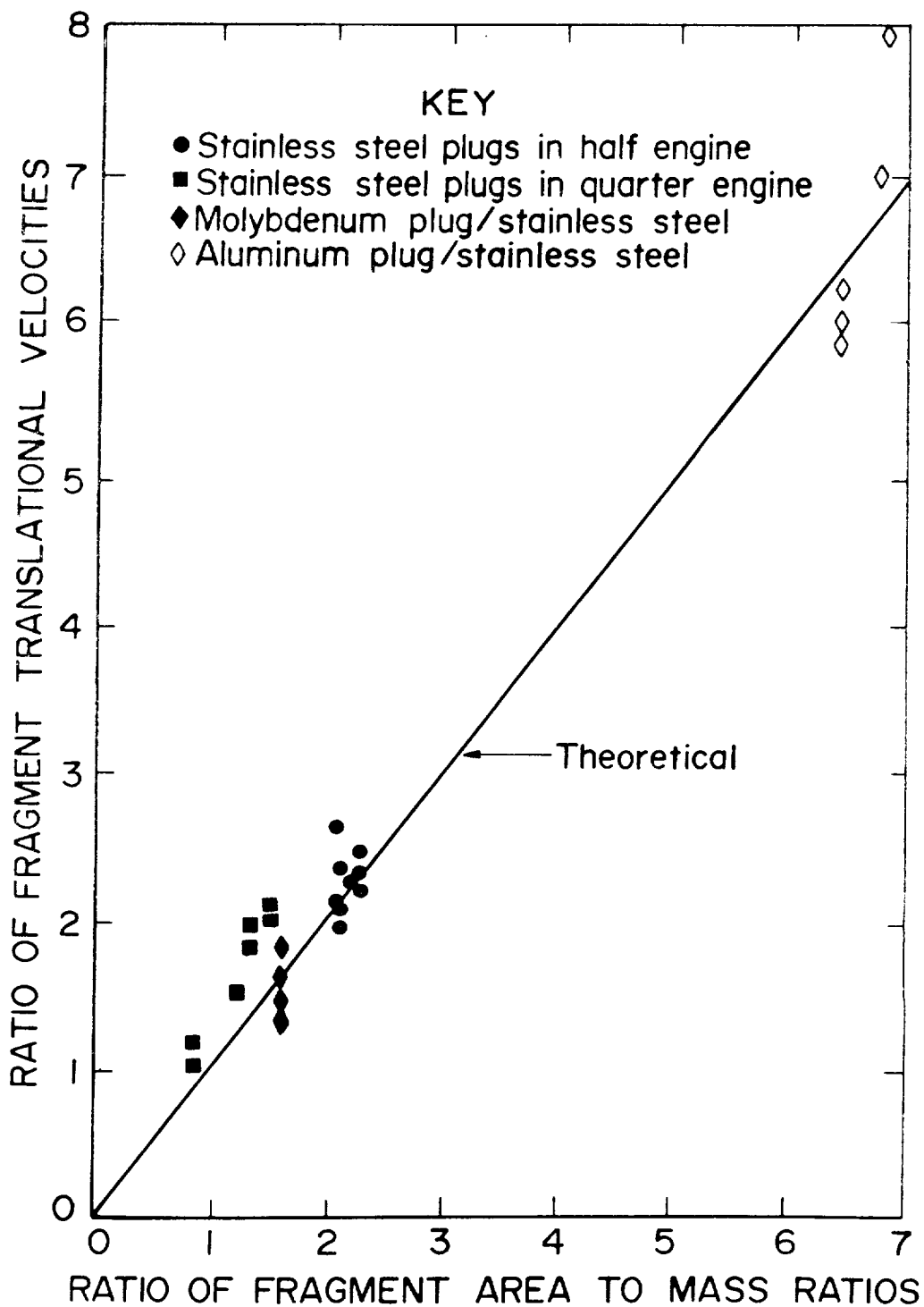
²/ In calculating the velocity range, fragments from the loaded and unloaded halves were included.

³/ NG-EGDN-cellulose.

⁴/ Primacord.

The results of these experiments using gas-phase detonations, shown in table 9, indicate that the quartered fragments have center of mass radial velocities greater than the halved sections. This is expected since the ratio of the fragment effective area⁹ to its mass (table 10) is larger for the quarter section than for the half section by a factor of $\sqrt{2}$. Similar data were obtained for the other fragments in that the highest radial velocities corresponded to those fragments having the largest area-to-mass ratio. This is best illustrated in figure 36 where the ratio of the velocities of two fragments common to an experiment were plotted against the ratio of their respective area-to-mass ratios given in table 10. As explained in the appendix, theoretically, the experimental points in figure 36 should lie on a 45-deg line if the impulse delivered to the fragments per unit of effective area were equal for fragments of equal area-to-mass ratios. The agreement between theory and experiment shown in figure 36 is satisfactory in view of the simplified theory.

⁹The effective area of a fragment is equal to the normal projection of the fragment geometry onto a plane normal to the resultant pressure vector.



P&H-73
524

FIGURE 36. - Ratio of the Fragment Translational Velocities as a Function of the Ratio of their Area-to-Mass Ratios Common to an Explosion.

TABLE 9. - Fragment velocities (m/sec) obtained in the
C₂H₄/O₂ detonation studies in sectioned
SS engines

Engine halves	Fragment type			
	<u>1/</u> Engine quarters	0.6-cm-diam blowout plug	1.3-cm-diam blowout plug	2.5-cm-diam blowout plug
5.91	-	14.75	-	-
6.19	-	<u>2/</u>	13.59	-
5.27	-	13.17	-	-
5.55	-	-	11.61	-
5.12	-	-	-	-
5.64	-	-	-	-
5.30	-	-	-	-
5.43	-	-	-	-
5.24	-	13.14	-	-
5.49	-	-	-	-
5.85	-	13.66	-	-
5.46	-	-	-	-
5.30	-	-	12.28	-
5.30	-	-	-	-
4.91	-	-	11.43	-
7.35	-	-	-	-
4.66	-	-	-	-
5.03	-	-	11.06	-
-	<u>2/</u> 6.49	-	12.13	-
-	6.40	-	-	6.92
-	6.00	-	14.02	-
-	3.75	-	-	-
-	7.01	-	-	-
-	5.79	-	-	-
-	9.91	-	11.70	-
-	9.91	-	-	9.91
-	7.44	-	-	-
-	7.13	-	-	-
-	4.60	-	-	-
-	6.74	-	-	-
Average velocity	5.50	6.76	13.75	11.97
<u>3/</u> σ	1.1	1.8	0.4	0.4

- 1/ In each test in which quarter sections were used, the velocity of two quarters only was measured because the photographs were taken in profile.
2/ Empty spaces indicate that the half or quarter sections did not contain blowout plugs or that the respective plug's velocity was not recorded.
3/ The 90 percentile standard deviation.

TABLE 10. - Mass and area-to-mass ratio for the SS,
aluminum, and molybdenum fragments

Fragment	Mass, g	1/Area/mass, cm ² /g
Stainless steel:		
Half	221.6	0.174
Quarter	109.3	.251
Half with 1/2-inch hole . . .	221.7	.172
Half with 1/4-inch hole . . .	223.3	.174
Quarter with 1-inch hole . . .	95.8	.259
Quarter with 3/4-inch hole . .	101.3	.240
Quarter with 1/2-inch hole . .	105.3	.351
Quarter with 1/4-inch hole . .	107.4	.385
1-inch plug	22.88	.221
3/4-inch plug	9.00	.317
1/2-inch plug	3.55	.357
1/4-inch plug	0.82	.386
Aluminum:		
1-inch plug	4.56	1.110
Molybdenum:		
1/2-inch plug	5.88	.274

1/Effective area of the fragment is equal to the normal projection of the fragment geometry onto a plane normal to the resultant pressure vector.

Fragment displacement, as depicted in figure 37 showed no measurable acceleration of the fragments following detonation of the gas mixture. This indicates that the hot combustion products pressurizing the chamber are exhausted out the engine nozzle, causing the combustion product gas pressure to decay to an insignificant level, in a time less than 0.2 msec (the time between frames). This result agrees with the estimated time of 0.5 msec (engine time constant) required for the engine to expel the product gases at such a rate that the internal chamber pressure drops to 90 pct of its initial value in this time interval. The position of the ignition source, whether in the throat or near the injector, made no perceptible difference in the resulting fragment velocities; theoretically, there should be a difference, but apparently it was too small to be observed in these experiments.

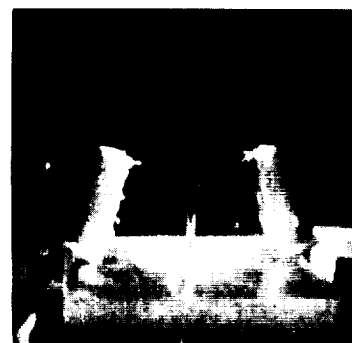
The force propelling fragments to a terminal velocity originates from two pressure sources, the high but narrow pressure region immediately following a gas detonation front and the eventual pressurization of the engine by the hot product gases. Although the peak pressure in the region behind the detonation front in a stoichiometric C₂H₄/O₂ mixture is approximately 34 atm, it is narrow (ca. 2 cm) and travels so rapidly (2.2 mm/μsec) across a fragment that the impulse delivered per unit area is only 77 dyne-sec, whereas the impulse delivered through product-gas pressurization is 4×10^3 dyne-sec, a factor of 50 larger than that from the detonation.



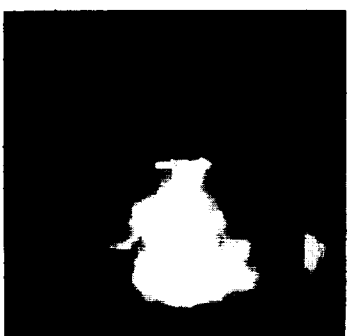
T = 0



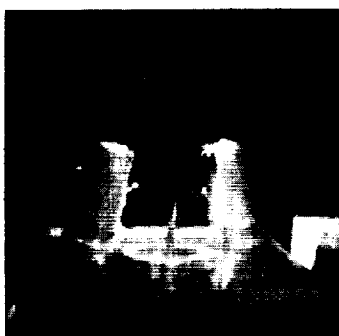
T = 5.32 ms



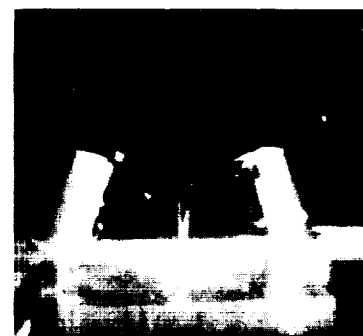
T = 10.6 ms



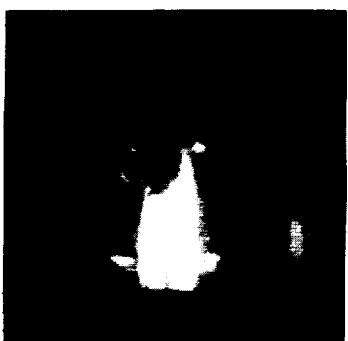
T = 1.77 ms



T = 7.09 ms



T = 12.4 ms



T = 3.55 ms



T = 8.87 ms



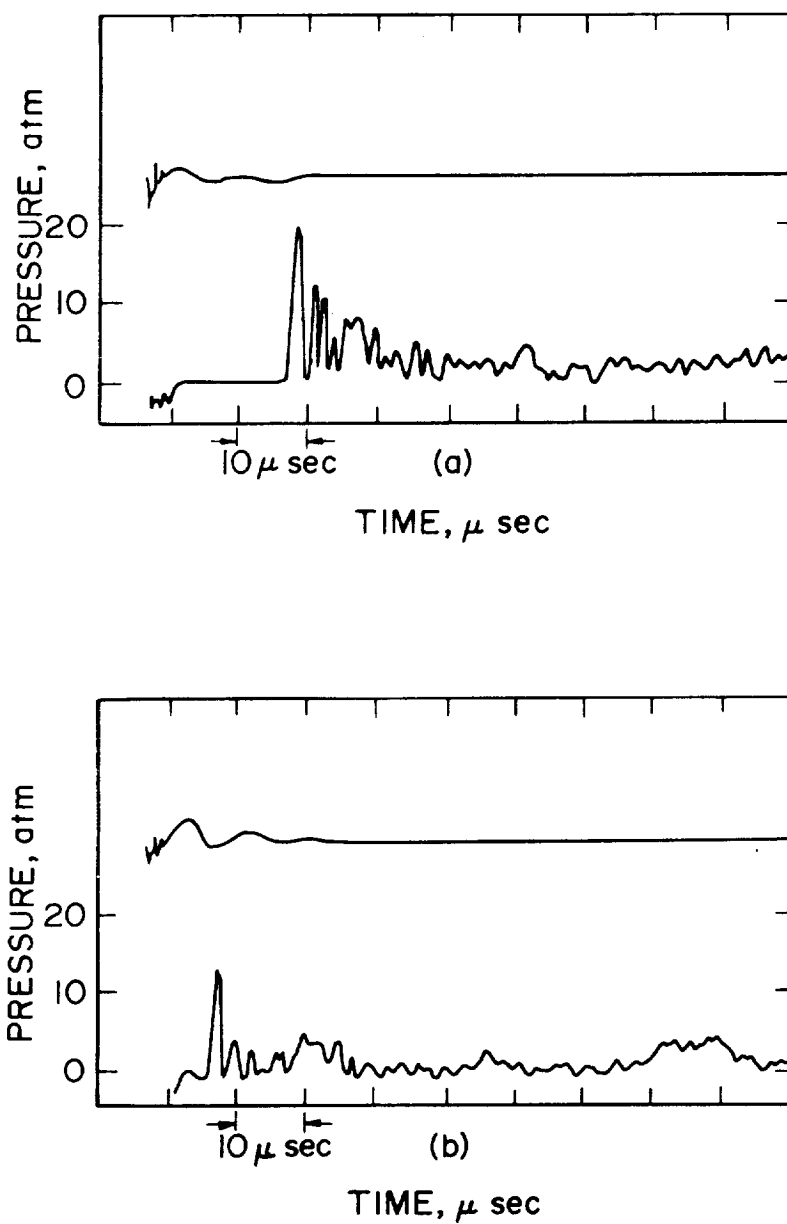
T = 14.2 ms

FIGURE 37. - High Speed Frame Sequence of Exploding Engine Halves.

These values illustrate that the major portion of the fragment terminal velocity occurs from the pressurization of the engine and not the high pressure region behind the detonation front. These results can be compared with those obtained previously and discussed on page 23 - - where we found that the reflection of the blast wave off the injector face contributed the major portion to the engine's impulse. These results are not contradictory since in the former case the blast wave reflected off the injector face has a higher pressure and longer duration than the side-on blast pressure seen by the fragment in the wall where there is a lower pressure and shorter duration. Pressure transducer records for the gas-phase detonation in these engines (fig. 38) illustrate the high oscillatory chamber pressure associated with a detonation. Fortunately, for analysis purposes, the time constant of the fragments is considerably larger than the period of the pressure disturbance so that the individual fragment sees a time average of these pressure oscillations. From this it can be assumed that the force accelerating the fragments is essentially the constant volume combustion pressure (fig. 39) for the C_2H_4/O_2 mixture, approximately 16 atms.

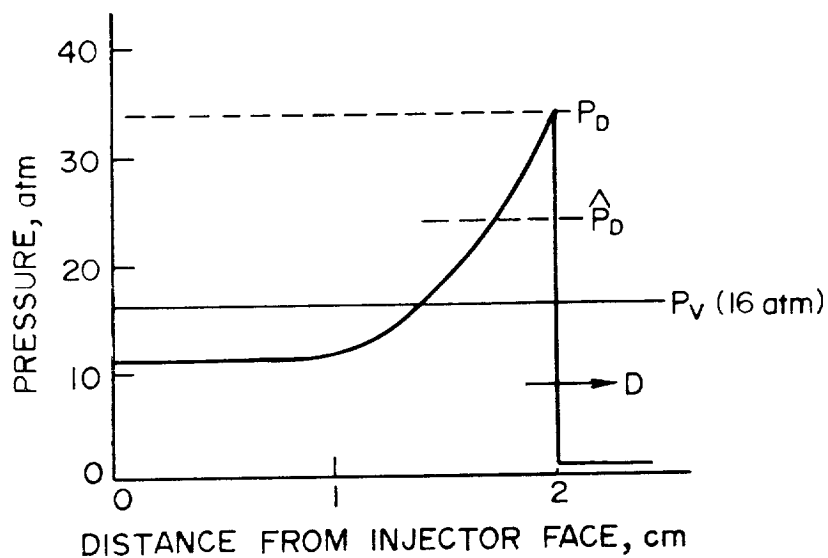
In addition to the translational or radial motion of the fragment mass center, there is also a rotational motion resulting from two mechanisms--one originating from the time required for the high pressure region following the detonation front to travel across a fragment, and the other from the eccentricity of the product gas pressurization vector and the fragment center of mass. Theoretically, as shown in the appendix, the angular velocity (radians/sec) of these fragments is approximately 5 times larger than the translational velocity (m/sec); this is depicted in figure 40. It also can be shown that the rotational energy of the fragments is approximately 23 pct of their translational energy, and this appears to be a maximum for the fragments generated in the molybdenum engine explosions. If it were not for the corrugated geometry of the molybdenum engines, the driving force vector would not be eccentric to the fragment mass center and the fragment rotational energy would be insignificant. (For this reason a noncorrugated geometry would be desirable.) In this discussion, the restriction to the fragment rotational motion due to adjacent fragments has not been considered.

The sectioned SS engines from the gas-phase detonation studies also were used in the thin layer explosives study. Unfortunately, due to the voluminous amount of opaque carbonaceous material produced in the detonation of the explosive layers, it was not always possible to see the smaller SS fragments on the high-speed films, so that most of the velocities measured in this study pertained to either half or quarter-engine sections. Fragment velocities versus the weight of explosive covering the wall, plotted in figure 41, show that for small weights of explosive, fragment velocity increases linearly with explosive weight. No more than 3.5 g of explosive was used because the SS engine sections were seriously deformed with larger weights.



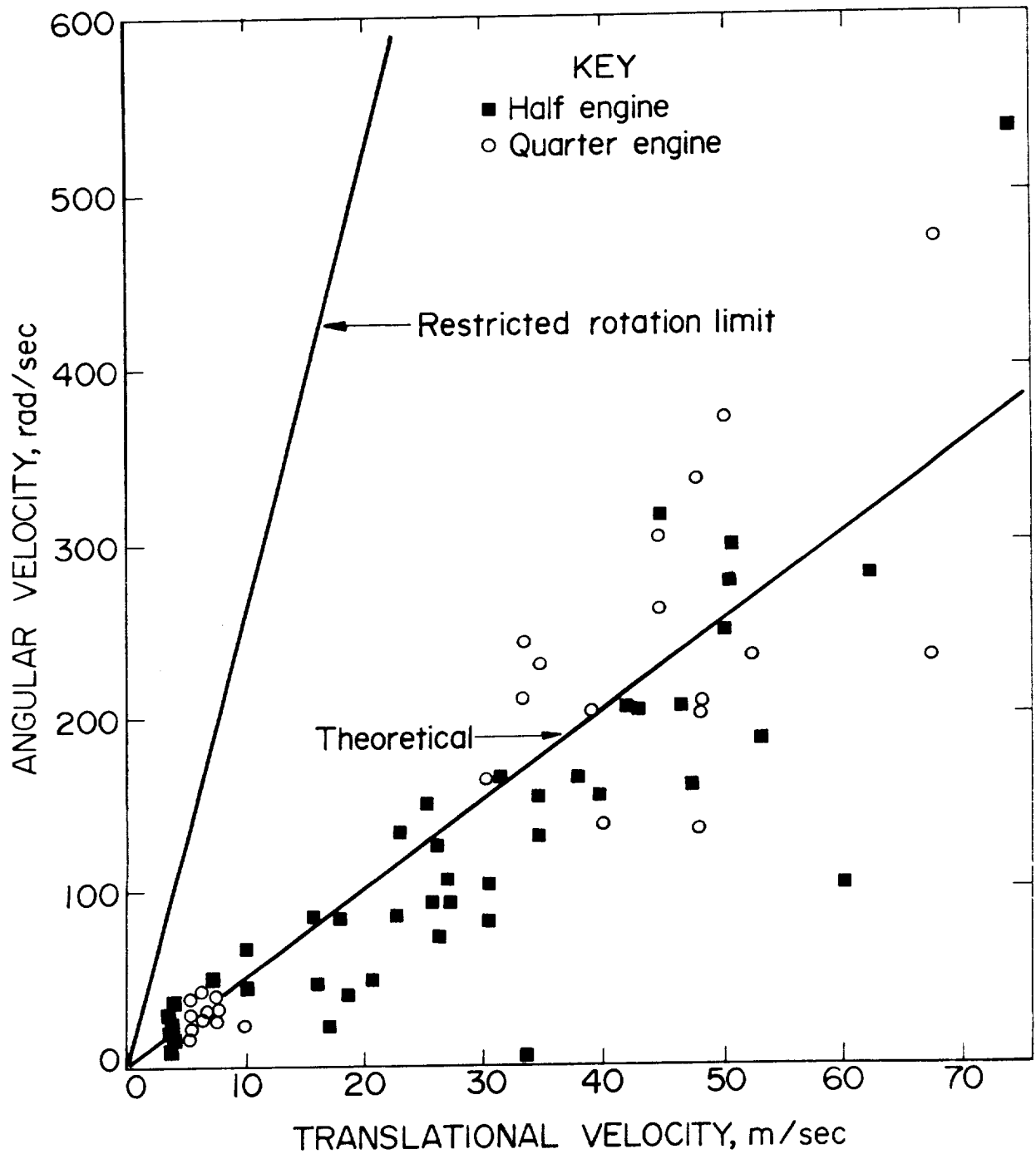
P6H-73
520

FIGURE 38. - Pressure Transducer Traces for Detonating Stoichiometric C_2H_4/O_2 Mixtures in the Stainless Steel Engines for Two Heights of the Ignition Source above the Transducer (a) 4.0 cm and (b) 1.4 cm.



PGH-73
529

FIGURE 39. - Pressure Distribution Behind an C_2H_4/O_2 Detonation Front Propagating from the Injector Face Towards the Throat; P_v is the Constant Volume Combustion Pressure, P_D the Maximum Detonation Pressure, and \hat{P}_D the Mean Detonation Pressure ($= 0.67 P_D$).



PGH-73
530

FIGURE 40, - Angular Velocity of Stainless Steel Fragments as a Function of their Translational (radial) Velocity.

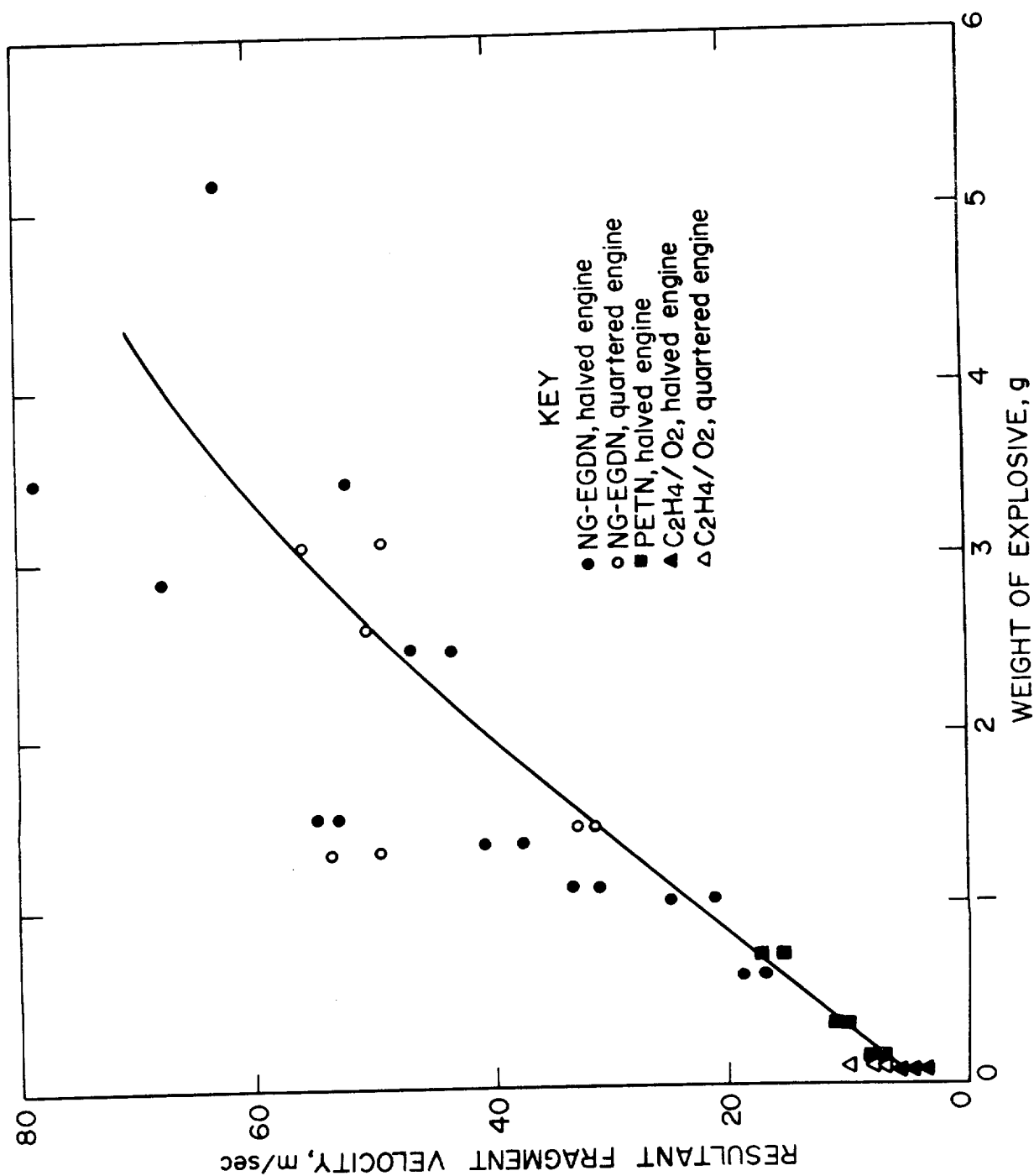


FIGURE 41. - Fragment Velocities from the Explosion of the Stainless Steel Engines with the NC-EGDN-Cellulose Layers, the PETN Cord, and the C₂H₄/O₂ Gas Detonations.

In the thin layer detonation, as in the gas-phase detonation, two mechanisms accelerate fragments to the terminal velocities, the very high pressure (7×10^3 atm), narrow (10^{-3} cm), high velocity (2mm/ μ sec) zone immediately following the detonation front, and the pressurization of the engine by the hot-product gases released in the detonation. Typically, the velocity resulting from the latter mechanism constitutes about 90 pct of the total velocity, illustrating again that the largest proportion of the fragment impulse comes from the pressurization of the chamber rather than the high pressure associated with the detonation. Our experiments have shown that the high pressure zone following the detonation is more significant in fragmenting the engine than in accelerating the fragments.

Similarly, the thin layer detonations also impart a rotational motion to the fragments. And likewise, rotation is attributed to two mechanisms, the travel time of the high pressure gas zone, following the detonation front, over the fragment, and the eccentricity of the applied driving force vector to the center of mass of the fragment. In the case of the molybdenum engine, with its corrugated outer surface, the latter mechanism contributes the greater proportion of the rotational energy. This is due to the fact that the thickness of the high pressure zone in the thin layers is much smaller than the fragments and consequently, when the delta function pressure distribution is integrated over the fragment area, the resultant impulse is zero. The experimental results (fig. 40) of fragment angular velocity as a function of linear velocity agree well with the theoretical. By calculation, it can be shown that the rotational portion of total fragment energy is about 300 times smaller than the translational contribution; demonstrating again that rotational energy constitutes only a fraction of the fragment energy and can be neglected. The fragments obtained in the two molybdenum engine experiments using 0.75 and 0.5 g of explosive had velocities ranging from 21 to 33 m/sec and from 6 to 9 m/sec, respectively; in the latter experiment one fragment weighing 111 g traveled at a velocity of 7 m/sec. In order to compare these velocities with those for the SS fragments, given in figure 41, it is necessary to correct for the difference in the area-to-mass ratio between the molybdenum and steel fragments. This is done by multiplying the velocity by the ratio of the corresponding effective area-to-mass ratio for the two fragment types. Using a mean area-to-mass ratio for the molybdenum fragment of 0.20 and the corresponding area-to-mass ratio for the SS half-engine fragment of 0.174, a correction factor of 0.87 when multiplied by the 21 m/sec velocity for the molybdenum fragment gives a value of about 18 m/sec. The corrected velocity agrees with the value of 15.5 m/sec found for the corresponding SS fragment.

After the major portion of the experimental work was completed, three additional molybdenum engines were given to the Bureau for destruction studies. In these latter tests, the engines were fired in a geometrical configuration simulating that of the IM vehicle to determine the hazards to vulnerable components, such as the Vycor window and the IM blanket structure consisting of 0.01-mm-thick

aluminum sheet and a 30-layer H-film blanket. Since the earlier tests demonstrated the significance of an explosion close to the wall in the fragmentation process, these experiments were conducted using a uniform charge of explosive covering the interior of the engine. The explosive consisted of 0.3-cm-diam Primacord coiled around the interior wall of the engine. The engines were destroyed in the same manner as previously and the resulting fragment velocities were obtained from high-speed motion picture photography. Two views of the arrangement of the LM materials surrounding the engine are shown in figure 42. Figures 43, 44, and 45 show the fragments generated in the engine explosions, and table 11 summarizes the results of these three experiments. Although the last shot was intended to be fired with a 1-g Primacord load, only 0.75 g of the Primacord actually detonated. The fragment sizes listed in table 11 compare favorably with those obtained in both the MSC and TMC engine destruct experiments, indicating that the amount of PETN required to cause this particular fragmentation pattern in molybdenum engines corresponds to about 0.75 g. When 0.5 g of PETN covered only half the engine, the average fragment weight of the covered portion was 6 g; when the same explosive weight covered the whole internal surface, the average fragment weight was 12.44 g; again, indicating the importance of the condensed-phase charge locality to resultant damage and fragment size. The ratio of the average weight is approximately 2. In the 0.75 g experiments in which the same two configurations were employed, the average weight of the fragment in which half the engine was covered with NG-EGDN was 0.8 g. The average weight of the fragment in which PETN covered the whole engine was 6.7 g. The respective ratio of average weight is more than 8. Not only the weight of the explosive and its locality affect fragment size, but also the type of explosive, or more specifically, the maximum detonation pressure of the explosive, which has been shown previously to be the major factor in resultant fragment sizes. The fragments generated in these explosions readily penetrated and shattered the Vycor plate. Only in one experiment in which no fragments impacted the plate was it not damaged. On the other hand, in only one instance did a fragment penetrate the entire IM blanket structure. The greatest majority of the fragments which impacted the blanket structure struck it obliquely and did not appear to cause extensive damage. It is certain that the Vycor window is vulnerable in the event of an engine explosion in its vicinity.

TABLE 11. - Number of fragments recovered, average weight, and velocity range obtained in the molybdenum engine explosions

Weight of PETN, ^{1/} g	Number of fragments recovered	Average fragment weight, g	$\frac{2}{\sigma}$, g	Velocity range, m/sec
0.50	21	12.44	10.47	10-21
.75	34	6.18	8.34	15-32
.75	38	7.35	11.64	14-25

^{1/} Explosive was evenly distributed on inner wall of engine.

^{2/} The 90 percentile standard deviation.

PH-173

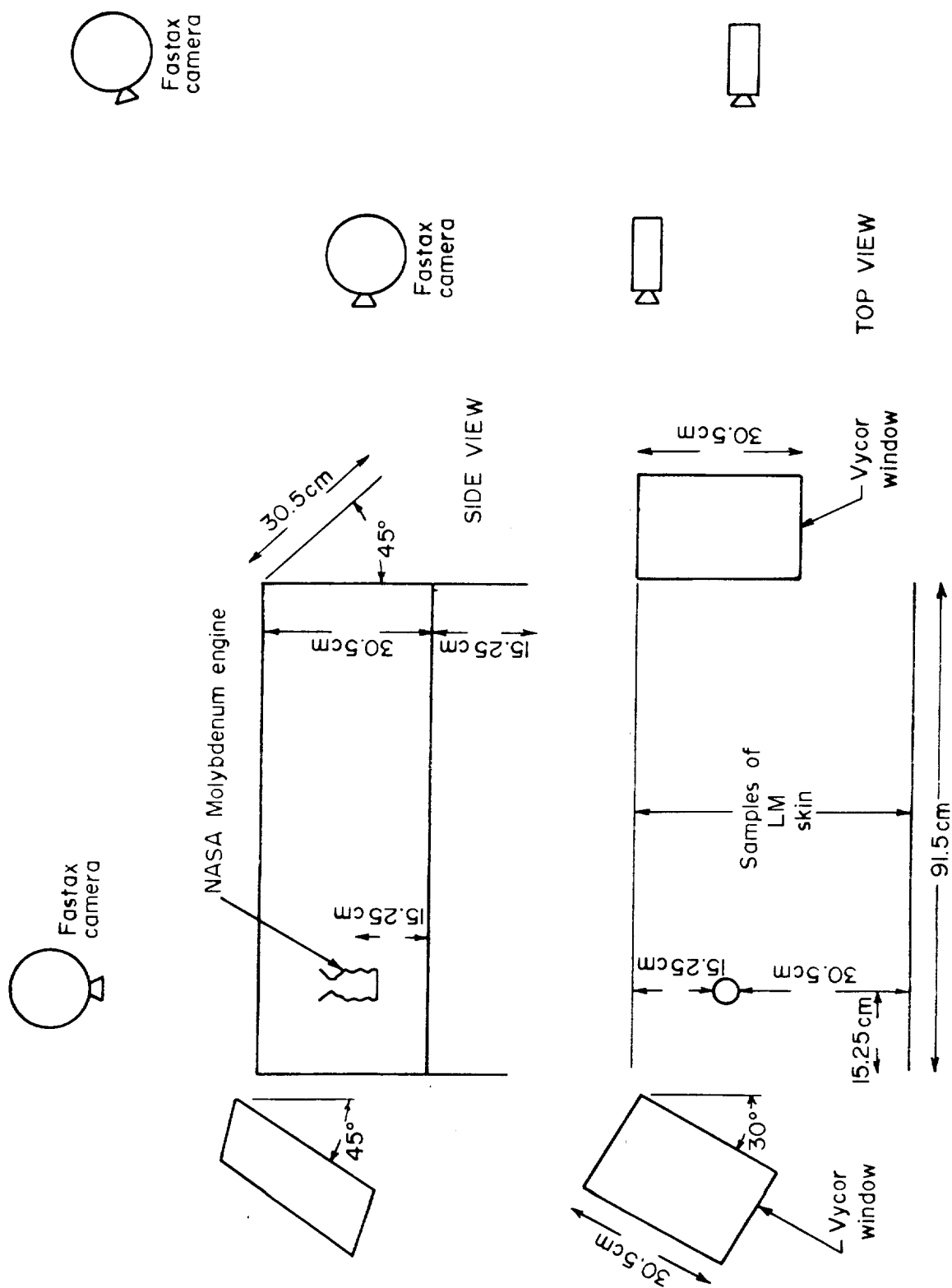


FIGURE 42. - Side and Top Views of the Experimental Arrangement of Components in the Engine Explosion Experiments.



FIGURE 43. - Molybdenum Engine Fragments Resulting from the Explosion of 0.50 g of PETN (Primacord) Completely Covering the Interior of the Engine.



FIGURE 44. - Molybdenum Engine Fragments Resulting from the Explosion of 0.75 g of PETN (Primacord) Completely Covering the Interior of the Engine.

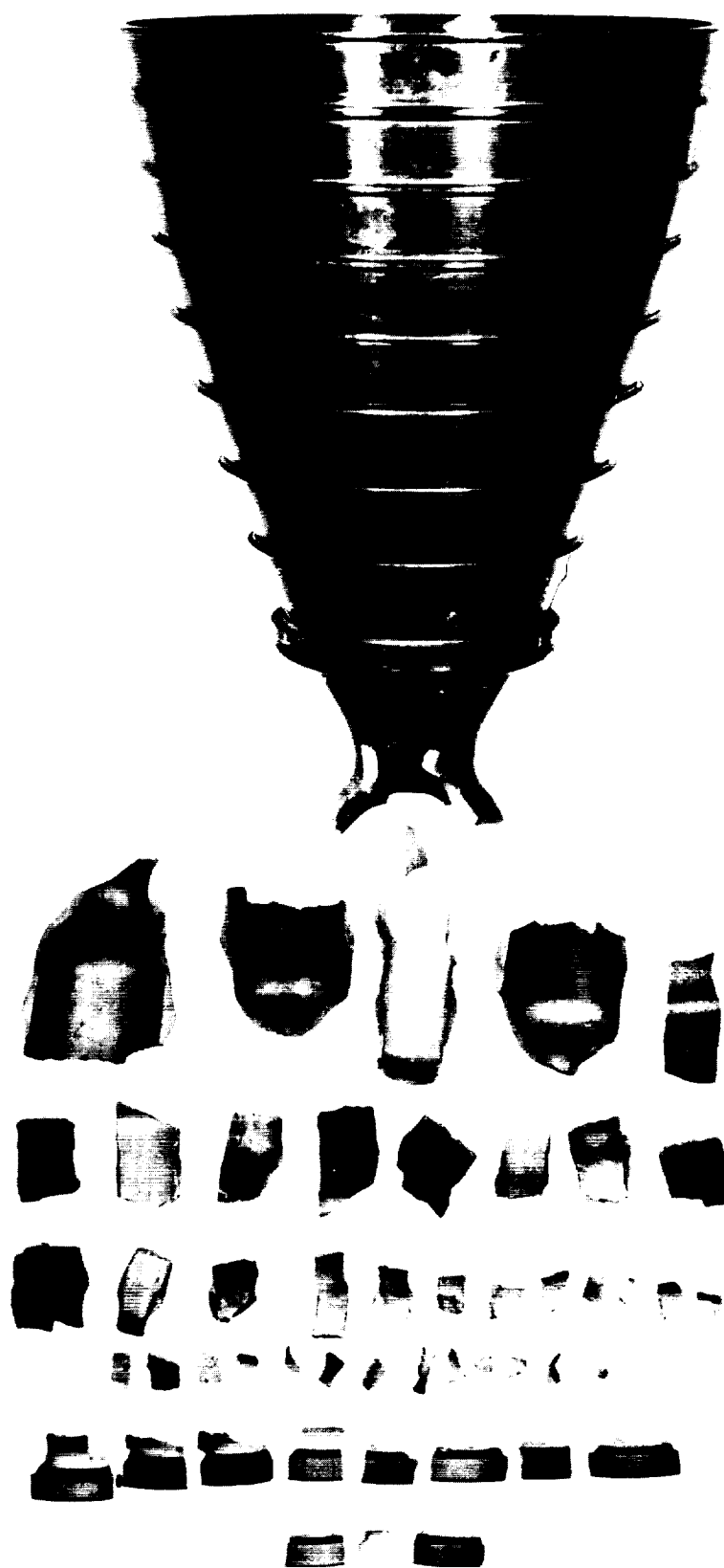


FIGURE 45. - Molybdenum Engine Fragments Resulting from the Explosion of 0.75 g of PETN (Primacord) Completely Covering the Interior of the Engine.

PENETRATION OF VYCOR WINDOW AND MYLAR H-FILM BLANKET BY STEEL PROJECTILES

In addition to the damage caused to the Apollo RCS engines and to their mounts, in an explosive event, there is also the damage incurred by adjacent areas (such as the IM vehicle) from flying fragments.

Experiments were conducted to study the relationship between energy and resultant damage. Lead and steel projectiles were used as fragment simulators. These projectiles were fired at Vycor window sections and H-film blanket sections by means of a Crossman¹⁰ compressed-CO₂ pistol and rifle. With the pistol it was possible to get lead-projectile velocities ranging from 0 to 91 m/sec; with the rifle, velocities as high as 152 m/sec could be obtained. Unfortunately, the lead projectile proved to be unsatisfactory for these tests due to its extensive deformation on impact. To circumvent this problem, steel projectiles were propelled by impacting them with the lead projectile. In this way, it was possible to obtain steel projectile velocities for 1.61 and 1.44 g projectiles ranging from 0 to 34 m/sec using the pistol and up to 52 m/sec with the rifle. A photoelectric timing device (velocity meter) was used to measure the velocities of the projectiles. Vycor plates were obtained from Corning Glass Works as a stock item. To check that the commercial Vycor was in fact similar to the Vycor used in the IM vehicle, a drop weight experiment was conducted on both the commercial glass and the glass used in the IM (Vycor is a specialty glass). A specimen of the IM Vycor material was supplied by MSC; its dimensions were 5 by 7.6 by 0.3 m. The samples of commercial Vycor which were tested, were all cut to the same dimensions of the IM sample window.

The test specimens were laid across two parallel knife edge supports approximately 5 cm apart, and a SS ball 1.6 cm in diameter and weighing 16.26 g was dropped at increasing heights until the plate under test broke. Eleven tests of this nature using the commercial plate gave a height required to break the glass, with this specific ball, ranging from 38 to 69 cm, with the average being 47 ± 12 cm.

The IM sample, broken in the same way, required a drop height of the same ball of 53 cm.

On the basis of these results, it was concluded that the commercial Vycor plate and the IM vehicle Vycor window have similar penetration characteristics.

To conduct a penetration experiment, the Vycor plate was clamped at six points in a metal frame in a vertical position. The steel projectile was placed inside the velocity meter, just ahead of its measuring section, and was impacted with the lead projectile from the compressed-CO₂ pistol. The projectile traveled only a few centimeters before striking the Vycor plate.

¹⁰See footnote 3 on page 7.

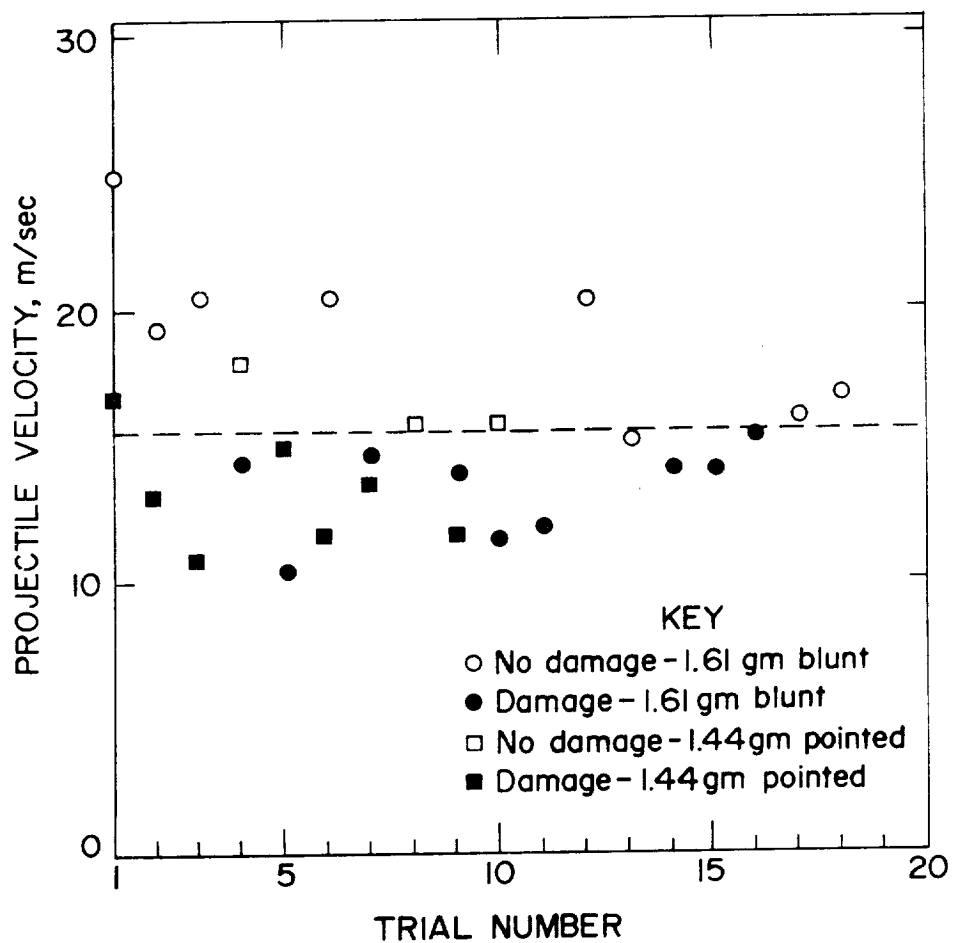
In the H-film penetration experiments, the same experimental arrangement was used as in the Vycor penetration tests. However, here it was necessary to use the compressed-CO₂ rifle to attain higher steel projectile velocities. A blanket of 12 layers of H-film was rigidly clamped at its four edges for test purposes.

The steel projectile which weighed 1.44 g was pointed, while the 1.66-g projectile was blunt. The size of either Vycor plate or the H-film tested was a 30- by 30-cm square.

The results of the experiments with the Vycor plate are depicted in figure 46. It was found that the Vycor window was damaged (either cracked or punctured) if the velocity of either of the two projectiles exceeded approximately 15 m/sec corresponding to an impulse of about 203 dyne-sec. This is considerably below the impulse delivered by even the smallest fragments generated in engine destruct experiments using as little as 0.5 g of explosive. Both the blunt-nosed and pointed projectiles were found to cause a similar degree of damage on impact. This is probably due to the fact that the blunt-nosed projectile is unlikely to strike the target "head-on" but, rather obliquely. As a result, the blunt-nosed projectile acts very similar to the pointed projectile. Thus, the fragments generated in even the smallest molybdenum engine explosions have sufficient energy to cause serious damage to the Vycor window. Probably, even more serious, is the fact that most fragments have sufficient energy not only to penetrate the protective Vycor window, but to possibly damage the window immediately behind it. The damaged Vycor is shown in figure 47.

In the H-film experiments, the H-film proved to be less susceptible to projectile penetration than the Vycor plate in that projectile velocities between 330 and 500 cm/sec were required to penetrate the film. These velocities correspond to momenta of 500 and 750 dyne-sec, respectively. The 111-g fragment produced in the molybdenum engine experiment using 0.5 g of explosive had a momentum of 2,500 dyne-sec, a factor of 5 larger than that required to penetrate the H-film. Fragments weighing less than 20 g and moving with the same velocity will not possess enough energy for penetration of the film. Figure 48 shows the results of the shots.

It has been shown by this series of tests that a real possibility exists that an exploding attitude control engine will create fragments that will damage either the Vycor windows or the blanket covering the LM vehicle.



P64-73
532

FIGURE 46. - Velocity of a 1.61 g Blunt and 1.44 g Pointed Steel Projectile Required to Crack or Puncture a 30-cm Square, 0.32-cm Thick Vycor Plate.

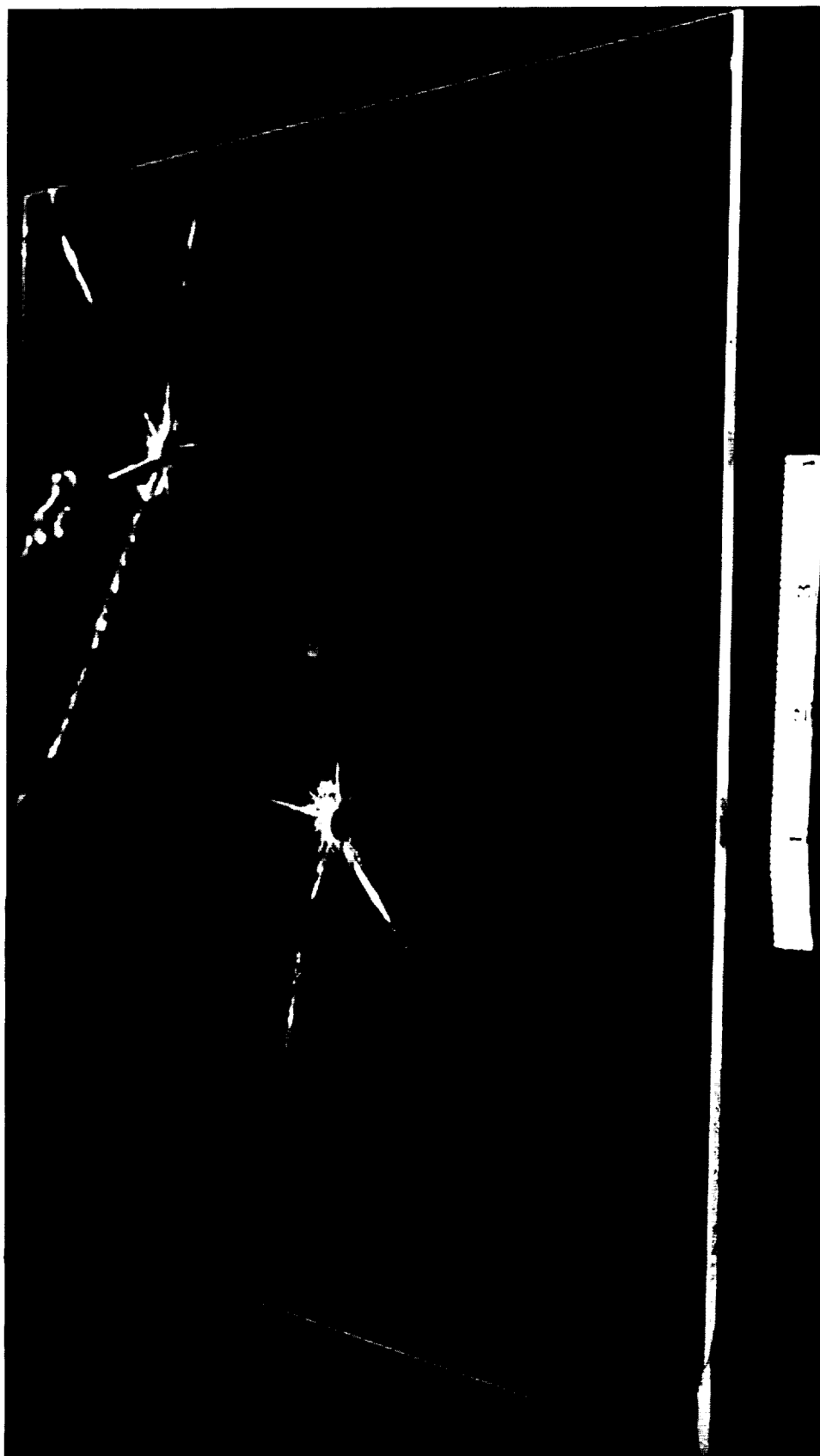
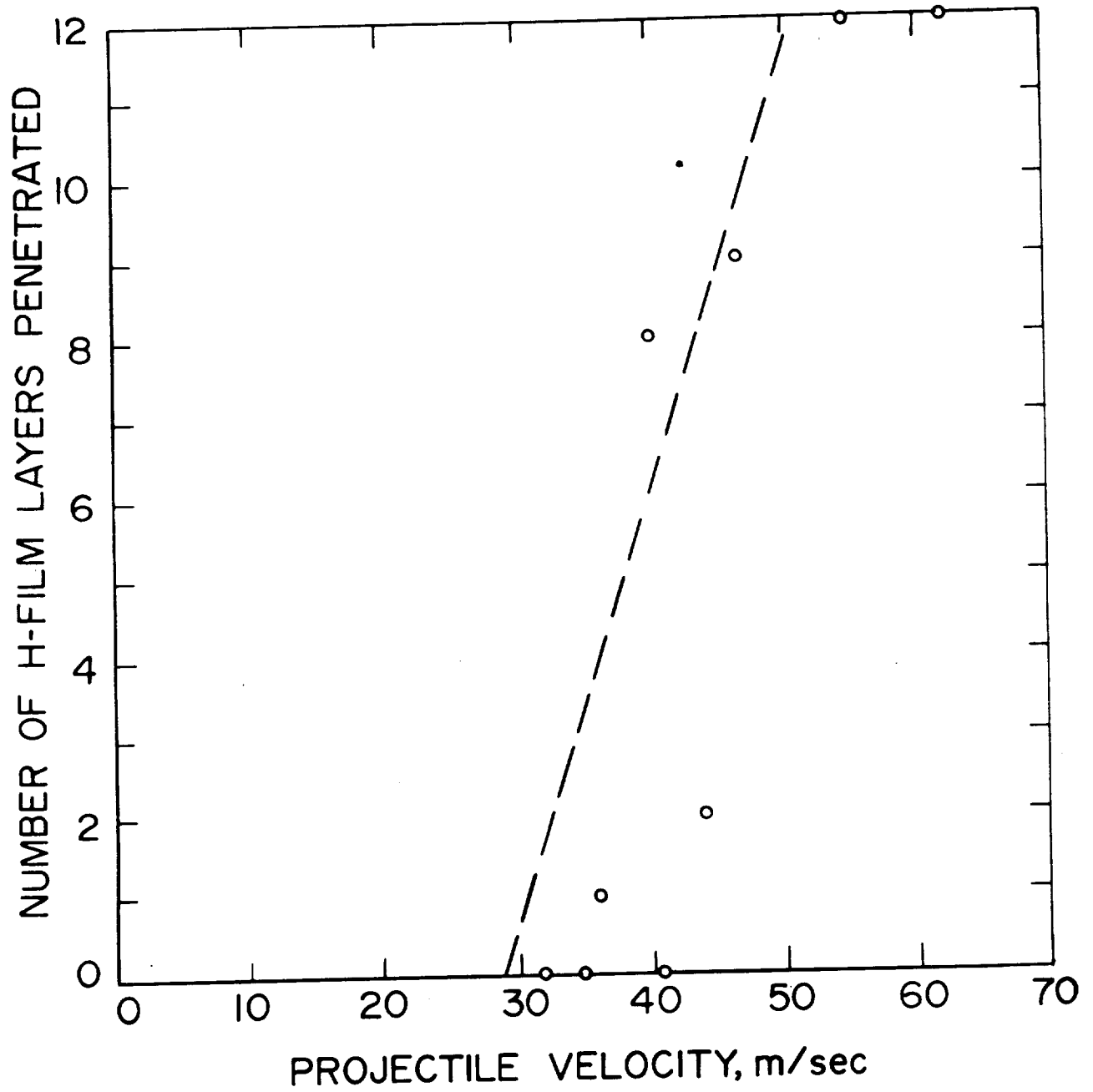


FIGURE 47. - Typical Maximum Damage to Vycor Plate by the Blunt Nose 1.61 g Projectile (also shown).



PGH-73
522

FIGURE 48. - Depth of Penetration of a 12-Layer H-Film Blanket by a Blunt 1.61 g Projectile as a Function of Projectile Velocity.

IMPULSE DUE TO AN EXPLOSION IN THE ENGINE

The size of the impulse delivered to the engine mount as a result of an explosion in the combustion chamber, which would not destroy the engine, should be small. A large impulse may loosen or shear the bolts that fasten the engine to its mount and render the engine useless for attitude control maneuvers.

The impulse for two explosive systems, gas-phase detonation and thin-layer explosion, was measured. The apparatus used for the tests consisted of a ballistic mortar weighing 5,085 g suspended from the ceiling of the bombproof by four steel cables 133 cm long (fig. 49). The internal geometry of the mortar, made of cold-rolled steel, was the same as the geometry of the SS engines. Two locations of the ignition source were tried to determine the effect of this variable on the impulse for the gas detonation tests, in which the chamber was purged with a stoichiometric ethylene-oxygen mixture in the same manner as were the SS engines in the experiments described earlier. The thin-layer explosive used was also the same NG-EGDN-Cellulose system. The reaction of the chamber to the explosion was recorded by means of a movie camera operating at 32 frames per second. The effect of the wick used to initiate the thin layer was measured by conducting a control experiment using the wetted wick only; appropriate corrections were introduced in the calculated results.

The gas-phase detonation, consisting of 0.5 g of explosive mixture, gave an initial chamber velocity of 5 cm/sec; whereas the 0.75 g of thin-layer explosive gave an initial chamber velocity of 31 cm/sec, and for 2 g of thin-layer explosive the velocity was 110 cm/sec. These velocities correspond to impulses of approximately 2.6×10^4 dyne-sec for the gas-phase detonation and 1.6×10^5 dyne-sec for the first thin-layer detonation, respectively. These results compare favorably with the impulse of 2.67×10^6 dyne-sec found for 9 g of tetryl. It also was found that the impulse increased linearly with the weight of explosive. The location of the explosive or the ignition source inside the engine did not influence the magnitude of the impulse.

RISE IN TEMPERATURE OF ENGINE WALL DUE TO AN INTERNAL EXPLOSION

To measure the temperature rise of the SS engines following either a gas-phase or thin-layer detonation, a chromel-alumel thermocouple was peened onto the wall of an unsectioned SS engine, approximately 2.5 cm from the base flange. The engine was set and clamped in the assembly (fig. 6). The thermocouple leads were connected in parallel to a potentiometer with a resolution of 10 μ V. Both gas-phase detonation and thin-layer detonation experiments were conducted in exactly the same manner as they were conducted for fragmentation studies. In the gas-phase detonation, there was no detectable increase in temperature. A small increase in temperature was noted when Primacord was used. The results of the experiments with Primacord are given in table 12.

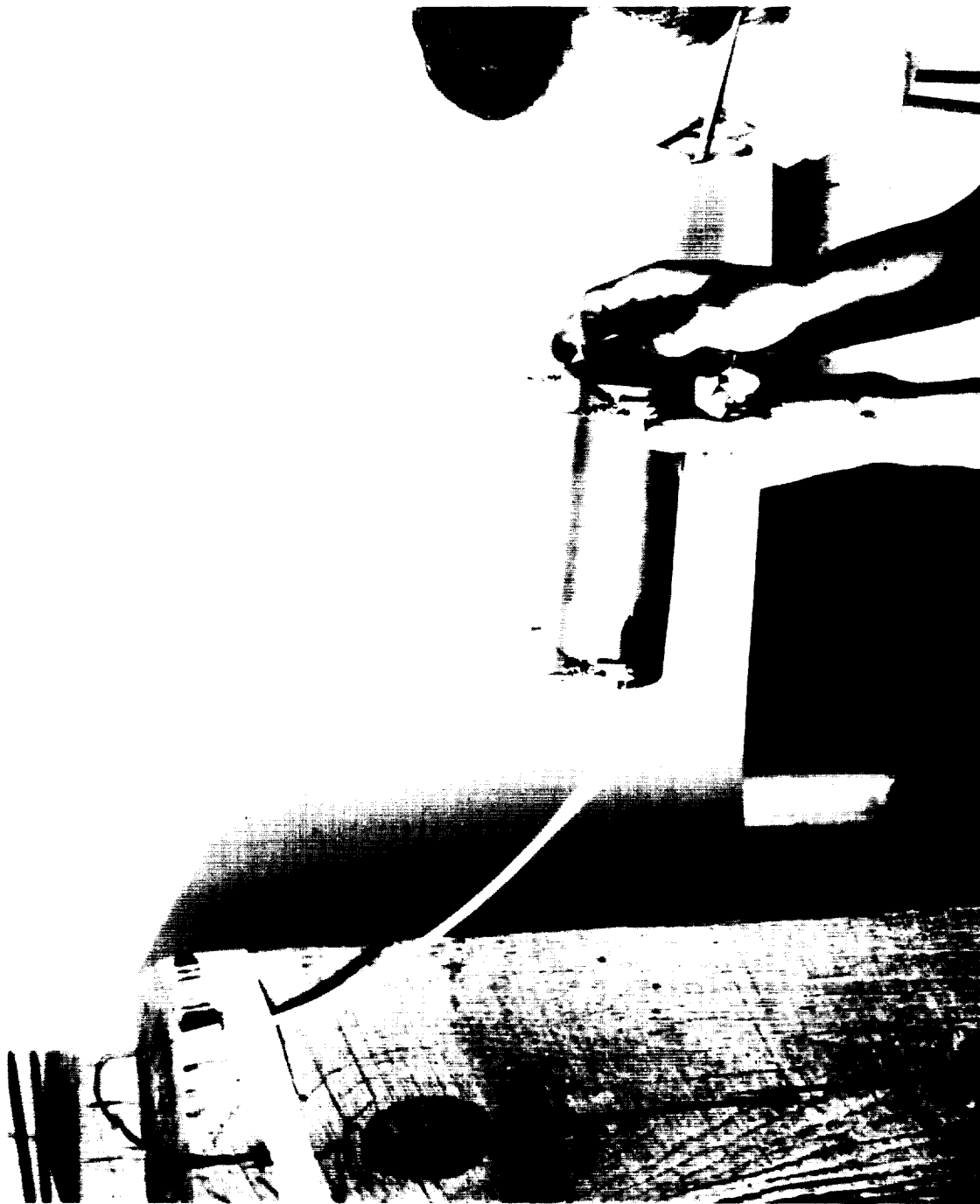


FIGURE 49. - Ballistic Pendulum Apparatus

TABLE 12. - Temperature rise of SS engines following detonation of various weights of Primacord

Primacord weight, g	ΔT , °C	1/Heat gained, calories
0.33	1.5	67
.39	1.1	49
1.00	2.5	112
1.00	2.5	112

1/ Based on engine weight of 450 g.

Heats of detonations of various explosives have been measured or calculated. The heat of detonation of PETN--which constitutes the major part of the Primacord--was measured and found to be 1.5 Kcal/g (7). This value varies somewhat with charge density, size, and confinement, and with the geometry of the vessel containing the charge, but the quoted value is sufficiently accurate to be used here for comparison calculations. Unreported percentages of the thermal energy of detonations that are transferred to the walls of the metal containers were determined by other researchers to be about 50 to 70 pct of the total heat of detonation released. Thus, theoretically, the heat to be transferred to the walls of the engine, in the 1 g test, should be approximately 700 cal, which is much higher than that actually measured. The difference probably lies in the distribution of the explosive on the walls of the equipment and the degree of confinement.

SUMMARY

This volume contains a large amount of data obtained from diverse experiments, but there is a connection between the various experiments in that each part contributes to a more complete understanding of the deformation and fragmentation problems.

Initially, the amount of explosive needed to deform SS engines was determined. Results, as expected, showed a larger degree of deformation with increasing weight of explosive. The restraining effects of flanges and thick-walled areas were noted. When equal amounts of explosive were used, the charge closer to the wall of the engine caused more damage.

The amount of explosive needed to fragment SS and molybdenum engines and the relationship between the amount of explosives used and the resultant fragment distribution were measured. Due to the marked difference in the mechanical properties of stainless steel and molybdenum and in their behavior under very high rates of loading, the results obtained with SS engines were not directly applicable to the molybdenum engines, molybdenum being much more brittle. Much smaller amounts of explosive were needed to demolish the molybdenum engines than were necessary for SS engines. It has been demonstrated that a thin layer of explosive on the molybdenum engine wall is significant in fragmenting the engine, but not in accelerating the fragments. The chamber pressure

produced by the combustion products provides the major mechanism for fragment acceleration.

When explosions occurred in molybdenum engines mounted on the Apollo Service Module panels, it was shown that 0.5 to 0.75 g of explosive PETN generate engine fragments that damage the panel. Also, the resultant fragments possess enough energy to damage Vycor windows but not the blanket covering the adjacent LM vehicle; fragments with higher energies are needed to damage the blanket.

The total impulse delivered to an engine as a result of an internal explosion was measured for three types of explosions: A solid explosive, a gaseous explosive system, and a thin-layer explosive. Impulse values were found to range from 30 to 600 g-sec, depending on the weight of the charge.

The peak-wall shock pressures resulting from the explosion of various weights of explosive fired at the center of the combustion chamber were measured. Pressures varied from 6×10^3 to 9×10^3 atm, for tetryl weights of 3 and 9 g, respectively.

The portion of thermal energy, resulting from the detonation of Primacord inside the engines, transferred to the engine was measured. The values obtained are lower than other reported values in similar experiments.

REFERENCES

1. Villemarette, R. J., J. W. Akerman, N. H. Chaffee, B. J. Rosenbaum, W. D. Taliaferro, and A. K. Watkins. Apollo Module Reaction Control System Panel B Plus Yaw Engine Failure Analysis. NASA Manned Spacecraft Center. N. MSC-IN-65-EP17, November 1965.
2. Loving, F. A. Barricading Hazardous Reactions. Ind. Eng. Chem., v. 49, October 1957, pp. 1744-1746.
3. Baumeister, Theodore, Ed. Mechanical Engineers' Handbook, 1964, pp. 3-5.
4. Rodean, H. C. Rocket Thrust Termination Transients. ARS J., June 1959, pp. 406-409.
5. Watson, R. W. The Perforation of Thin Plates by High Velocity Fragments. Proc. Fifth Symp. Hypervelocity Impact, Denver, Colo., Oct. 30-Nov. 1, 1961, v. 1, pt. 2, pp. 581-592.
6. Miyagishima, T. I., E. Rosman, and E. P. Pertman. Investigation of High Strain Rate Behavior of Refractory Alloys and Coatings. Final Rept., February 1966, Contract NAS-9-4905, 212 pp.
7. Staff of the Explosives Chemistry Section of the General Chemistry Division, University of California. Properties of Chemical Explosives. Dec. 16, 1965.
8. Gray, Dwight E., Ed. American Institute of Physics Handbook, 2d ed., 1963.

APPENDIX I. THEORETICAL BACKGROUND

Additional background theory of combustion dynamics and fragment-kinematics are presented in this appendix.

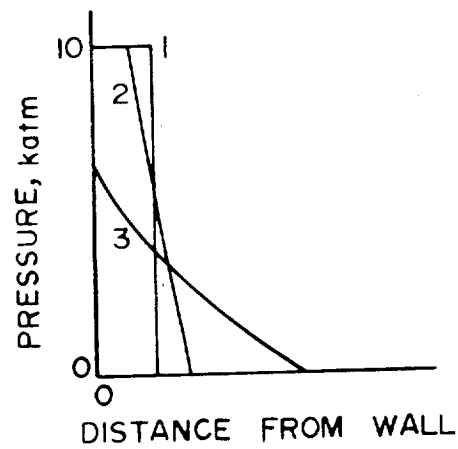
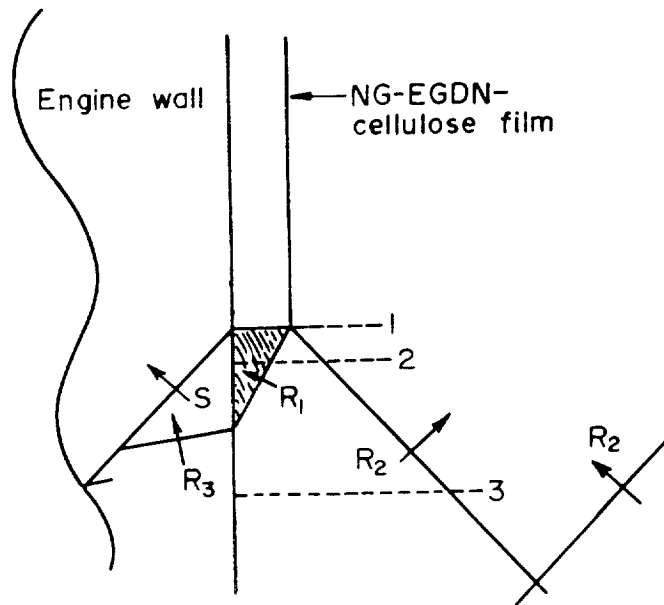
Combustion Dynamics

A C_2H_4/O_2 gas-phase detonation originating at the injector face in RSC engines traveling toward the throat at a velocity of $2.2 \text{ mm}/\mu\text{sec}$ has a pressure distribution similar to that shown in figure 39. At the detonation front, the pressure rises abruptly from 1 to 34 atm and then falls gradually to a relatively steady-state pressure of approximately 70 pct the constant volume combustion pressure.

Upon reaching the throat, part of the detonation moves out of the engine and part reflects from the converging section as a pure shock wave and moves back towards the injector. The width of the triangular pulse (fig. 39) is equal to about half the distance of travel from the point of ignition. For example, in the case where the detonation wave has traveled approximately 2.5 cm, the base of the triangular pulse would be about 1.25 cm. If the chamber were sealed so that the gases could not exhaust to the environment, the pressure oscillations in the chamber would eventually subside to a constant pressure (constant volume combustion pressure), represented by the horizontal line in figure 39. However, because of the continual exhausting of the chamber contents under actual conditions, constant pressure is never realized although it is usually assumed that this is the effective driving pressure accelerating the fragments.

The thin-film detonation process (fig. A-1) is more complicated since this is a two-dimensional phenomenon, as opposed to the one-dimensional gas-phase detonation. To construct the wave diagram shown in figure A-1, it was assumed that the engine was initially evacuated. If this were not the case, the rarefactions (R_2) would be shock waves. Behind the detonation front is a high pressure zone (shaded in the figure), into which rarefactions (R_3) are propagating. The pressure in this shaded area is usually about 8-10 kb for nitroglycerin (NG).

The high pressure zone immediately behind the detonation front compresses the wall of the molybdenum chamber behind the shock wave (S) which propagates at a speed slightly greater than the speed of sound in molybdenum. The shock wave is followed by a rarefaction wave (R_3) that originates at the point of contact of the rarefaction wave (R_1) and the chamber wall. Since the rarefaction wave (R_3) travels in the shock compressed medium, its velocity is slightly higher than the shock and it eventually intersects the shock wave. The shock intensity decays continually thereafter until it reflects from the outer wall of the chamber. The cylindrical rarefaction wave (R_2) travels back into the combustion chamber eventually coalescing on the engine axis. This intersection produces other waveforms that contribute to the confusion. Figure A-1 shows the pressure distribution in the plane of the engine cross section at three distances behind the detonation front. The length of the high pressure zone behind the front is typically the same order of magnitude as the thickness of the layer.



PGH-73
526

FIGURE A-1. - Wave Pattern and Pressure Distribution Associated with Thin Film Detonation.

Fragment-Kinematics

The two pressurization mechanisms accelerating the fragments in both the gas-phase and thin-film detonations relate to the high pressure zones immediately following the detonation fronts, and the pressure of the product gases filling the engine. As is noted in the following sections, the latter results in the major influence, although the former probably plays a significant role in fragmenting the molybdenum engines. It can be shown that the impulse per unit volume (I) delivered to the fragments via the high pressure zone immediately following the gas-detonation front is approximately equal to the mean pressure (\bar{P}_D) in this zone divided by the detonation velocity (D): $I = \bar{P}_D/D$. For the C_2H_4/O_2 mixture initially at 1 atm pressure, the mean detonation pressure is 0.67 times the peak pressure (34 atm) and the detonation velocity is 2mm/ μ sec; therefore, the impulse amounts to approximately 160 dyne-sec. If this were applied to a 3-g molybdenum fragment (the weight of a molybdenum fragment with a cross-sectional area of 1 cm² is approximately 3 g), it gives a fragment velocity of approximately 53 cm/sec. This value is considerably lower than the experimentally measured value of 13.7 m/sec for the 0.82-g SS fragment used in the gas-phase detonation studies. Therefore, we conclude that the major pressure accelerating the fragments is not the high pressure zone but the pressure of the product gases in the engine. As a matter of fact, it is a simple exercise using the conservation of momentum (equation 1) to show that if the constant volume combustion pressure is 16 atm¹ and the engine time constant is 0.5 msec, for a product gas temperature of 3,000° K, then the product of the mean chamber pressure ($\bar{P}_V = 8$ atm, half the constant volume combustion pressure) and the engine time constant (T) gives an impulse ($I = \bar{P}_V T$) of approximately 4,000 dyne-sec. For the 3-g fragment with an effective area of 1 cm² (area-to-mass ratio of 0.3) this gives a velocity of approximately 1,000 cm/sec, in reasonable agreement with the observed velocity for the 0.6 cm SS fragment (area-to-mass ratio 0.39) of 13.7 m/sec. The fact that fragment velocity is proportional to its area-to-mass ratio follows from the conservation of momentum expression,

¹Refers to constant volume combustion pressure of C_2H_4/O_2 .

$$Mv_t = A\hat{P}_v\tau$$

$$\text{or} \quad v_t = (A/M)\hat{P}_v\tau \quad (1)$$

where A is the effective area of the fragment to which the pressure is applied, M is the mass of fragment, \hat{P}_v is the time average pressure in the chamber (one-half the constant volume combustion pressure), τ is the time constant for the engine (that is, the time required for the combustion chamber pressure to drop 90 pct of its initial value), and v is the fragment velocity. The product of \hat{P}_v and τ should be constant in a given experiment. If equation 1 applies, then the ratio of the velocities of any two fragments in a given explosion should be directly proportional to the ratio of their effective area-to-mass ratios:

$$\frac{v_1}{v_2} = \frac{(A/M)_1}{(A/M)_2} \quad (2)$$

Figure 36 shows a plot of fragment velocity ratios to the ratio of their effective area-to-mass ratios; the satisfactory agreement of the experimental data and the theoretical curve justify the use of the mathematical expressions. The validity of these mathematical expressions makes the calculation of fragment velocities fairly straightforward if one has available information concerning the constant volume combustion pressure. This is correct if it is assumed that the fragment acceleration is not sufficient to displace the fragments any significant distance in the time required for the engine to depressurize out the throat. If this were not the case, it would be necessary to consider, in addition to the throat area, the total area of the growing cracks between the fragments as a means of exhausting the product gases. However, it can be shown for these engines and for explosive weights less than about 1 g that τ is considerably shorter than the time required for the fragments to move an appreciable distance.

An additional point of interest is the effect of the high-frequency oscillation pressure in the engine on fragment acceleration. A mathematical analysis of the application of a highly oscillatory sinusoidal pressure to a fragment, superimposed on a steady-state pressure, shows that the fragment will see a time average of the sinusoidal pressure if the frequency of the oscillation obeys the following relationship:

$$f > \frac{P_1}{2n} \sqrt{\frac{L}{P_0 M}} \quad (3)$$

where f is the frequency of the sinusoidal pressure disturbance, P_1 the peak-to-peak pressure of the oscillatory signal, L the characteristic length of the fragment, P_0 the steady-state pressure, and M the fragment mass. For a molybdenum fragment having an effective area of 1 cm^2 and a mass of 3 g, this expression reduces to 6,000 cycles/sec, showing that if the applied sinusoidal pressure has a frequency greater than 6,000 cycles/sec, the fragment will be subjected to an effective pressure equal to the steady-state pressure, since the time average of the sinusoidal pressure is zero. The pressure oscillograms in figure 38 have a frequency of approximately 500,000 cycles/sec. Although this frequency is not extremely meaningful since the pressure transducer has a natural frequency of 100,000 cycles/sec, the example demonstrates that the fragments generated in these explosions are not influenced by the presence of the oscillatory component of the pressure.

A final topic of interest concerns the partition of fragment energies into rotational and translational components. Using the fragment whose rotation is calculated on the next few pages, we see that the translational energy is approximately 33 times larger than the rotational energy; therefore, the rotational energy of a fragment can, in general, be neglected in comparison to its translational energy.

The above arguments apply to the kinematics of fragments associated with either gas or thin-layer detonations so that it can likewise be shown that the high pressure zone immediately following the detonation in the thin layer contributes little to the fragment translational and rotational velocities. However, because of the larger weights of explosives used in these experiments, the crack growing between the accelerating fragments is significant in depressurizing the chamber and consequently in affecting fragment terminal velocity. Figures 40 and 41 show the experimental results obtained for the sectioned SS engines using the thin-layer explosive. The scatter in the points (fig. 41) results primarily from the nonreproducible nature of the combustion process associated with these thin layers because the film thickness is near the limit required to sustain a stable detonation. Of the experiments with the NG-EGDN-cellulose explosive layer, only one-third resulted in stable and complete combustion. The remaining two-thirds either did not

completely consume the film or the film did not initiate at all. Figures 40 and 41 show the results of only those experiments which were considered to achieve complete combustion; however, there was no absolute criteria for establishing this fact. It is possible, using figures 40 and 41 and the conservation of angular and linear momentum, and the mass-to-area ratio for the fragments, and their moments of inertia, to calculate the fragment translational and rotational velocities for any given weight of explosive. Furthermore, the experimental results justify neglecting the contribution of the growing crack between fragments in affecting the terminal velocity of the resulting fragments as long as the weight of explosive does not exceed 1 g. The results of the gas and condensed-phase detonation studies using SS presectioned engines, demonstrates the validity of using simple conservation of momentum expressions to calculate realistic fragment velocities. It has been demonstrated that the rotational contribution to fragment total energy can, for the most part, be neglected. The location of the ignition source does not contribute significantly to the fragment velocities.

Fragment rotation due to the passage of a detonation across its surface can be calculated in the following manner.

From the conservation of angular momentum:

$$T = \dot{L} = I\dot{w}, \quad (A-1)$$

where T is the torque due to the applied detonation pressure about the fragment center of mass (CM) (fig. A-2), L is the rate of change of angular momentum, I is the fragment moment of inertia, and w is its angular acceleration. For a square fragment of length L and mass M ,

$$I = \frac{2}{3} ML^2. \quad (A-2)$$

For a triangular pressure pulse (fig. 39), the torque on the fragment at any time, t , can be expressed by:

$$T = \frac{L}{2} \hat{P}_D (2L - Dt) Dt, \quad (A-3)$$

where \hat{P}_D ($\hat{P}_D = 0.67 P_D$) is the mean pressure in the triangular portion of the pulse, and D the detonation velocity. Integrating (A-3) over the time for the detonation to travel across the fragment we find,

$$w_t = \hat{P}_D L^2 / MD, \quad (A-4)$$

where w_t is the terminal angular velocity. For a C_2H_4/O_2 detonation, $P_D = 23$ atm and $D = 2\text{mm}/\mu\text{sec}$, and for $L = 1$ cm and $M = 3$ g, (A-4) gives,

$$w_t = 38 \text{ rad/sec.}$$

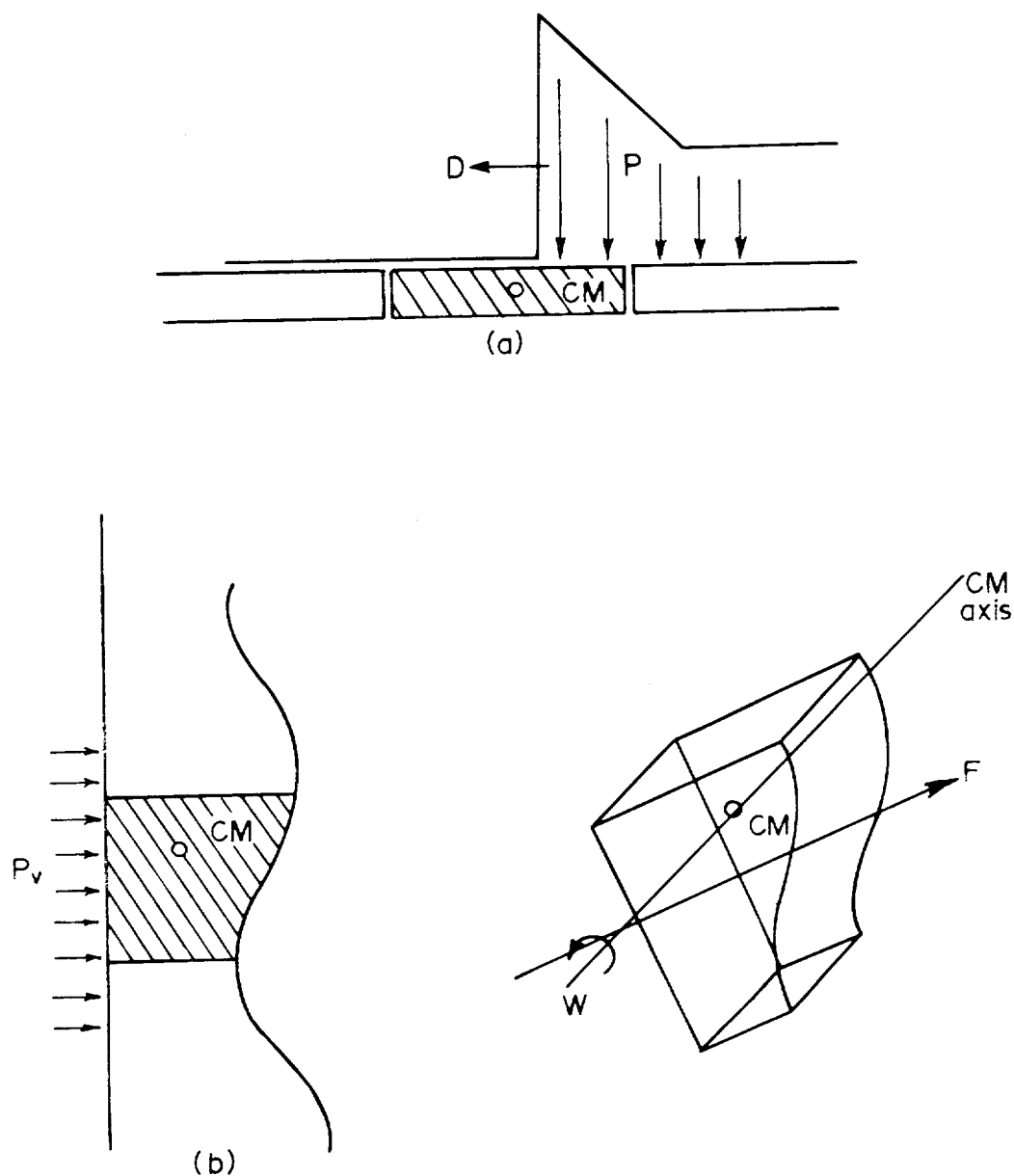


FIGURE A-2. - Illustration of (a) the High Pressure Zone Behind the Detonation Front and (b) the Quasi-steady Chamber Pressure (P_v) in Producing Rotation of a Fragment.

Fragment rotation also results when the force vector, due to the chamber pressure, does not pass through the fragment center of mass (fig. A-2). The force vector is obtained from the relation

$$\bar{F} = \int P_v d\bar{A}, \quad (A-5)$$

where P_v is the combustion chamber pressure and $d\bar{A}$ the infinitesimal surface area vector, where the integration is carried out over the fragment's interior surface. For the molybdenum fragment,

$$I = 1.0 \text{ g-cm}^2 \quad \underline{2/}$$

$$\text{and } T = 0.1 P_v \quad (A-6)$$

For impulse forces, equation (A-1) gives

$$\tau \hat{T} = I w_t,$$

$$\text{or } w_t = \frac{\tau \hat{T}}{I}, \quad (A-7)$$

where τ is the engine time constant and \hat{T} the time-average torque ($= 0.1 \hat{P}_v$). Substituting (A-6) into (A-7),

$$w_t = \frac{\tau(0.1) \hat{P}_v}{1.0} \quad (A-8)$$

and for $\tau = 5 \times 10^{-4}$ sec and $\hat{P}_v = 8$ atm (one-half of the constant volume combustion pressure), $w_t = 850$ rad/sec.

From equations (A-7) and (1), we can obtain the ratio of the rotational and translational velocities,

$$\frac{w_t}{v_t} = \frac{\tau \hat{T}}{I A P_v} \quad (A-9)$$

For a rigid body, \hat{T} can be written

$$\hat{T} = K \hat{P}_v, \quad (A-10)$$

where K is a constant specific to a fragment. From (A-9) and (A-10),

$$\frac{w_t}{v_t} = \left(\frac{\tau}{I} \right) \left(\frac{K}{A} \right) \quad (A-11)$$

so that the ratio of the fragment's angular and translational velocities is constant independent of both τ and P . Since a fragment rotational and translational (kinetic) energies are given by the relations,

^{2/}Note the moment of inertia for the fragment in figure 44 is not the same as for the fragment in figure 43.

$$RE = 1/2 I w_t^2, \quad (A-12)$$

$$\text{and } TE = 1/2 M v_t^2,$$

then

$$\frac{TE}{RE} = \left(\frac{M}{I} \right) \cdot \left(\frac{v_t}{w_t} \right)^2; \quad (A-13)$$

using (A-9)

$$\frac{TE}{RE} = \left(\frac{M}{I} \right) \cdot \left(\frac{IA}{MK} \right)^2$$

or

$$\frac{TE}{RE} = \left(\frac{A}{K} \right)^2 \cdot \left(\frac{I}{M} \right) \quad (A-14)$$

Equation (A-14) shows that the ratio of the translational and rotational energies depends on only physical characteristics of the fragment, exclusive of P and τ . If $I = 2 \text{ g-cm}^2$, $K = 0.1 \text{ cm}^3$, $M = 3 \text{ g}$, and $A = 1 \text{ cm}^2$, then

$$\frac{TE}{RE} = 33$$

demonstrating that the rotational energy is small compared with the translational energy.